2-1-2020

COMPUTATIONAL MODELING OF LAMINATED VENEER BAMBOO (LVB) DOWEL JOINTS

Niloufar Khoshbakht

COMPUTATIONAL MODELING OF LAMINATED VENEER BAMBOO (LVB) DOWEL JOINTS

A Dissertation Presented

by

NILOUFAR KHOSHBAKHT

Submitted to the Graduate School of the
University of Massachusetts Amherst in partial fulfillment
of the requirements for the degree of

DOCTOR OF PHILOSOPHY

February 2020

Environmental Conservation
Sustainable Building Systems

COMPUTATIONAL MODELING OF LAMINATED VENEER BAMBOO (LVB) DOWEL JOINTS

A Dissertation Presented

by

NILOUFAR KHOSHBAKHT

Approved as to style and content by:

Peggi L. Clouston, Chair

Alexander C. Schreyer, Member

Sanjay R. Arwade, Outside Member

Curtice R. Griffin, Head
Department of Environmental Conservation

DEDICATION

To my kindhearted mother and my loving father.

ABSTRACT

COMPUTATIONAL MODELING OF LAMINATED VENEER BAMBOO (LVB) DOWEL JOINTS

FEBRUARY 2020

NILOUFAR KHOSHBAKHT, BSc. UNIVERSITY OF TEHRAN

MSc. UNIVERSITY OF TEHRAN

Ph.D., UNIVERSITY OF MASSACHUSETTS AMHERST

Directed by: Professor Peggi Clouston

Laminated veneer bamboo (LVB) is a sustainable building material that has been gaining interest in the construction industry of late. As a relatively new product, little is known about its connection performance, specifically, its failure behavior in dowel type joints and possible similarities it may have to engineered wood products in terms of failure mechanisms. Research is needed to aid in the understanding of LVB dowel connection failure behavior and to quantify the failure mechanism and key factors associated with LVB dowel connection strength. Modeling, as conducted in this research, is a valuable tool to help devise safe standards and formulations for future LVB product adoption, design, and implementation.

In this dissertation, a finite element model was described to investigate dowel bearing failure when loaded parallel-to-grain. The model was calibrated and validated through comparison with experimental results. Frictional contact was incorporated in the model and the coefficient of friction was proved to be a key factor in finding the maximum shear stress location. According to both the FE model and experimental results, the high shear stress-to-strength ratio is the major cause of failure when the dowel is loaded parallel-to-grain.

Moreover, tensile stress perpendicular-to-grain is observed to be an influential secondary cause of failure.

Once the FE model was established and the primary study was done, a quantitative comparison was carried out between the two test methods offered by ASTM5764 standard (full-hole and half hole specimen) for timber products to see if the same condition holds for LVB and other similar wood engineering products. Followed by a study conducted to investigate the effectiveness of Hankinson formula for LVB dowel joints which subsequently resulted in devising the formulation, so it can calculate bearing strength at different angles to the grain for LVB material.

This research study will contribute to safer design and implementation of LVB bolted connections and development of standard test method for wood-composite materials including LVB.

TABLE OF CONTENTS

Page

LIST OF TABLES

Table Page

LIST OF FIGURES

Figure Page

TERMINOLOGY

Abbreviations

EN383= European standards;

EYM = European Yield Model;

GLG= Glued laminated guadua bamboo;

LVL= Laminated veneered lumber;

LVB=Laminated veneered bamboo;

LSL= Laminated strand Lumber;

NDS= National Design Specification® for wood construction;

PSL=Parallel strand lumber;

Q (8 or 9) = Quadrilateral element;

SCL=Structural composite lumber;

Symbols

L = Length of specimen;

W = width of specimen;

CV= coefficient of variation;

SD = standard deviation;

b = width of specimen;

d = fastener diameter;

e= end distance;

E= elastic moduli;

$E_L^{||}$= Local modulus of elasticity when the specimen is loaded parallel to grain;

$E_L^{\perp}$= Local modulus of elasticity when the specimen is loaded parallel to grain;

$E_{aa,}$ E_{bb}andE_{cc}= Modulus of elasticity in three fiber direction;

F = load;

Fij = components of strength tensor;

Fyb = Fastener bending yield strength;

Fe =Dowel bearing strength of wood member;

G = in-plane shear modulus;

g = gap distance in normal contact condition;

go or gn= standard gravity

h= height;

k=spring stiffness;

L = length;

m= mass;

n= sample size;

R: The specimen width-to-fastener diameter ratio;

S = in-plane shear strength;

SD = standard deviation;

t: value of t statistic from table 1 ASTM D2915;

u, v, w = displacement in x, y, z directions;

V = volume;

Vo = output voltage;

Vs = input voltage;

$\bar{X}$: Specimen mean value;

s_L = parallel-to-grain strength;

s_L^+ = parallel-to-grain tensile strength;

s_L^-, s_{LU}^- = parallel-to-grain compressive yield and ultimate strength, respectively;

s_T = perpendicular-to-grain strength;

s_T^+ = perpendicular-to-grain tensile strength;

s_T^- , s_{TU}^-) = perpendicular-to-grain compressive yield and ultimate strength, respectively;

Z= reference design value (fastener load capacity);

δ = displacement;

ε (i,j,k)= strain components;

θ = grain angle;

μ = mean value; coeff of friction;

ϑ_{ij} = Poisson's ratio;

σ_i = stress components;

τ = Shear stress;

τ_{ij}=in plane shear stress;

λ : normal contact force(Lagrange multiplier);

π =Energy of the system;

Subscripts

x, y, z = coordinate directions;

1, 2, 3= principal material directions;

max = designates maximum value;

u = designates ultimate value;

y = designates value at incipient yield;

CHAPTER 1

INTRODUCTION & BACKGROUND

1.1 Introduction

Bamboo is a fast-growing plant that has been used in construction for centuries in many parts of the world where it is naturally grown (Lee, Bai, & Peralta, 1994). Its sustainable attributes are well known; for example, its maturation cycle for harvest is a mere 3 to 8 years (Mahdavi, Clouston, & Arwade, 2011), its rate of carbon sequestration is more efficient than that of other wood species, and its processing is low energy intensive and creates minimal pollution (Diesen & Clouston, 2014). Consequently, bamboo is becoming an attractive material in regions of the world where it is not a native plant.

Although the natural cylindrical form of the bamboo culm is inherently strong, it is not overly practical, particularly in consideration of structural connections. Laminated Veneered Bamboo (LVB), however, is composite material made from bamboo that possesses bamboo's desirable mechanical properties but has the added benefit of being prismatic, produced in stock sizes, and allows for standard connection hardware, similar to engineered wood products (Mahdavi, Clouston, & Arwade, 2011).

1.2 Background & literature review

1.2.1 Wood based Composite Materials

Structural Composite Lumber is a type of engineered wood product in which a combination of wood (in the form of sheets or strands or small wood elements) with

adhesives is used to form a lumber-like member with an efficient usage of fibers in order to achieve the desired mechanical properties. Some of the most well-known products are Laminated Veneer Lumber (LVL), Glulam, Parallel Strand Lumber (PSL) and Laminated Strand Lumber(LSL).

The advantages of structural composite lumber over ordinary sawn lumber include strength, the predictive performance, dimensional stability, consistency, and treatability. The dimensional stability of LSL is not as good as LVL and PSL.

Laminated Veneer Bamboo (LVB) is also relatively new, which is the main topic of this Dissertation. Bamboo is less likely to be used in construction applications because it is hard to connect bamboo in its natural shape. Bamboo, in this study, is being used in the form of LVB laminated veneer bamboo. However, even in the form of rectangular lumber, robust research is needed in understanding bamboo connection behavior. One must study its orthotropic behavior to see how it varies compared to other wood products.

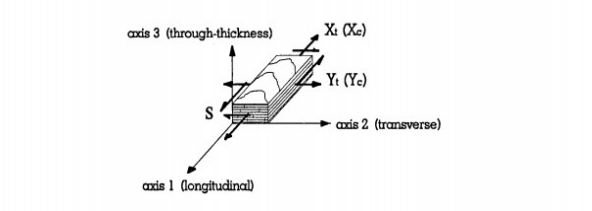

Figure 1.1: Three principal axes of LVB (Clouston,1995)

The strength of a composite material is highly directional in nature (Gibson, 1994). The strength varies according to the angle of the loading relative to the direction of the fiber (Figure 1.1) .In composites, the strength is characterized by strength in the longitudinal direction(s_L) and strength in the transverse direction(s_T) both in compression and tension (s_L^+ / s_L^-, s_T^+/s_T^-) and also by in-plane shear strength(s_{LT}).Usually, $s_T^+$is the lowest of all, which is known to contribute to failure in wood composites. Therefore, these five factors,

or a combination of them, have been incorporated to construct failure yield models for composite materials.

Failure criteria can be used to predict strength in wood composites. They can help us simply estimate the lamina strength under complex loading conditions and to quantify when and how the structure fails. Below are brief descriptions of most relevant phenomenological failure criteria : Maximum Stress criterion, Maximum Strain criterion, Hankinson formula, Quadratic Interaction criteria, Tsai-Hill Yield criteria and Tsai-Wu failure criterion.

1.2.2 Phenomenological failure criteria

1.2.2.1 Maximum stress criterion

Maximum stress criterion for orthotropic materials is an extension of Normal Stress Theory (Rankine's Theory) for isotropic materials. It suggests that failure occurs when stress in any principal direction goes beyond the strength value in that same direction.

$$-s_L^- < \sigma_1 < s_L^+$$

$$-s_T^- < \sigma_2 < s_T^+ \quad (1.1)$$

$$|\tau_{12}| < s_{LT}$$

Figure1.2 shows that for maximum stress criterion, all stress components are independent. Thus, the failure surface forms a rectangle.

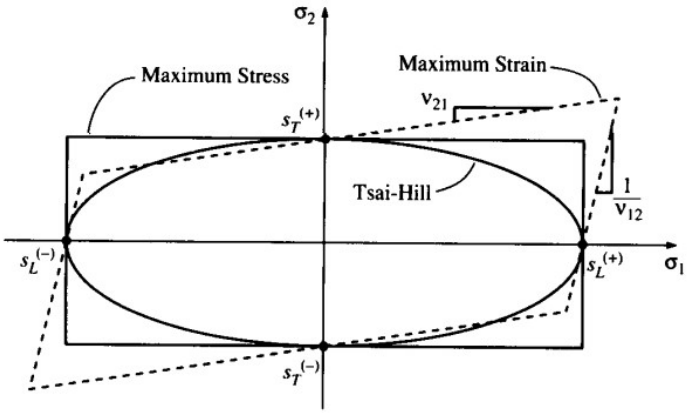

Figure 1.2: 2D Failure surfaces for different failure criteria(Gibson,1994)

1.2.2.2 Maximum Strain criterion

Maximum Strain criterion is an extension of Saint Venant's Theory (Maximum Normal Strain Theory), considering the orthotropic behavior of wood. In this context, failure occurs when principal strains exceed the ultimate corresponding strain.

$$\begin{aligned} -e_L{}^- < \varepsilon_1 < e_L{}^+ \\ -e_T{}^- < \varepsilon_1 < e_T{}^+ \\ |\gamma_{12}| < Se_{LT} \end{aligned} \qquad (1.2)$$

The shape of the failure surface is a skewed parallelogram (Figure 1.2.) that shows that there is an interaction between σ_1 and σ_2 due to the effect of the Poisson ratio.

$$\varepsilon_1 = \frac{\sigma_1}{E_1} - \frac{\nu_{12}\sigma_2}{E_2} \qquad (1.3)$$

1.2.2.3 Hankinson formulation

If we consider biaxial stress in orthotropic material, the simplest way to address strength interaction criterion is to use a linear form:

$$\frac{\sigma_1}{s_L} + \frac{\sigma_2}{s_T} + \frac{\tau_{12}}{s_{LT}} = 1 \quad (1.4)$$

For off-axis stress state at angle θ, after transformation of stresses we have:

$$\sigma_1\left(\frac{\cos^2\theta}{s_L} + \frac{\sin^2\theta}{s_T} + \frac{\cos\theta\sin\theta}{s_{LT}}\right) = 1 \quad (1.5)$$

Hankinson formula is an empirical formula developed from Equation 1.5 by excluding shear term since in wood products the interaction equation is found to be insensitive to shear stress.

$$\sigma_1 = s_\theta \rightarrow s_\theta = \frac{s_L s_T}{s_L \sin^2\theta + s_T \cos^2\theta} \quad (1.6)$$

s_θ: Failure strength at angle θ in the loading direction

The Hankinson formula is not exactly a failure criterion but has been widely used (Hankinson, 1921) as a measure for prediction of strength at different angle-to-grain loading for wood products. Hankinson criterion has been employed in Euro code 5 and most widely used for timber, glulam and LVL products.

Hankinson formula has been generalized as it shown in Equation 1.7 in which n is a constant that is determined from experiments. For original Hankinson equation n equals to 2 and has been used for many wood products. However, for the general formulation the value n can differ based on different strength ratio in orthotropic direction and loading type (compression and tension) and the range of its variation can be found in the literature (Wood Handbook 2010).

$$s_\theta = \frac{s_L s_T}{s_L \sin^n\theta + s_T \cos^n\theta} \quad (1.7)$$

1.2.2.4 Quadratic interaction criteria

In general, the quadratic failure criterion can be simply written in form of ellipsoid:

$$\left(\frac{\sigma_1}{s_L}\right)^2 + \left(\frac{\sigma_2}{s_T}\right)^2 + \left(\frac{\tau_{12}}{s_{LT}}\right)^2 = 1 \qquad (1.8)$$

The letters in denominator represent strength in orthotropic directions. Quadratic criterion is a modified version of Von Mises (Maximum distortional energy) criterion in which the effect of material anisotropy is considered. For three-dimensional space the Quadratic criteria(Hill,1948) is given by:

$$A(\sigma_2 - \sigma_3)^2 + B(\sigma_3 - \sigma_1)^2 + C(\sigma_1 - \sigma_2)^2 + 2D\tau^2{}_{23} + 2E\tau^2{}_{31} + 2F\tau^2{}_{12} = 1 \quad (1.9)$$

If the term in the left-hand side of equation 1.9 is equal or bigger than one, failure occurs. The value of A, B, C, D, E and F are parameters attained from experiment (i.e. uniaxial test, shear test) tests.

For 2D planar surface, the Quadratic criteria has been generalized and extended in form of Tsai- Hill criterion:

$$\frac{{\sigma_1}^2}{{s_L}^2} - \frac{\sigma_1\sigma_2}{{s_L}^2} + \frac{{\sigma_2}^2}{{s_T}^2} + \frac{{\tau_{12}}^2}{{s_{LT}}^2} = 1 \qquad (1.10)$$

Another quadratic interaction criterion is achieved if we normalize von Mises equation by relevant strengths:

$$\frac{{\sigma_1}^2}{{s_L}^2} - \frac{\sigma_1\sigma_2}{s_L s_T} + \frac{{\sigma_2}^2}{{s_T}^2} + 3\frac{{\tau_{12}}^2}{{s_{LT}}^2} = 1 \qquad (1.11)$$

The quadratic criteria couldn't account for differences between tensile and compressive strengths. Hence, the work was followed by (Tsai & Wu, 1971)and formed a general quadratic interaction criterion in which the given failure surface is in the form of tensor polynomial:

$F_i\sigma_i + F_{ij}\sigma_i\sigma_j = 1$ for i,j=1,2,…,6 (1.12)

F_i : First rank stress tensor

F_{ij}: Fourth rank stress tensor

Figure 1.3 shows a pictorial description of stresses and conventional stress signs in 3D space.

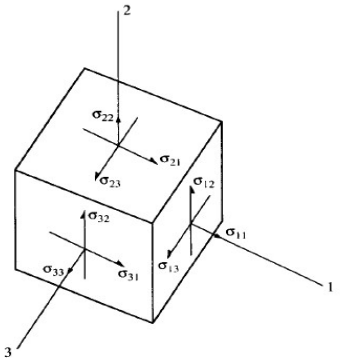

$$\sigma_{11} = \sigma_1 \qquad \epsilon_{11} = \epsilon_1$$
$$\sigma_{22} = \sigma_2 \qquad \epsilon_{22} = \epsilon_2$$
$$\sigma_{33} = \sigma_3 \qquad \epsilon_{33} = \epsilon_3$$
$$\sigma_{23} = \sigma_{32} = \sigma_4 \qquad 2\epsilon_{23} = 2\epsilon_{32} = \gamma_{23} = \gamma_{32} = \epsilon_4$$
$$\sigma_{13} = \sigma_{31} = \sigma_5 \qquad 2\epsilon_{13} = 2\epsilon_{31} = \gamma_{13} = \gamma_{31} = \epsilon_5$$
$$\sigma_{12} = \sigma_{21} = \sigma_6 \qquad 2\epsilon_{12} = 2\epsilon_{21} = \gamma_{12} = \gamma_{21} = \epsilon_6$$

Figure1.3: Stresses in 3D space(Gibson,1994)

Given that $\sigma_3 = \sigma_{33} = 0, \sigma_4 = \tau_{23} = 0,\ \sigma_5 = \tau_{31} = 0$ for plane stress, Tsai & Wu equation is reduced to :

$$F_{11}{\sigma_1}^2 + F_{22}{\sigma_2}^2 + F_{66}{\sigma_6}^2 + F_1\sigma_1 + F_2\sigma_2 + 2F_{12}\sigma_1\sigma_2 = 1 \quad (1.13)$$

F parameters are experimentally determined and can be expressed in terms of uniaxial and shear strength except for F_{12} that needs biaxial test to be determined.

Among all these criteria (Figure.1.4)Tsai-Wu is considered to be a reasonable tool to determine wood composite strength since it allows for considering material strength both

in compression and tension and also reflects interaction between stresses in either direction using term F_{12} in the equation .The only thing that should be carefully taken care of is to see how sensitive the specific material model is to interaction parameter F_{12} .According to (Clouston, Lam, & Barrett, 1998) F_{12} is strongly dependent on grain angle and performing sensitivity data analysis for Douglas Fir laminated veneer, they revealed that F_{12} is more stable for smaller grain angles.

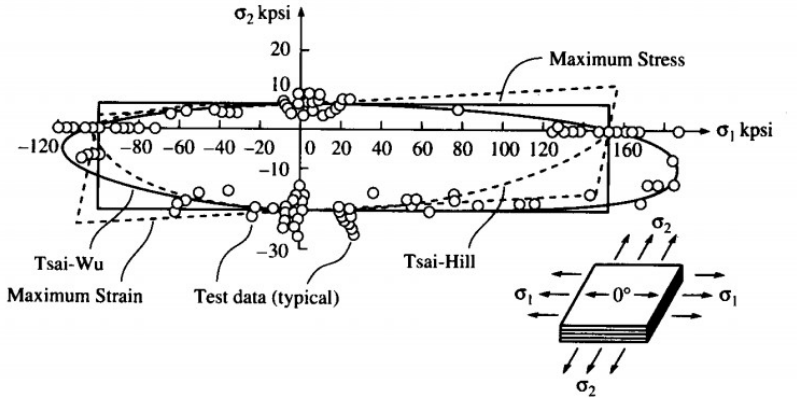

Figure1.4: Comparison of predicted failure surfaces for graphite/epoxy (Gibson,1994)

Tsai-Hill and Tsai-Wu theories are the quadratic polynomial failure criteria that are widely used. There are several theories, i.e., Hoffman theory, Norris theory (1950), Hill theory (1948) and Tan-cheng theory (1993) that are not discussed here.

1.2.3 Design and modeling of a bolted connection

1.2.3.1 Overview

Bolted joints are mostly used in laterally loaded applications connecting wood-wood, wood-metal and wood-concrete and they can have several shear planes.

The National Design Specification (NDS) for Wood Construction (AWC, 2015) employs a reference design value (Z) representing the basic capacity of a dowel fastener under short-term lateral load where the yielding of various elements in the connection contributes to failure. The analysis of a laterally loaded fastener is based on the yielding of various elements in the connections (i.e. Fastener diameter, dowel bearing length, fastener bending yield strength etc.).The Z term derives from the European Yield Model (EYM) originally proposed by Johansen (Johansen, 1949); and is widely used for design of laterally loaded fasteners. The EYM considers the connection geometry and wood/fastener material properties to evaluate strength, while assuming the wood to be a rigid plastic material (Figure 1.5).

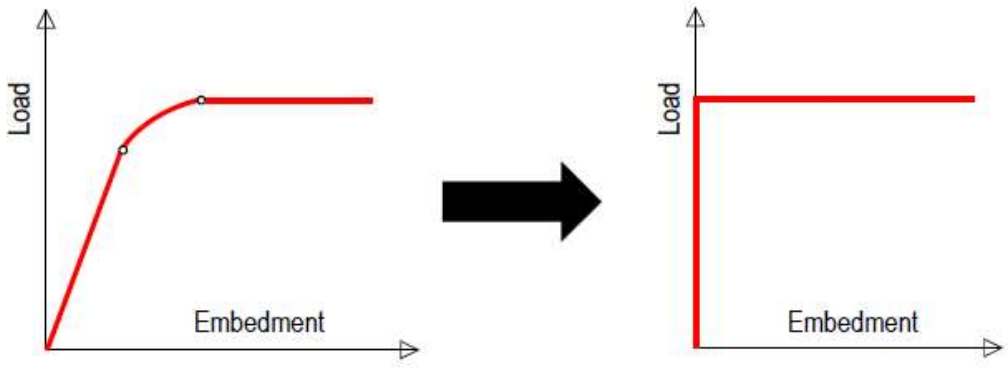

Figure1.5: Embedment load-slip curve a) Typical curve b) rigid-plastic material model (EYM)

According to Johansen's yield model (EN383), the embedment strength is expressed as the maximum applied load divided by the contact area (Eq. 1.8).

$$f_h = \frac{F_{max}}{t*d} \quad \left[\frac{N}{mm^2}\right] \tag{1.14}$$

Hilson (Larsen and whale) et al found that there is a linear relationship between $f_h$and density being used in Euro code 5 (BSI, 2009)

$$f_h = C_2(1 - 0.01d)\rho_k \quad (1.15)$$

ρ_k: Density at moisture content 12%

C_2: 0.082 for spruce (loaded parallel to the grain)

It is notable that as the hole diameter becomes larger, the embedment strength decreases due to increase in compressed area beneath the fastener. Fahlbusch (Jorrisen,1998) proposed formulation below to show how the diameter of the fastener affects embedment strength:

$$f_h = f_{h;10}\left(0.9 + \frac{1}{d}\right) \quad (1.16)$$

$f_{h;10}$: embedment strength for a fastener diameter of 10 mm

d: fastener diameter [mm]

However, Noren suggests a linear relation between diameter and embedment strength:

$$f_h = f_{h;10}\frac{166-d}{56} \quad \left[\frac{N}{mm^2}\right] \quad (1.17)$$

And finally, Euro code 5 (BSI, 2009) uses equation below to find embedment strength(Figure 1.6) :

$$f_h = f_{h;10}\frac{100-d}{90} \quad \left[\frac{N}{mm^2}\right] \quad (1.18)$$

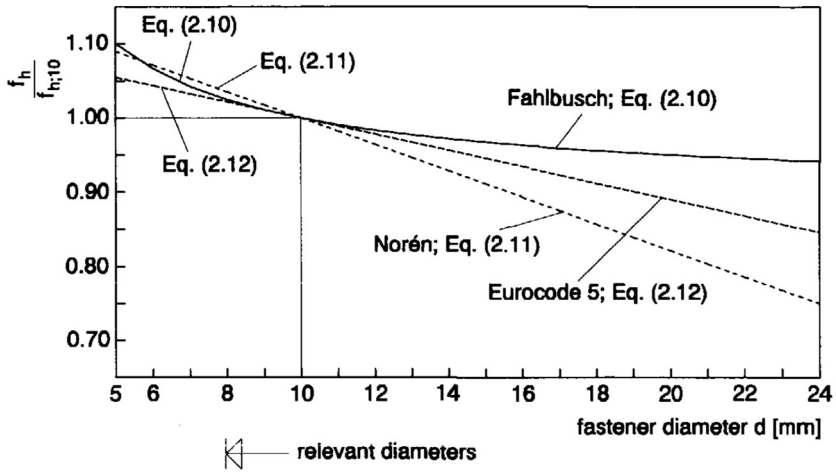

Figure1.6: The relation between embedment strength and fastener diameter (Jorrisen,1998)

According to NDS (NFPA, 1986) six failure modes can be considered in yield limit calculation based on whether crushing happened to the main member, the side member or to both; and also by considering the development of plastic hinge in the dowel. Figure 1.7 shows basic failure modes mentioned in NDS documents.

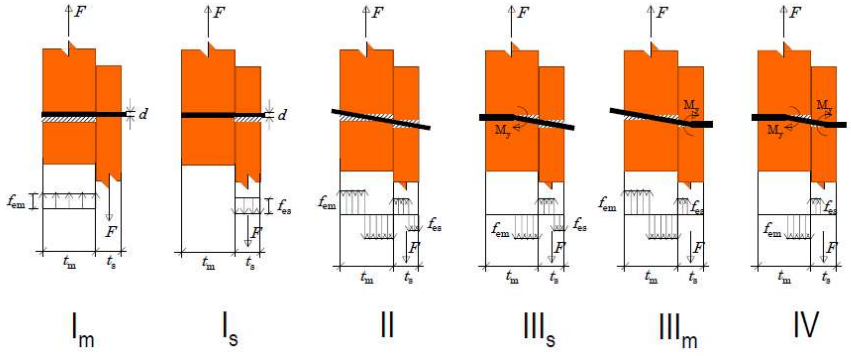

Figure1.7: Basic failure modes in NDS design handbook

For example, for ModeI_m , Z will be defined as follows:

Mode I_m(NDS Eq. 11.3-1)

$$Z = \frac{Dl_m F_{em}}{4K_\theta} \quad (1.19)$$

And for mode IV we have:

$$Z = \frac{D^2}{3.2K_\theta}\sqrt{\frac{2F_{em}F_{yb}}{3(1+R_e)}} \quad (1.20)$$

In which:

$$R_e = \frac{F_{em}}{F_{es}}$$

$$R_t = \frac{l_m}{l_s}$$

$$K_\theta = 1 + \frac{\theta}{360}$$

D: Fastener Diameter

l: Dowel bearing length

F_{yb}: fastener bending yield strength (F_{yb} can also be useful when material property for specific fastener is not available. It can predict the load capacity of mechanism and contributes to estimate the formation of plastic hinge).

F_{em}:Fe of metal in case of metal side plates

Fe: dowel bearing strength of wood member, (Varies with specific gravity , angle of load to grain ɵ, relative size of fastener)

1.2.3.2 Literature review on computational modeling of dowel joints

Based on the EYM, the embedment strength is most influential for a Mode I failure strength (Soltis, 1991), whereby wood crushing is the main mode of failure. Wood crushing failure occurs around the bolt hole due to high stress concentrations in this area (Oudjene & Khelifa, 2009). While the EYM estimates a design strength and corresponding failure

mechanism, it does not provide an understanding of the complex stress-state in the material beneath the contact surface. Because of the cellular and porous characteristics of wood (and presumably bamboo), the problem is geometrically and materially nonlinear and demands more investigation.

The most predominant failure modes of the wood in the connection were reported to be initiated by shear and tension perpendicular-to-grain stresses (Branco, Cruz, & Piazza, 2009). Shear pull-out (aka plug shear failure), which is caused by combined shear and tensile perpendicular-to-grain stresses along the outer edge of the dowel/wood contact zone, was noted as a related failure mode. In terms of loading direction, compressive loading in parallel-to-grain direction was reported to be the cause of brittle failure in wood connections (Kharouf, McClure, & Smith, 2003).

The embedment strength of a wood dowel connection depends on geometric parameters, such as hole diameter and hole end-distance, as well as material properties. Santos et al. (Santos, de Jesus, Morais, & Lousada, 2010) investigated the embedment strength of a dowel-type connection with maritime pine loading in the longitudinal and tangential directions. They did a comparison between different standard test methods and conducted research by presenting linear elastic finite element model of the two test methods, EN383 and ASTM D5764 one with complete and the other with the half-hole specimen as suggested in the relevant instruction. Shear splitting was observed in the longitudinal-tangential plane when loading parallel to the grain, while low tension strength seems to be responsible for failure when loading perpendicular to the grain direction. They also found a positive relation between embedment strength and density for ASTM D5764 standard method. It is noteworthy that according to their outcomes, in ASTM method bolt

has less tendency to bend and resulted strength is clearly higher than EN 383 for the radial compression test.

Bamboo products are sometimes assumed to behave like hardwood material (Dixon and Gibson,2014). While many studies and formulations involving bearing strength are derived from softwood species, a handful of studies have focused on hardwood. For example, a 2007 study was conducted on the tropical hardwood Shorea obtusa (Awaludin, Smittakorn, Hirai, & Hayashikawa, 2007) to find dowel bearing properties for several test configurations, and the results were compared with formulations from NDS and Euro code 5 standards. The authors found that the estimated bearing strengths using equations from the NDS were higher than that of their experiments and other empirical equations. Moreover, no previous studies nor standards on loading perpendicular to the grain were capable of properly predicting failure testifying to the fact that more research is needed in this area.

Using elasto-plastic material model, obtained load-displacement curves become closer to experimental results as a result of nonlinear assumptions in the model according to Oudjene et al. (Oudjene & Khelifa, 2009).Using anisotropic elasto-plastic constitutive law in compression for spruce , the model shows much higher ability to predict connection behavior rather than using linear elastic orthotropic material model (Oudjene & Khelifa, 2009) . Their Finite Element model coupled anisotropic plasticity with ductile densification, which led to a better description of wood nonlinearity in compression. For loading parallel to grain, this model shows high accuracy to capture the nonlinear behavior of the joint whereas in the perpendicular direction fails to predict the joint failure properly.

Patton-Mallory et al. (Patton-Mallory, Cramer, Smith, & Pelican, 1997) focused on bolted connections loaded parallel-to-grain. The author used a trilinear stress-strain relationship to predict the strength behavior of the bolted connections. When loaded parallel-to-grain, the prediction of the connection failure showed good conformity with experimental results for loading up to 0.762 mm displacement. However, it was noted that the model was not sensitive to small changes in material properties and thus, shows the same failure mode prediction. He (Patton-Mallory, Pelicane & Smith,1998) also evaluated the effect of end distance (e/d) and aspect ratio (L/d) on strength and failure behavior of connection when loaded parallel to the grain. Using Tsai-Wu criteria failure theory Patton Mallory predicted stress distribution and failure modes of a single bolted connection by implementing a 3d FE model.

Using digital image correlation method, Stelmokas et al (Stelmokas, Zink, Loferski, & Dolan, 1997) measured the load distribution of wood connections as a group with different patterns parallel to the grain. They examined which bolt carries the major load in the group and the way the load transmitted among the bolts.

Applying theory of plasticity to wood , Kharouf (Kharouf, McClure, & Smith, 2003) modeled glued-laminated timber with two regimes: a) elasto-plastic orthotropic in regions of bi-axial compression considering Hill criteria as a yield function b) linear elastic orthotropic for other regions considering maximum stress/strength as the failure criteria. Based on this model, they implemented a code in ADINA software to run the analysis of bolted connections. Using this material model, an improved model was achieved which is more consistent than assuming wood as a linear elastic orthotropic material.

A few studies have been published on failure analysis of bamboo-laminated products. Yang et al. (Yang, Lam, & XIao, 2014) performed failure analysis of Glubam, an engineered bamboo material that is assumed bidirectional in terms of fiber direction. The authors revised the Hankinson formula to explain the material behavior at different fiber angles based on an off-axis tension test. Further, they worked on finding Tsai-Wu parameters, specifically, the interaction parameter F_{12} at an angle of 15 degrees. Based on the experimental data, the Tsai-Wu failure criterion was unable to explain the failure behavior of Glubam.

Work was done by Ramirez et al. (Ramirez, Correal, Yamin, Atoche, & Piscal, 2012) on laminated Guadua bamboo dowel joints to experimentally determine the effect of different hole diameters and different loading directions on bearing strength. The author found a meaningful relation between bearing strength and fastener geometry, including diameter and width-to-diameter ratio. They also developed an FE model based on their experimental results and determined an experimental formula to explain the local behavior of the loading zone around the bolt hole as a function of bulk material properties. However, in the FEM results failure mechanism and failure mode were not discussed.

Recent work by Reynolds et al. (Reynolds, Sharma, Harries, & Ramage, 2016) revealed a meaningful difference in failure mechanism between Moso bamboo dowel joints and timber dowel joints. Based on digital imaging experiments and full-field strain measurements, it was deduced that high shear stresses around the bolt hole are responsible for bamboo dowel failure, while failure in timber joint is attributed to tensile strain perpendicular to the grain. The authors used a numerical model based on the Lekhnitskii stress function (Lekhnit͡skiĭ, 1968) and explained that the different failure behaviors of

laminated bamboo products are due to coefficient of friction and orthotropic material property differences between timber and engineered bamboo.

1.2.4 Contact mechanics and contact stresses in dowel joints

As the dowel joint is loaded gradually, the contact area (boundary condition) between a bolt and a hole changes at the end of each load increment (Figure 1.8). This leads to a nonlinear boundary value problem which should be solved in the contact mechanics framework. The classical analytical approach -in linear elastic context - was introduced by Hertz (1882) in which it was assumed that the contact surfaces are continuous and strains are small (Frastia 2006). However, with a fast growing rate of computing methods in FEM software, numerical methods using discretization techniques have added value to the robustness of contact solutions. Finite element software are able to solve contact problems with complicated geometry and material properties. However, relying on the computational solution is still challenging (Wiggers, 2006)and the experiments still needed to confirm the results.

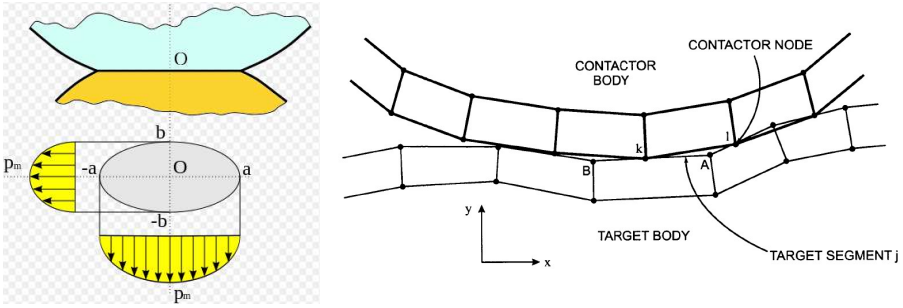

Figure1.8: Contact pressure and varying contact area between two bodies(ADINA,2012)

To conduct preliminary study on an LVB dowel connection (presented in chapter three) ADINA software was used to model a two-dimensional joint followed later by a three-dimensional ANSYS model described in chapters four and five.

Some basic definitions of contact algorithms are as follows (ADINA, 2012):

1.2.4.1 Normal contact formulation

The term normal contact (Figure 1.9) is used when a contact surface is treated as a unilateral constrained problem. It has been used as a classical strategy to formulate contact in the literature (Johnson, 1985 or Kikuchi and Oden 1988). Basically, in a normal contact condition, we assume a constraint for non-penetration state that can be expressed as:

$$g \geq 0 \quad ; \quad \lambda \geq 0 \quad ; \quad g\lambda = 0 \qquad (1.21)$$

Where g is a gap, and λ is the normal contact force. Contact occurs when $g\lambda$ equals to zero.

Different algorithms exist to impose contact condition. However, two basic methods can be used to enforce constraints for bodies in contact: Lagrange multiplier method and penalty method.

Let's assume that a point mass is touching the rigid surface (Figure 1.9). For simulating contact between two bodies, condition below must be met:

$$C(u)=h-u\geq 0 \qquad (1.22)$$

$C(u)> 0$: gap exists,

$C(u)=0$: contact occurs

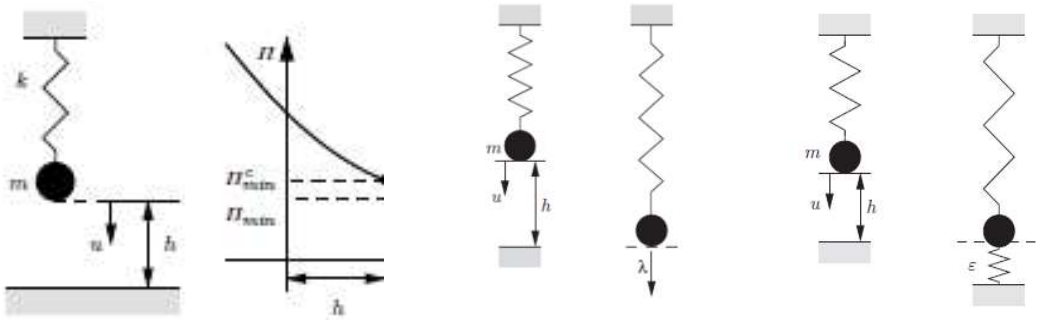

a) b) c)

Figure1.9: Normal contact condition simulated with point mass and spring a) Lagrange multiplier method b) penalty method (Wiggers,2006)

Based on variational formulation of structural model (Wiggers, 2006) , the energy for spring mass can be written as:

$$\Pi(u) = \frac{1}{2}ku^2 - mgu \qquad (1.23)$$

Without imposing restrictions, the extremums will be derived from equation below:

$$\delta\Pi \prod(u) = \frac{1}{2}ku\delta u - mg\delta u = 0 \qquad (1.24)$$

Lagrange method imposes constraint to the system by adding an independent term including Lagrange multiplier (λ) to the energy of the system which fulfils constraint equation properly.

$$\Pi(u,\lambda) = \frac{1}{2}ku^2 - mgu + \lambda c(u) \qquad (1.25)$$

We often use the penalty method for applying the penalty term to the energy of the system as an active constraint in an approximate manner. Figure 1.9.c shows the application of penalty term as an added spring between point mass and contact surface.

Hence, there would be no additional variable in the energy equation. However, it is sensitive to the choice of the penalty factor.

$$\Pi(u) = \frac{1}{2}ku^2 - mgu + \frac{1}{2}\epsilon[c(u)]^2 \ \ with\ \epsilon > 0 \qquad (1.26)$$

A combination of the penalty and the Lagrange multiplier methods leads to the Augmented Lagrangian method. The Augmented Lagrangian method has been proposed as a procedure to partially overcome the two preceding methods' difficulties. The augmented lagrangian method removes the requirement that the penalty factor be large.

In both ANSYS and ADINA software Penalty, Lagrange and Augmented Lagrange methods are available/There are some other algorithms that use special techniques to enforce contact constraints (i.e. barrier method, mortar method, NITSCHE method) (Wiggers, 2006) .However, in this dissertation, only algorithms implemented in ADINA (and ANSYS) software are discussed.

Based on descriptions of Lagrange and Penalty method, two approaches are available in ADINA as a finite element general purpose algorithms for solving contact problems:

- Constraint-function method
- Segment (Lagrange multiplier) method

1.2.4.2 The Constraint-function method (node to segment contact algorithm)

Bathe (1996) proposed a function of g and λ named ω(g , λ) to apply a constraint to the system so that it satisfies contact condition ω(g , λ)=0 according to equation 2.20 .The constrained-function method can be applied by using either Lagrange multiplier method or Penalty method. The variable λ (Normal contact force) can be considered as

Lagrange multiplier (Bathe, 1996).This method is suggested by Bathe (Bathe, 1996)so it can improve convergence solution of full newton method by applying appropriate constrained function. Here is the function suggested in ADINA (Bathe, 1996)

$$\omega(g,\lambda) = \frac{g+\lambda}{2} - \sqrt{(\frac{g-\lambda}{2})^2 + \epsilon_n} \quad and\ \epsilon_n \ll 1 \tag{1.27}$$

However, this algorithm is sensitive to large incremental time steps and it may lead to convergence difficulties (Bathe, 1996)

1.2.4.3 The Segment (Lagrange multiplier) method

For segment method (Figure 1.10), Lagrange multipliers are used to enforce condition as mentioned above. The contact surfaces are discretized by two/three-node linear segments. If both nodes of a segment are in contact with the target surface, the contactor segment is defined to be in contact. The number of Lagrange multiplier equations due to contact is dynamically adjusted in each iteration based on frictional condition of the contact segments: If the node is in sticking contact, there are two equations for the node and if the node is in sliding contact, there is only one equation for the node.

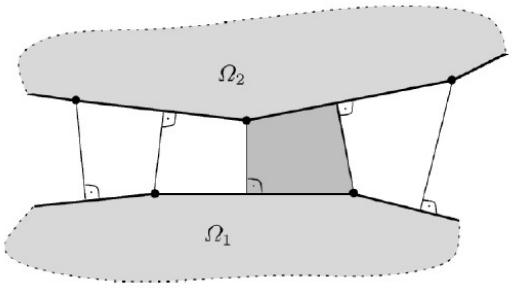

Figure1.10: Segment method: contact surface discretization (ADINA,2012)

However, to achieve a more accurate result, it is recommended to try the constraint-function method first((ADINA theory and modeling guide,2012). Alternatively, in ANSYS software, augmented Lagrangian method is the default and is the most-commonly used option.

1.3 Objectives and scope

In wood dowel connections, different stresses and stress combinations often lead to some level of wood failure. The most influential stresses are longitudinal shear and tension perpendicular-to-grain. In previous studies in dowel connections, the major emphasis is placed on softwood species and there are only a limited number of studies available on engineered bamboo connections. Moreover, these few studies only partially explain the failure behavior of dowel connections; and thus, a need for more rigorous study remains in order to clarify the modes responsible for mechanism failure.

The focus of this dissertation is to describe the behavior of Moso (*Phyllostachys heterocycla var. pubescens*) LVB dowel connections under compressive loading using conventional failure criteria assuming LVB as elastic-plastic orthotropic material. The aim

is to understand how LVB dowel connection behavior differs from that of timber, so we can use this understanding for designing codes and developing standards.

One primary objective is to numerically and experimentally investigate application of two different specimen types (full-hole versus half-hole) suggested by ASTM standard method for testing dowel bearing strength and to determine which method best describes LVB connections. A second objective is to numerically and experimentally investigate loading at different angles to the grain to propose a model that can predict LVB dowel connection for safe connection design.

CHAPTER 2

MODELING LVB DOWEL BEHAVIOR

2.1 Introduction

The most predominant failure modes of wood in the dowel connection is initiated by shear and tension perpendicular-to-grain stresses. Chapter Three aims to progress from this body of knowledge by examining a simple LVB dowel connection through experimental testing followed by computational modeling of the connection. The objective of this chapter is thus to elucidate LVB dowel failure mechanisms in compression loading parallel to grain through interactive stress analysis and to further understand LVB dowel connection behavior for design and evaluating codes and standards.

It is noted that the content of this Chapter has already been published as follows:

Khoshbakht, N, Clouston, P. L, Arwade, S. R., & Schreyer, A. C. (2017). Computational modeling of laminated veneer bamboo dowel connections. Journal of Materials in Civil Engineering, 30(2), 04017285.

2.2 Experimental program

2.2.1 LVB material property tests

The material properties of LVB: shear, tension/compression strengths parallel-to- and perpendicular-to-grain, were experimentally determined and applied as input parameters for subsequent FEM studies of the dowel joints. In the experimental tests, commercially

available LVB boards were used made from Moso bamboo (*Phyllostachys heterocycla var. pubescens*). The LVB was purchased from Lamboo company and consists of 1/4" x 3/4" bamboo culm slats that are bonded together with ANSI/HPVA type 1 adhesive.

The boards were conditioned for a minimum of 2 months in constant ambient environmental conditions. The mean moisture content of the samples was 5.4% (C.V. 5%) as measured by the oven dry method (ASTM D2016).

2.2.1.1 Compression tests

To evaluate compression strength and elastic properties, ten specimens (calculated based on ASTM D2915 with a confidence level of 99%) were machined from 3000 mm × 150 mm × 35 mm LVB boards for each sample. For parallel-to-grain loading direction, specimen dimensions were 25 mm × 25 mm × 100 mm, while 50 mm × 50 mm × 150 mm specimens (ASTM D143, 2009) were used for perpendicular-to-grain direction.

Loading was applied continuously at a rate of 0.012 in. (0.305 mm/min) using a 150 kN Material Testing System (MTS) machine. The displacement was measured using a uniaxial extensometer (MTS634.11F-24) for the parallel-to-grain compression test (Figure2. 1) and a Linear Variable Displacement Transducer (LVDT) for the perpendicular-to-grain test (Figure2.2).

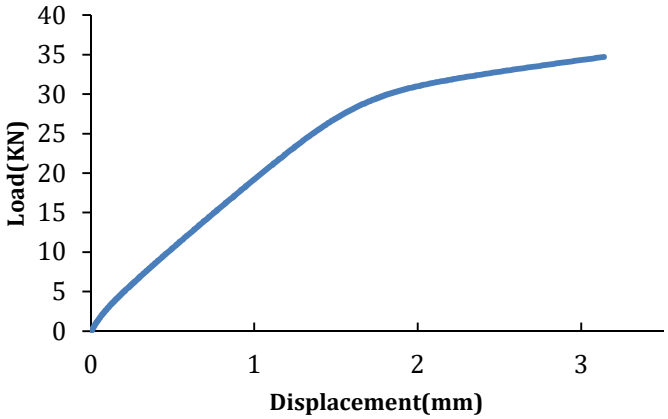

(a) (b)

Figure 2.1: a) Compression test setup parallel-to-grain; b) typical load-displacement curve

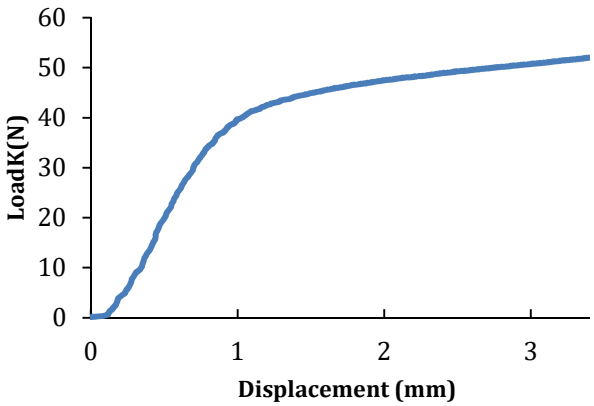

(a) (b)

Figure 2.2: a) Compression test set up for perpendicular-to-grain direction; b) typical load-displacement curve

2.2.1.2 Tension tests

Samples were prepared in accordance with ASTM D3500 for small tension specimens of structural panels. The samples were cut from 300 mm × 150 mm × 35 mm LVB boards with a CNC machine to ensure that the exact profile and dimensions were achieved. Tension loading was applied according to ASTM D3500 so that the failure occurred within 3-10 minutes (Figure2. 3b). Ten specimens were tested, and Table 2.1 displays the material property values with corresponding loading direction. The load-displacement curve in

Figure2.3c confirms the expectation that LVB in tension follows a linear, brittle failure behavior.

Table 2. 1:Material properties of Moso Laminated Veneer Bamboo

		Compression		Tension		Shear
Loading Direction	**Density Kg/m^3**	**MOE (MPa)**	**Strength (MPa)**	**MOE (MPa)**	**Strength (MPa)**	**Strength (MPa)**
Parallel	650	11600	62	9219	95	13.15
C.V.		7%	3.2%	15%	12%	11%
Perpendicular	650	1440	28	200	5.43	-
C.V.		30%	11%	9%	22%	

The tension test for the perpendicular-to-grain direction was performed on ten specimens in accordance with ASTM D143 at the same loading speed (0.305 mm/min) (Figure2. 4). The results are provided in Table 2.1.

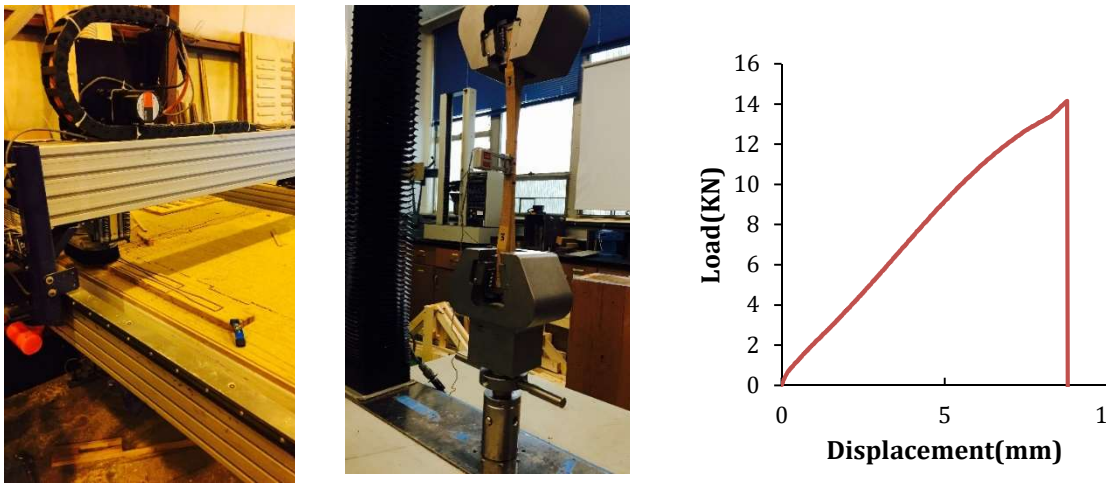

(a) (b) (c)

Figure2.3: Tension test: a) fabrication, b) test setup, c) typical load-displacement curve

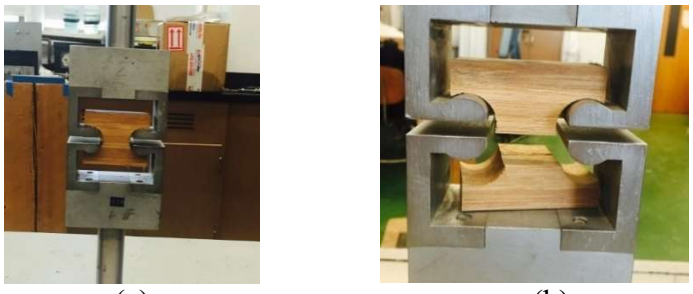

(a) (b)

Figure2.4: Tension test: a) setup perpendicular-to-grain; b) failure due to loading perpendicular-to-grain

2.2.1.3 Shear tests

The shear test was performed according to ASTM D143 and at a loading rate of 0.6 mm/min. Figure2. 5 shows the test equipment and the shear block subjected to continuous loading. According to the standards, the shear area was 2 in. × 2 in. and the average shear strength was found to be 13.15 Mpa. No glue failure was observed in the sample.

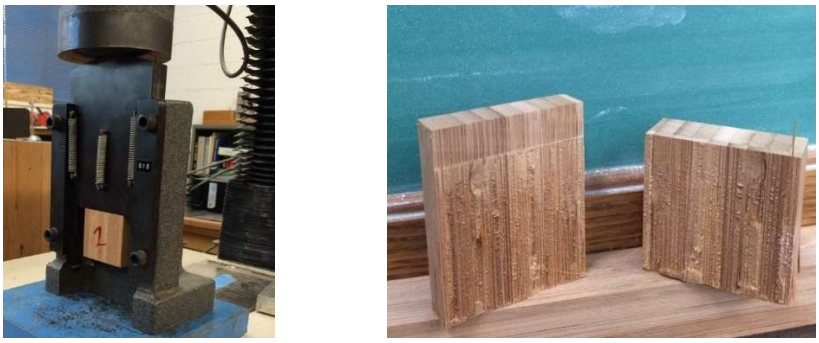

(a) (b)

Figure2.5: Shear test: a) test setup; b) specimen shear failure surface

2.2.2 LVB embedment test set setup

The material preparation and test procedure for evaluation of embedment properties followed ASTM D5764 for a single dowel joint using wood-based products (Figure2. 6). The sample consisted of 15 replications as determined by ASTM D2915. An MTS3000 testing machine was utilized in combination with an LVDT and extensometer to measure displacement both at the contact surface and beneath the contact area of a single dowel joint.

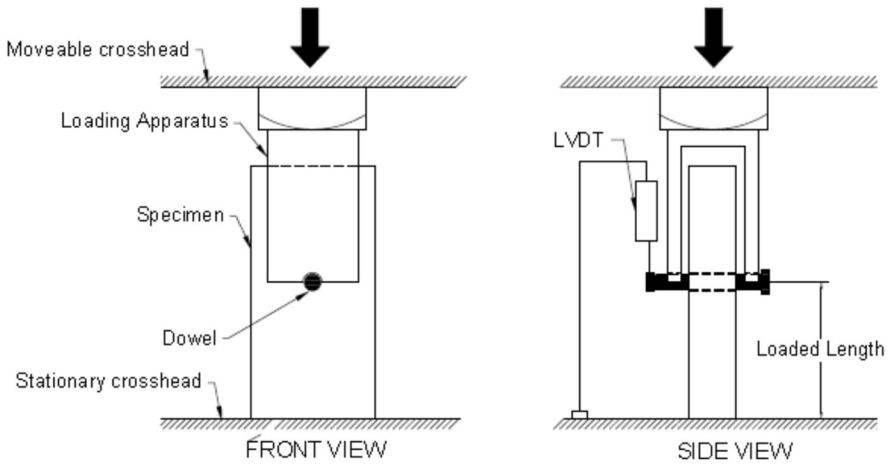

Figure2.6: Embedment test setup based on ASTMD5764

ASTM D5764 guidelines recommend using full-hole specimens instead of half-hole specimens for specimens that tend to split before the completion of the test. Therefore, to provide a more realistic measurement of dowel joint behavior, we decided to use full-hole specimens.

The LVB specimens measured 152x63x32 mm^3. The hole was bored with a 17.5mm ($11/16^{th}$ inch) diameter drill bit to accommodate a 15.9mm ($5/8^{th}$ inch) diameter steel (grade5.5) bolt. The steel loading apparatus was fabricated to ensure application of the load onto the wood contact surface was imparted directly through the smooth surface of the steel bolt. A crosshead rate of 1 mm/min produced failure within 1-10 minutes. Displacement directly beneath the contact zone was obtained by means of an LVDT (Figure2. 7). An MTS634.11F-24 extensometer was also employed to observe the material strain at a 25 mm distance beneath the mid-point of the contact surface.

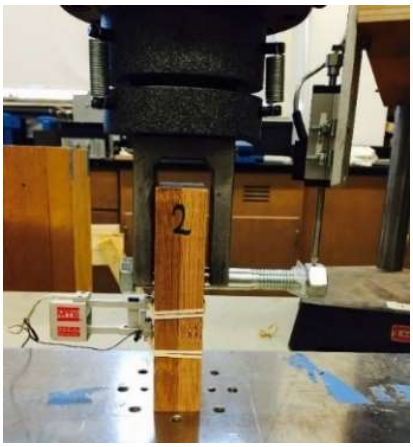

Figure2.7: Embedment test setup: displacement was measured in contact zone (LVDT) and beneath the contact zone (Extensometer)

2.2.3 Test results

Table 2.2 shows the stiffness values (N/mm) at the contact surface and beneath the contact surface (extensometer zone). The results indicate that the material stiffness at the contact surface is 10.6 times less than the stiffness measured in the extensometer zone. In view of this result, two definitions for material elasticity is employed for the subsequent stress analysis in this paper: bulk modulus of elasticity and local modulus of elasticity at the contact surface.

Table 2. 2:Stiffness measured at contact surface and beneath the contact surface

	Stiffness in extensometer zone (N/mm)	Stiffness at contact surface (N/mm)	Embedment strength Parallel-to-grain (MPa)
Mean	343600	32400	49
C.V.	14.4%	5.6%	8%

Figure2. 8 displays a failure pattern of the dowel joint after loaded parallel-to-grain until it reached its maximum strength within 0.9-1.2 mm LVDT displacement. In 80% of the specimens, the crack started and continued to grow at between 4 to 4.7 mm off-center (ie. $1/6^{th}$ of the hole perimeter left or right of center) beneath the loaded area. Another split occurs on the top of the bolt hole during the last stage of loading as a result of plane

separation in the bottom section. It is important to note that no glue failure was observed. These tests suggest that a combination of tension perpendicular to grain and shear stresses on the specimen is responsible for failure.

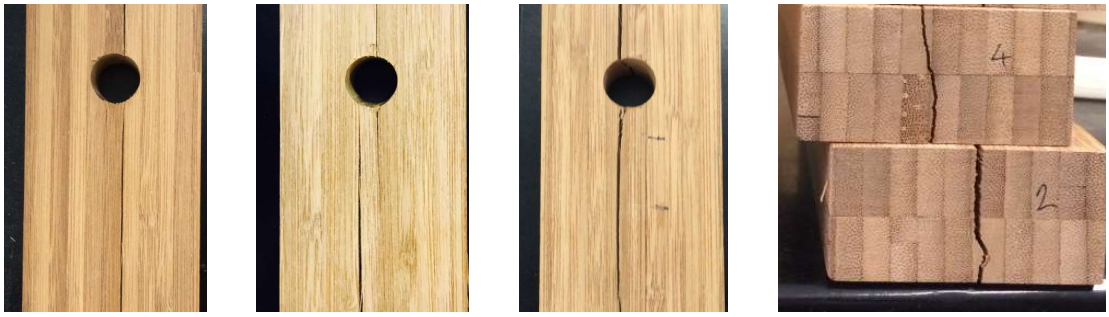

Figure2.8: Splitting failure in LVB dowel joint when loaded parallel-to-grain

2.3 Finite Element Model and Analysis

In order to investigate the stress distribution at and beneath the contact surface, a 2D plane strain F.E. model was developed using ©ADINA 9.2 software. The model geometry was the same as the experimental full-hole test setup described in ASTM D5764. Fixed displacement was assumed at all bottom nodes and compressive load was applied to the bolt in the form of displacement. The effect of a $1/16^{th}$ inch larger bolt hole to bolt diameter (tolerance per NDS) was also considered in the model.

A contact surface was defined between the steel bolt and the LVB hole. The bolt was assumed to be a rigid body under a condition that is called a rigid-target contact problem often used for cases when the two bodies have substantially different material stiffness (e.g. $E_1 = 10^{10} E_2$) (Frastia, 2007). According to Kim(2015), the stiffness matrix becomes ill-conditioned when the stiffer body of the two is not assumed rigid, which leads to uncertainty in the accuracy of the solution.

Incremental loading steps of a 0.001 mm displacement was applied, to start, by controlling the time function value. After validation of the results, the applied displacement was increased to 1 mm by changing the time points gradually until the LVB dowel joint reached its maximum strength according to the load-displacement curve.

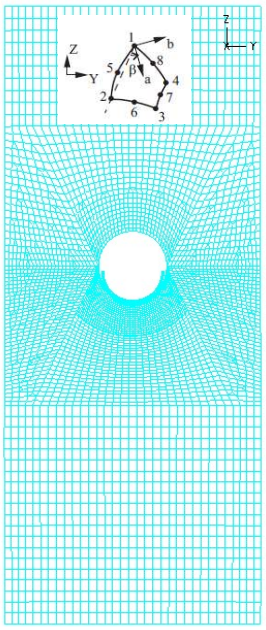

Figure2.9: FEM element local and global coordinates and mesh

2.3.1 Material property assumptions

The Moso LVB was modeled as linear elastic, orthotropic material with constitutive properties from Table 2.1. Values for the less influential parameters, Poisson ratio and shear modulus, were selected from the literature: the former value being between 0.22-0.25 as noted by Yu et al. (2011) and the latter value being 745 MPa as reported for Moso bamboo (Askarinejad et al. 2015).

The material axes directions were modeled to coincide with the global axes directions (ADINA Primer, 2014). To ensure that the stiffness and compliance matrices were positive

definite, in order to reach a solution, the material property input values complied with ADINA nomenclature for Poisson ratio per Equation 2 (ADINA, 2012), which differs from the general notation(Jones,1999) of Poisson's ratio (Equation 2.2).

$$\frac{\vartheta_{ij}}{E_j} = \frac{\vartheta_{ji}}{E_i} \qquad \text{i,j = a,b,c} \qquad (2.1)$$

$$\vartheta_{ij(ADINA)} = (\frac{E_j}{E_i})\vartheta_{ij(Jones)} \qquad \text{i,j = a,b,c} \qquad (2.2)$$

2.3.2 Element selection

A 2D plane strain model was developed with both eight-node and nine-node quadrilateral elements (Q8 and Q9). Mesh refinement was performed in the area of interest around the bolt hole. Both Q8 and Q9 elements converged to the same solution results. Based on this convergence study, Q9 with side lengths of 0.5 mm at the area of interest was chosen.

2.3.3 Model calibration

It was found that several important parameters affect the FE model contact behavior. They are explained in detail below:

-Contact stiffness: This value is defined as a penalty parameter that is based on the material stiffness and contact element size. A larger value allows for less penetration but it may lead to difficulties in convergence. In ADINA, contact stiffness is defined by a scale factor known as the compliance factor, which is usually assumed as a value of 0.001. The ADINA software manual suggests a penetration value in the order of 1% of the element

size (ADINA, 2012). Thus, the compliance factor is chosen so that it allows appropriate penetration.

-Mesh at contact area: The relative mesh size of the contact/target surface was selected to avoid penetration of the contact body into the target body (Kim, 2015) by making certain that the target body had a coarser mesh than the contact surface (Figure2. 10-a). Usually, the flat or stiffer body is selected as the target to decrease penetration and minimize numerical error.

Moreover, the element size should be tested in the most probable contact zone so that the normal of the contact and target surfaces interact properly with each other. Because of the C0 continuity across the contact boundary, the contact force is very sensitive to mesh discretization. It was found that the results change abruptly with mesh refinement so careful consideration should be placed on mesh refinement at the contact boundary.

-Contact tolerance: This value is the minimum distance that the program searches for contact and calculates contact force with lower computer cost. The contact tolerance is usually 1% of the contact element length (Kim, 2015). It is important because choosing proper contact tolerance, together with proper load increment, leads to converged and more accurate results.

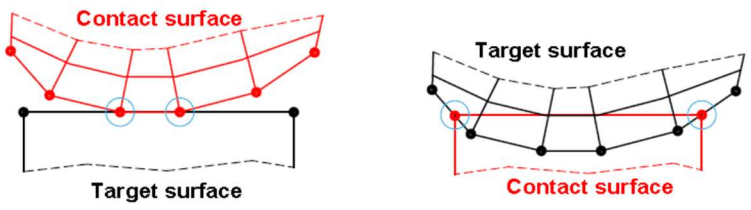

(a) (b)

Figure2.10: Contact area mesh model effect on penetration: a) target surface with coarser mesh; b) contact body with coarser mesh

In both Lagrange multiplier and penalty methods, the contact is treated as a constraint (Kim, 2015) in the structural equilibrium, which is why the contact formulation is independent of the material constitutive models.

By considering all of the above, the model was calibrated to experimental results by using different combinations of mesh size, contact stiffness, load increments, and contact tolerance. Table 2.3 presents the FE model stiffness results assuming value 0.2 for coefficient of friction between LVB and steel dowel (Reynolds et al. 2016). Ideally, the displacement in the contact zone (U_Z) should be equal to the applied displacement on the rigid bolt, which should lead to zero penetration; however, in practice, for choosing a realistic model there should be a compromise between penetration and contact stiffness. Accordingly, the optimal FE model (No. 4) was chosen based on Table 2.3, which has a reasonable U_Z and the closest stiffness to that of the experimental results. The value for K from the FE model No. 4 is 34240 N/mm, which is the closest to the K mean value (32400 N/mm, C.V. 5%) from the embedment tests.

Table 2.3:FEM calibration in compressive loading parallel to the grain

Model:			**Results:**				
FEM Model	**Mesh size (mm)**	**Compliance factor**	**Displacement (mm)**	**U_Z (mm)**	**Contact force on contact line, F_Z (N/mm)**	**Contact pressure (MPa)**	**Contact stiffness, K (N/mm)**
1	0.5	0.0001	1	0.96	1257	37760	37760
2	0.5	0.0002	1	0.93	1140	36480	36480
3	0.5	0.0003	1	0.9	1170	35200	35200
4	0.5	0.0004	1	0.87	1070	34240	34240

2.3.4 Local Elastic Moduli Evaluation

The localized moduli of elasticity (E_L) (as opposed to the bulk modulus of elasticity (E_B)) is necessary as input to the FE model. Two distinct values for $E_L$were considered: parallel-to-grain and perpendicular-to-grain to account for the significant orthotropicity of the material (i.e. E parallel >> E perpendicular). Also, the splitting failure in LVB is due in large part to tensile stresses perpendicular-to-grain and the respective E values play an important role in the accuracy of the model.

The local elastic modulus (E_L) parallel-to-grain was determined following an empirical approach. The method is based on embedment test data and Equation (2.3), derived from Hooke's law, where K is the mean slope of the linear portion of the load-displacement curves slope of the embedment test.

$$E_L = K * \frac{L}{A} \qquad (2.3)$$

K: slope (N/mm)

A: bolt projected area (mm^2)

L: Bearing zone depth (mm)

According to Hong et al. (2011) the most important parameter that affects the bearing zone depth, L, is the dowel geometry. The depth of bearing zone for their calculations was assumed to be equal to the dowel diameter, D. Later, Ramirez et al. (2012) based on experimenting varying dowel diameters in their FEM model for Guadua bamboo, suggested the simple equality that L=1.6D. Following the same path, according to the present FEM model, the bearing zone depth was found to be 1.4D for Moso LVB.

Based on calculated bearing depth, the E_L parallel-to-grain value used in the stress analysis was considered to be 1007 MPa (C.V.15%) from Equation (2.3).

The local elastic modulus (E_L) perpendicular-to-grain was calculated from the tension perpendicular-to-grain test data where K was found from the mean slope of the linear portion of the load-displacement curves. The E_L perpendicular-to-grain mean value used in the stress analysis was calculated to be 200 MPa. The results are summarized in Table 2.4.

Table 2.4:Finding local modulus of elasticity based on embedment and tension test results

Test	Sample size	Failure Load (N)	Failure Displacement (mm)	Local Modulus of elasticity (MPa)
Parallel-to-grain (Embedment Test)	15			
Mean value		28197	1.18	1007
C.V.		8%	15%	15%
Perpendicular-to-grain (Tension Test)	10			
Mean value		4450	0.55	200
C.V.		22%	19%	9%

2.4 Results and discussion

The calibrated FE model was employed to examine the stress state of Moso LVB in the zone under the dowel; the purpose being to gain insight into the progressive nature and exact cause of failure. The investigation focused on the progression of key individual stresses as displacement was increased to near failure. 1mm was the upper limit chosen as the experimental embedment tests indicated that failure occurred, on average, at 1.18mm (C.V. 15%).

Figure2. 11 illustrates the magnitude of compressive stress in the Z (parallel-to-grain) direction as it decreases with vertical distance from center point of hole at three stages of incremental displacement: 0.1mm, 0.5mm, and 1mm. For this stress, the stress-distance curve for each load increment follows a similar trend; this is not so for other stresses, as will be shown. At 1mm displacement, the maximum elemental stress in the Z direction is less than mean strength per Table 2.1 (56 MPa < 62MPa), suggesting that, while certainly an influence on incipient failure in that zone, σ_{zz} is not the primary cause.

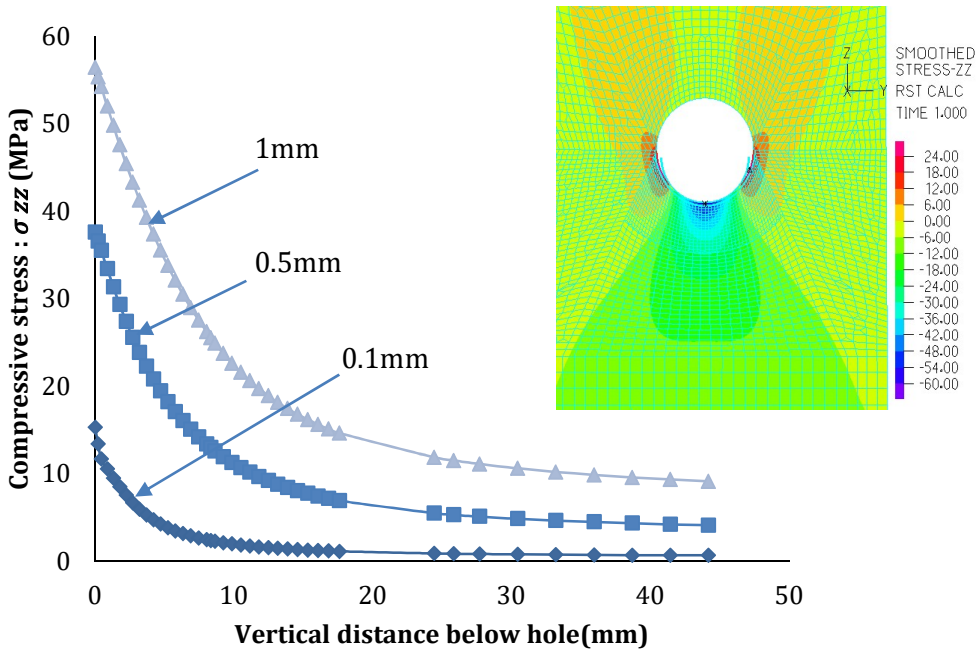

Figure2.11: Parallel-to-grain compressive stress distribution below hole for three displacements

Figure2. 12 and Figure2.13 depict stress contours around the bolt hole at high levels of load for tensile stress perpendicular-to-grain (σ_{yy}) and in-plane shear stress (σ_{yz}), respectively. Notably, the stress levels shown exceed strength values given in Table 2.1 for both stresses indicating that failure (at least at the elemental level) has already occurred. The location of highest stress for both stresses match closely with the visual results for splitting failure that were observed in the experimental tests except for the contact edges

of steel bolt and LVB material. In Figure2.13, the model predicted that the dowel joint begins to fail at approximately 0.95 mm of applied displacement, 18% off from the experimental mean value (1.18 mm).

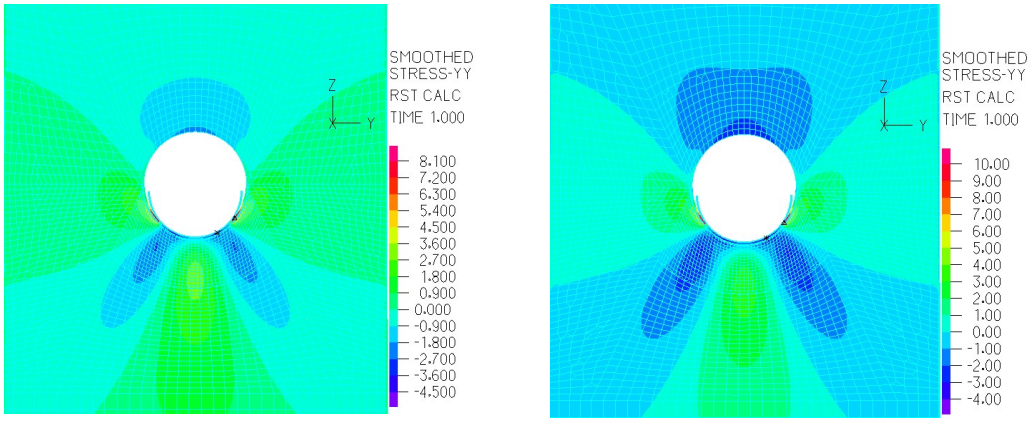

(a) (b)

Figure2.12: Perpendicular-to-grain tensile stress contours with a) 0.8 mm displacement and b) 1 mm displacement

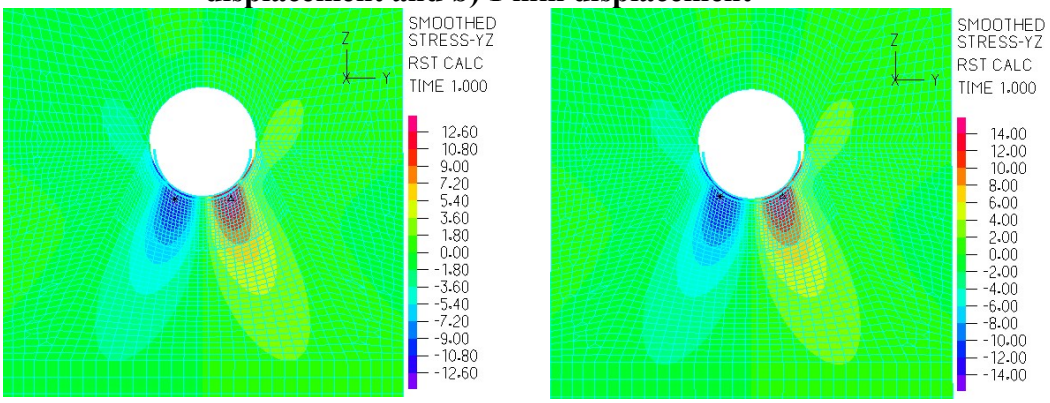

(a) (b)

Figure2.13: In-plane shear stress contours with a) 0.8 mm displacement and b) 0.95 mm displacement

Figure2. 14 and Figure2.15 illustrate how tensile stress perpendicular-to-grain varies with vertical and horizontal distance from center point of hole at four stages of incremental displacement. According to the data points selected in the vertical distance from the contact surface in Figure2.14, the maximum tensile stress occurs at 7.4 mm underneath the contact surface. Figure2. 14 indicates that as the loading increases, the stress distribution changes

because of the change in the contact surface area. Also, as the loading increases, the contact surface enters the stage of slip contact (Figure2. 16). The maximum tensile stress is 3.6 MPa at 1 mm displacement (roughly failure), which is slightly less than 5.4 MPa (experimental LVB strength in Table 2.1). However, the coefficient of variation for strength from the embedment test results (22%) would suggest that tension stress perpendicular-to-grain clearly also contributes to the cause of failure.

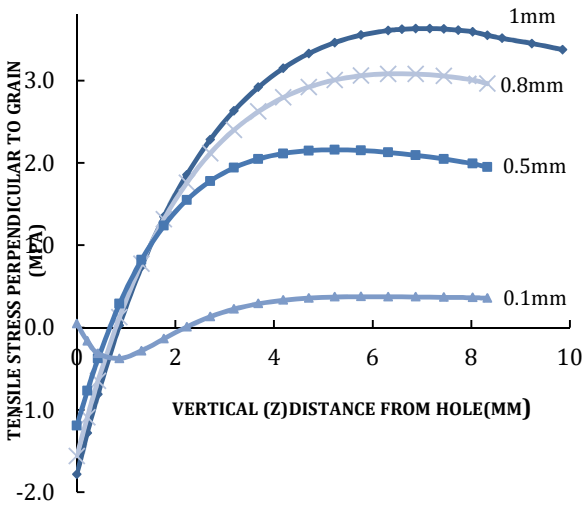

Figure2.14: Perpendicular-to-grain tensile stress distribution on plane below contact surface for four displacements

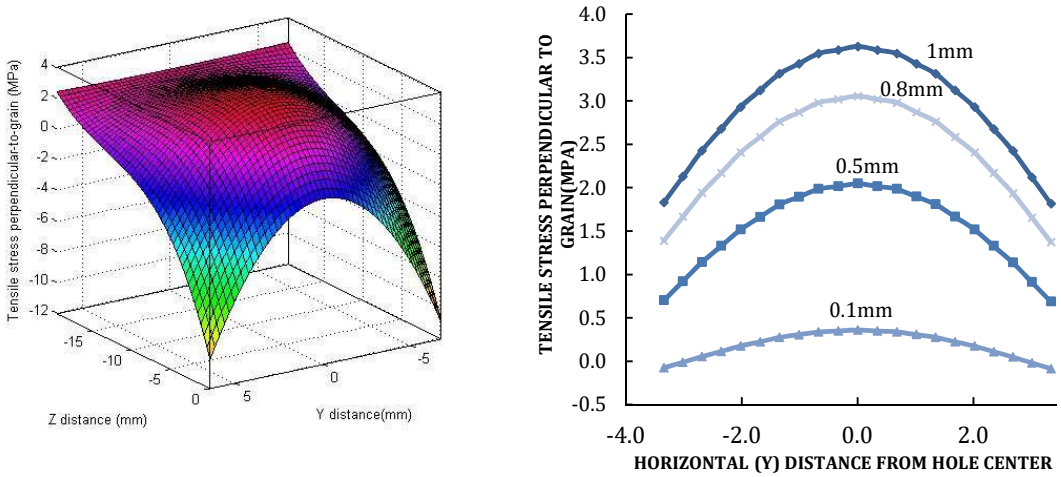

Figure2.15: Perpendicular-to-grain tensile stress distribution a) in 3D space b) across horizontal plane at 7.4 mm below hole for four displacements

Figure2. 17 illustrates how the location of the maximum shear stress changes as the loading increases, and also shows how the maximum shear stress is affected by friction. Because there are only normal contact forces in the contact region, the maximum shear stress is very close to the contact center when a 0.1 mm load increment is applied (Figure2. 17a). When the load increases, the contact surface enlarges (Figure2. 16) and tangential forces appear. In this case, the stress pattern is also affected by slip and frictional forces (Figure2. 17b), which cause the location of maximum shear stress to move outward and away from the contact surface. Given this stress state, the FE model predicts the location of the maximum shear stress at 4.75 mm horizontally off-center, which is confirmed by the embedment experiment results. For 80% of the sample size (reference Figure2. 8), the fracture initiated between 4-4.7 mm off-center (lower $1/6^{th}$ of the hole perimeter), and the other 20% displayed a fracture on-center.

As depicted in Figure2. 17.b, the maximum shear stress occurs at 1mm beneath the contact zone. This is consistent with the experimental observations in which the fracture starts underneath the surface and develops up to the surface as the loading increases.

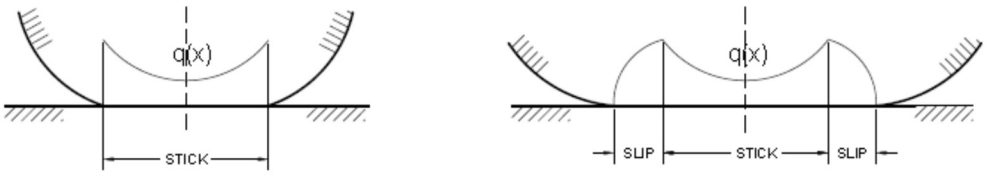

Figure2.16: As the vertical loading increases the contact surface enters to slip region

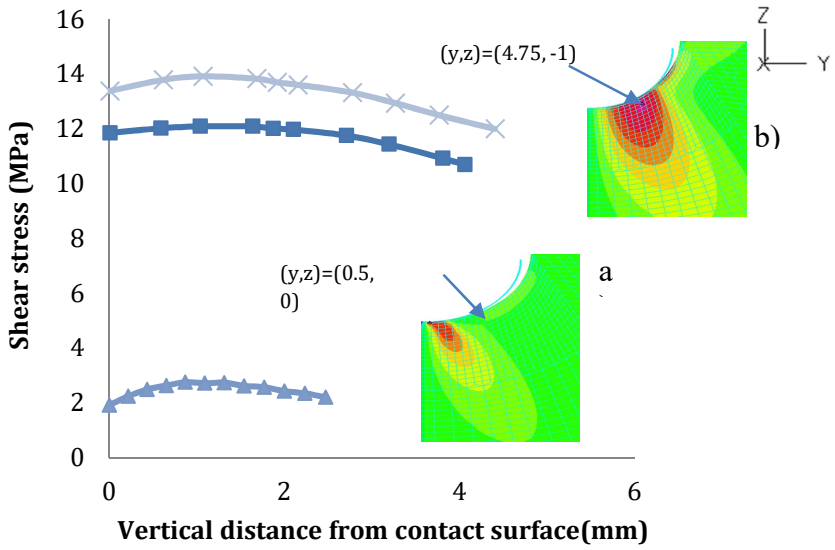

Figure2.17: Shear stress values on vertical distance from the contact surface and shear stress contours: a) surface stress field in sticking contact; b) the location of maximum shear stress moves outwards due to sliding contact

CHAPTER3

EVALUATION OF ASTM D5764 DOWEL CONNECTION TESTS FOR LAMINATED VENEER BAMBOO (LVB)

3.1 Introduction

Being a relatively new building material in North America, LVB was only recently added to the material testing standard ASTM D5456 "Standard Specification for Evaluation of Structural Composite Lumber Products" in 2013. This standard recommends the test same protocols for LVB and wood alike. Recent research, however, on LVB dowel connections (Reynolds et al. 2016 , Khoshbakht et al. 2018) has indicated that bamboo lumber exhibits different failure mechanisms than softwood lumber, especially for dowel bearing response. This finding raises questions about the appropriateness of adopting a wood standard for LVB.

A handful of research studies compare standard test methods and specimens for dowel bearing response, but their focus has been primarily softwood species. For example, Santos et al. (2010) used maritime pine wood and did a comparison between two standard test methods: EN383 (2007) and ASTM D5764 (2017), one with full-hole specimen and the other with half-hole specimen as described in the respective standards. The authors concluded that embedment strength measured for both standards are essentially the same. They also found a positive relationship between embedment strength and density following the ASTM D5764 method. It is noteworthy that according to their outcomes, in the EN383 (2007) method, the average specimen displacement at yield was nearly twice as much as

that of the specimens following the ASTMD5764 method for the longitudinal compression test because of the proposed half-hole geometry (Santos et al. 2010).

Similarly, but using spruce specimens, Franke and Magniere (2014) evaluated different dowel embedment testing methods and highlighted the major differences between standards. The authors showed that the variation in the specimen geometry and loading and differences in evaluation method of finding stiffness and bearing strength, affects the embedment strength significantly.

Importantly, recent work by Reynolds et al. (2016) and Khoshbakht et al. (2018) revealed a meaningful difference in failure mechanism between Moso LVB dowel joints and timber dowel joints: both studies found that high shear stresses around the bolt hole were primarily responsible for bamboo dowel failure while tensile stresses perpendicular to the grain were the primary cause of failure in timber joints - the latter also being affirmed by Reynolds et al. (2016).

ASTM D5764 recommends using half-hole specimens "unless the specimens tend to split before the completion of the test", in which case the full-hole test is required. To the authors' knowledge, the effect of using these different test set-ups (specifically full-hole vs. half-hole specimens) on dowel failure behavior of LVB and other similar hardwood materials has not yet been fully investigated. In this paper, we evaluate the ASTM method specifically with regards to the embedment test procedure for LVB specimens to recommend an appropriate test method for LVB dowel joints. We base our work on experimental data and non-linear FE simulations by describing the behavior of Moso LVB dowel connections under compressive loading using orthotropic material properties for both the full and half-hole arrangement. In so doing, we aim to provide

insight into LVB failure mechanisms which can further support development of codes and standards for bamboo connection detailing and design to facilitate worldwide adoption of bamboo in modern construction.

One additional factor that has not been considered in the Standards for dowel bearing properties is the surface roughness of the dowel hole. This effect has been addressed in past studies (Rodd 1973 , Jorissen 1999) and recent papers (Sjodin et al. 2008) and is shown to be a critical factor in determining load bearing capacity of the connection. The foci of these studies, however, are softwood species. Hence, in this chapter, the effect of surface roughness on load bearing capacity of the LVB dowel joint is also addressed.

It is noted that the content of this Chapter has already been published as follows: N. Khoshbakht, P. Clouston, S. Arwade, and A. Schreyer, "Evaluation of ASTM D5764 Dowel Connection Tests for Laminated Veneer Bamboo (LVB)," Journal of Testing and Evaluation 47, no. 4 (2019): 2717-2736.

3.2 Experimental program

3.2.1 Embedment Test Setup

Prior to conducting the embedment test, the material properties of LVB (shear, tension and compression parallel-to- and perpendicular-to-grain), were experimentally determined per ASTM D143 (1994). These values were necessary as input parameters for subsequent FE studies of the dowel joints. In the experimental tests, commercially available LVB boards were used made from Moso bamboo (*Phyllostachys heterocycla var. pubescens*) procured by the company Lamboo® Technologies. The boards were

conditioned for a minimum of 2 months in constant ambient environmental conditions. The mean moisture content of the samples was 5.4%.

The material preparation and test procedure for evaluation of embedment properties followed ASTM D5764 which is designed for testing a single dowel joint of wood-based products (Fig3.1). The sample consisted of 10 replications for each full/half hole arrangement as determined by ASTM D2915 (1999). An MTS3000 testing machine was utilized in combination with an LVDT to measure displacement at the contact surface of dowel joints to obtain load-displacement curves.

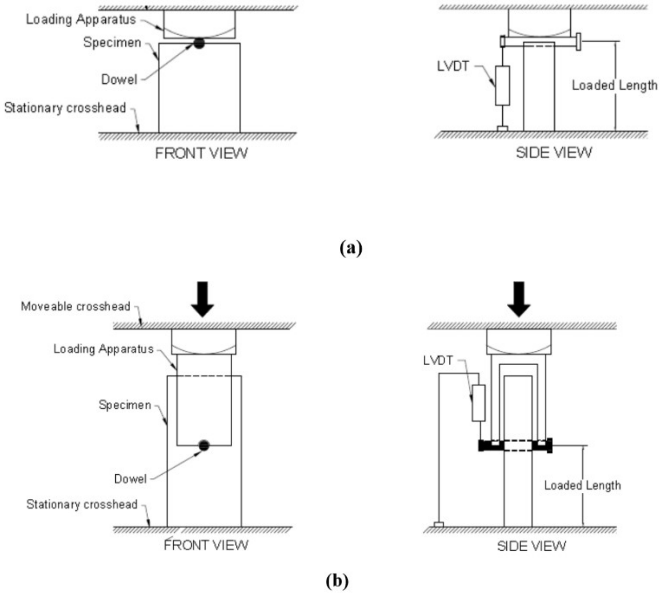

Figure 3.1: Embedment test setup based on ASTMD5764: (a)half-hole and (b) full-hole test

The LVB specimens measured 152by 63 by 32 mm^3 and 90 by 63 by 32 mm^3 for full-hole and half-hole specimens respectively. Using a 17.5mm (11/16th inch) diameter drill bit, a hole was drilled in the middle of the block to accommodate a 15.9mm (5/8th inch) diameter steel (grade5.5) bolt. Different steel loading apparatus was used for full and half hole specimens to ensure application of the load onto the wood contact surface follows

the standard. Per the standard, a crosshead rate of 1 mm/min was used to produce failure between 1-10 minutes. Displacement directly beneath the contact zone was obtained by means of an LVDT (Fig3.2).

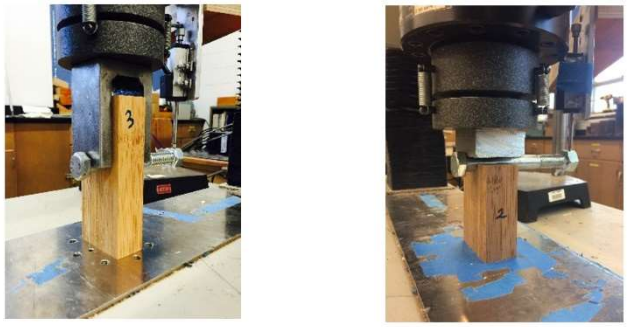

(a) (b)

Figure 3.2: Embedment test setup: displacement was measured in contact zone for (a) full-hole and (b) half-hole specimens

3.2.2 Embedment Test Results

The embedment test results, shown in Table 3.1, reveal the stiffness at the contact surface, which in turn leads to finding local modulus of elasticity in the contact zone.

Table 3.1:Stiffness measured at contact surface

	Stiffness at contact surface (N/mm)	Ultimate Displacement (mm)	Yield load (%5 dowel diameter) (kN)	Embedment strength Parallel-to-grain (MPa)
Full-hole Test				
Mean	32400	1.18	27.1	34.4
C.V.	5.6%	24%	8%	8%
Half-hole Test				
Mean	45900	1	28.8	36.6
C.V.	15%	25 %	10%	10%

In Figure 3.3, representative curves for full-hole and half-hole tests are shown where the difference in load bearing capacity of LVB from each test is noticeable. Although measured embedment yield load in the half-hole arrangement is higher than that of full-hole, fracture occurs at approximately the same displacement for both. The rationale behind

this phenomenon will be explained in a later discussion section of this chapter through FE results. Figure 3 illustrates failure of the full-hole and half-hole dowel joint after being loaded in compression parallel-to-grain up to their maximum stress.

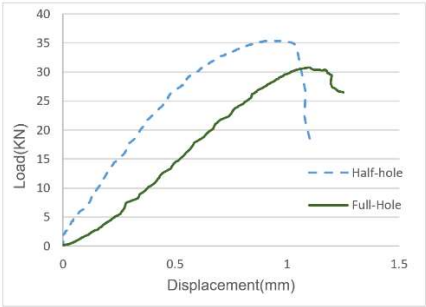

Figure 3.3: Load bearing capacity comparison between full-hole and half-hole LVB dowel joint

(a) (b)

Figure 3.4: Splitting failure in LVB dowel joint when loaded parallel-to-grain: (a) full-hole (b) half-hole

For the full-hole test, in 80% of the specimens, the crack started and continued to grow at between 4 to 4.7 mm off-center (ie. lower $1/6^{th}$ of the hole perimeter) and in 20% of the specimens an on-center crack was also detected beneath the loaded area. These tests suggest that a combination of tension perpendicular to grain and shear stresses on the specimen is responsible for failure.

For half-hole test, on the other hand, the fracture consistently occurred off-center in the lower $1/6^{th}$ of the hole perimeter (Fig3. 3 b) which suggests that shear stress (only) is the primary cause of failure.

3.3 Finite Element Model and Analysis

To find a more detailed explanation of the different failure behavior of LVB dowel joint in full and half-hole set up, a non-linear 3D FE model was built using ANSYS Mechanical APDL17.2 (ANSYS, Inc., Canonsburg, PA). The two test setups described in ASTM D5764 (full-hole and half-hole) were followed explicitly.

The model was developed with hexahedra homogenous 20-node elements (SOLID186) to investigate the stress distribution, and clarify the cause of failure, in each test method. Displacement-controlled compressive loading was applied to the steel bolt and the specimen model was fixed at the bottom. The bolt hole diameter was modeled as $1/16^{th}$ inch larger than the bolt diameter to reflect realistic building practice as specified in the National Design Specification for Timber Construction (NDS,2015). Because of symmetry, half of the dowel was modeled, and symmetric planes were restricted in the direction normal to the plane of symmetry. Mesh refinement was performed in the area of interest around the bolt hole. The number of elements used in the model is 6142 and 4186 for full-hole and half-hole model, respectively.

Contact elements (CONTA174 and TARGE170) were employed for creating flexible surface-to-surface contact for the steel bolt and the LVB hole. Then, an Augmented Lagrange algorithm was used to solve the contact problem implementing parameter *FKN*=0.1 to adjust the contact stiffness in the contact area. The other important contact parameter is contact tolerance (*FTOL*), which is the minimum distance that the program searches for, for contact, and calculates contact force with lower computer cost. The *FTOL* parameter is important because choosing proper contact tolerance, together with proper load increment, leads to converged and more accurate results. For our work, after choosing

different values (given in Tables 3.2 and 3.3) *FTOL* was considered as 0.15. and 0.01 for full-hole and half-hole models, respectively. Finally, value 0.2 for coefficient of friction between LVB and steel dowel was chosen (Reynolds et al. 2016).

Table 3.2:Full-hole model calibration results

Model:					**Results:**
FE Model	Mesh size (mm)	FKN	FTOL	Constraint method	Contact stiffness in elastic zone, K (N/mm)
1	1	0.1	0.15	Penalty	31300
2	1	0.1	0.15	Augmented	31500
3	1.5	N/A	0.1	Lagrange	38800
4	1.5	0.1	0.15	Augmented	32000
5	1.5	0.1	0.1	Augmented	34300

Table 3.3:Half-hole model calibration results

Model:					**Results:**
FE Model	Mesh size (mm)	FKN	FTOL	Constraint method	Contact stiffness in elastic zone, K (N/mm)
1	1	0.1	0.01	Augmented	Not converged
2	1	0.1	0.1	Augmented	39000
3	1.5	0.1	0.15	Augmented	36000
4	1.5	0.1	0.05	Augmented	41000
5	1.5	0.1	0.01	Augmented	43000

3.3.1 Contact modeling

To define the most efficient mesh at the contact area and to decrease the amount of unrealistic penetration, there are two things that should be considered:

- Choice of contact/target surfaces: considering target element characteristic and definition, no penetration is allowed between the target element nodes (Kim,2015). Hence, target element is usually selected for modeling a stiffer body which in our case is the steel bolt (Fig3.5).

- Contact/target surface relative mesh size: a finer mesh was considered for target surface (steel dowel) to allow a permissible penetration to the contact surface (wood surface) in the FE model (Fig3.5).

It is notable that - regarding choosing the proper mesh size - because of the C0 continuity across the contact boundary, the contact force is very sensitive to mesh discretization. It was found that the results change abruptly with mesh refinement, so mesh refinement at the contact boundary doesn't necessarily lead to converged results.

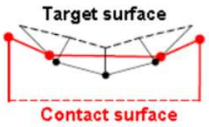

Figure 3.5: The effect of contact area mesh on penetration: contact body with coarser mesh

3.3.2 Material model

An orthotropic bilinear material model with hardening was assumed for Moso LVB and the constitutive properties were chosen from the experiment results given in Table 2.1 for the elastic region. To calculate the required parameters for the plastic region - which is defined by yield stress and tangential modulus - the average slope and yield load of 10 embedment tests were used and the calculated stress and tangential modulus were incorporated in the FE model (reference Fig3.6).

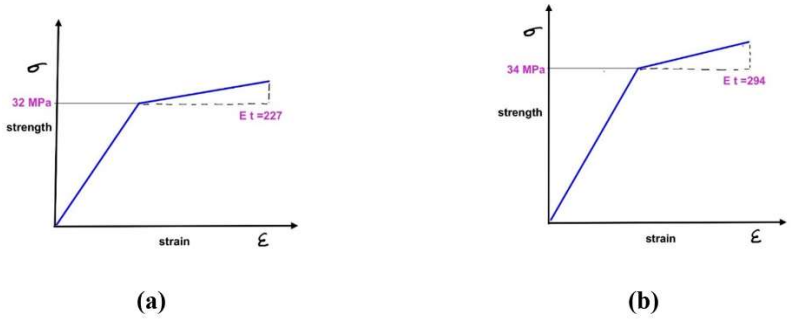

Figure 3.6: Elastic-plastic material model for full and half-hole specimens based on embedment test curves(a) Bilinear material model(full-hole) (b) Bilinear material model(half-hole)

The choice of Poisson ratio and shear modulus values didn't affect the stress results noticeably. Hence, they were selected from the literature: the former value being between 0.22-0.25 as noted by Yu et al. (2011) and the latter value being 745 MPa as reported for Moso bamboo (Askarinejad et al. 2015). The second and third shear moduli were estimated to be ½ and 1/10th (respectively) that of the first shear modulus based on similar mechanical properties for hardwood given in the Wood Handbook (2010).

For the steel bolt, the elastic material model was assumed with the yield stress of 210 GPa and Poisson's ratio of 0.3.

In orthotropic material modeling, care should be taken for choosing the right direction of input material properties, especially for Poisson ratio, to ensure that the stiffness and compliance matrices were positive definite. As a result, the material axes directions were modeled to coincide with the software global axes and the strongest direction of LVB aligned with global X-axis to avoid any confusion (Fig3.7).

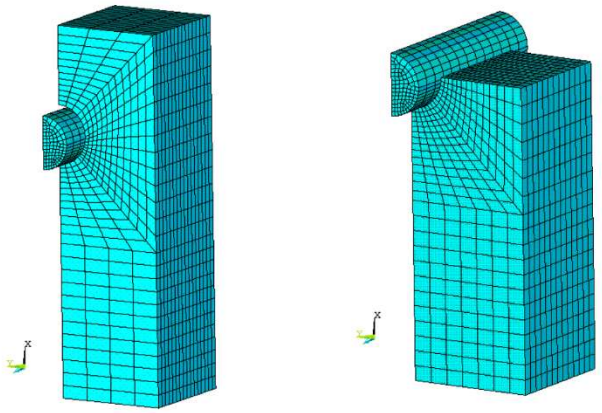

Figure 3.7: FEM element mesh: a) full-hole model b) half- hole model. The strongest direction of LVB is aligned with global X-axis

In both Lagrange multiplier and penalty methods, the contact is treated as a constraint (Kim,2015) in structural equilibrium, which is why the contact formulation is independent of the material constitutive models. In this case, the modulus of elasticity values from the conventional LVB test in Table 2.1 was used. After running the FE model and achieving the results, for contact surface validation of our FE model, the contact surface load-displacement curve (in the longitudinal direction) was obtained and compared with the measured load-displacement results by means of an LVDT.

By considering all the above, full and half-hole models were calibrated to experimental results by considering different combinations of mesh size, load increments, and contact tolerance. Calibration results are presented in Fig3.8 and Tables 3.2 and 3.3. Correspondingly, for obtaining experimental curves shown in Fig3.8, an LVDT was employed to observe the material load-displacement curve in the mid-point of the contact surface for a sample size of ten. The measured stiffnesses (i.e. load/displacement) at the contact zone were 32400N/mm for full-hole and 45500 N/mm for half-hole specimens in the linear elastic region of the curves.

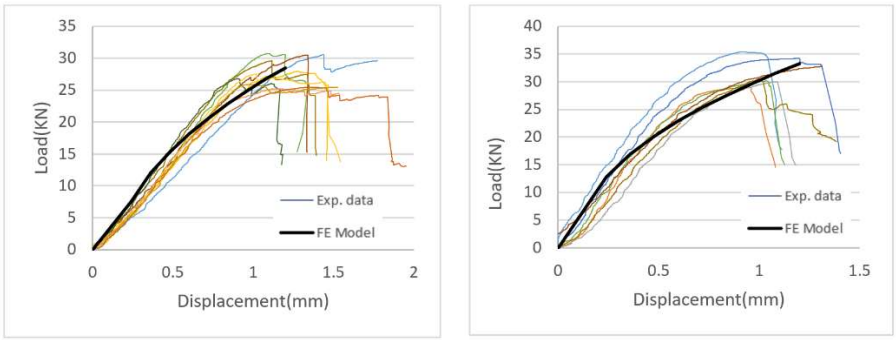

Figure 3.8: FEM calibration in compressive loading parallel to the grain (a) Full-hole model and (b) Half-hole model

An initial bulge in the experimental curves was observed, which is the result of self-alignment and self-adjustment between the hole and steel bolt. The applied incremental displacement was increased to 1.2 mm until the LVB dowel joint reached its maximum stress according to experimental results in Table 3.1. Comparison of the FE models and experimental test results in Fig3.8 led to a verified FE model with the element length of 1.5mm at the contact edge.

3.3.3 Local Elastic Moduli Evaluation

The local elastic modulus (E_L) parallel-to-grain (needed for the FE model) was determined following an empirical approach that uses the slope of the load-displacement curves of the embedment test. The method is fully explained in the authors' previous work (Khoshbakht et al. 2018) in which the attained local modulus of elasticity is calculated based on dowel geometry and joint stiffness (N/mm). Also, the assumed MOE corresponded to that of the lowest strength direction (i.e. perpendicular-to-grain) because, in ANSYS, only one tensile or compressive elastic modulus (independent of material

direction) is allowed in the material property input section. Results are summarized in Table 3.4.

Table 3.4:Calculated local modulus of elasticity for full-hole and half-hole model

Test data used for calculations	Sample size	Failure Load (N)		Displacement at failure (mm)		Calculated Local Modulus of Elasticity (MPa)	
		Full-hole	Half-hole	Full-hole	Half-hole	Full-hole	Half-hole
Parallel-to-grain (LVB Embedment Test)	10	28197	35100	1.18	1	1007	1400
Perpendicular-to-grain (LVB Tension Test)	10	N/A	N/A	N/A	N/A	200	200

3.4 Results and discussion

In this analysis, the validated FE models for full-hole and half-hole tests as described above, were implemented to study the internal stresses in the LVB joint contact area as displacement was increased to near failure (1.18 and 1mm upper limits based on the experimental results of the embedment tests).

It is noted that in some FE models, contact points may oscillate between an open and closed status. This is called "chattering" and in our case (shown in Fig 3.9) contact chattering occurred at the point of separation between contact and target surface (LVB and steel dowel). This phenomenon created a singular point at this location which led to false high stresses in this point. They were ignored wherever found in the following analysis.

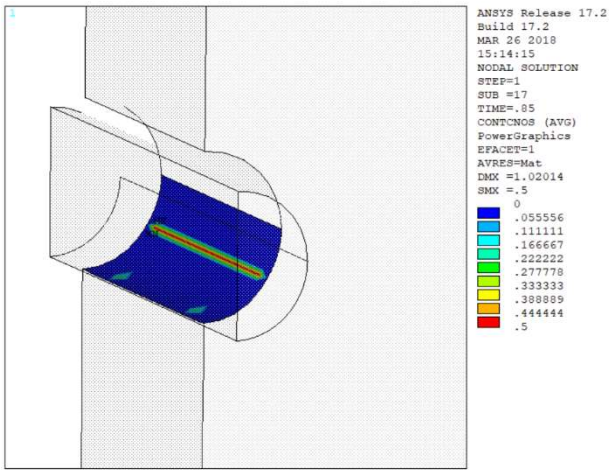

Figure 3.9: Contact chattering occurs at the point of contact/target separation

3.4.1 FE Analysis Results and Discussion

The maximum tensile stress perpendicular to grain for the full-hole model (Fig3. 10 a) was 4.5 MPa and occurred at 8.5 mm beneath the contact surface. This value is slightly less than the experimental strength given in Table 2.1 (5.4 MPa). The coefficient of variation of strength in the experimental results of 22% would suggest that tension stress perpendicular to grain would be a substantial contributing factor to material failure. On the contrary, for the half-hole specimen, shown in Fig3.10 b, the maximum tensile stress reaches only 1.5 MPa (13 mm beneath the contact surface) which is far less than the experimental strength or 5.4 MPa and thus, has little contribution to material failure.

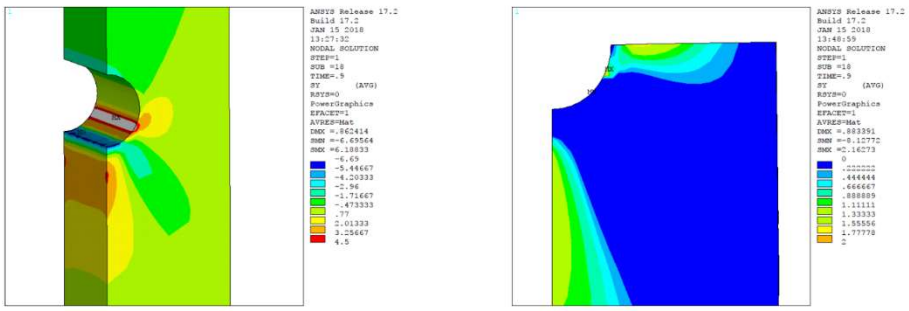

(a) (b)

Figure 3.10: Tensile stress pattern perpendicular-to-grain for: (a) Full-hole model at 1.1 mm loading (b) Half-hole model at 0.9 mm loading

Figure 11 depicts the maximum in-plane shear stress pattern at failure. In both the full and half-hole model, the maximum shear stress occurs at the lower 1/6th of the hole perimeter which coincides with the location of fracture initiation observed in the experiments (Fig 3.4).

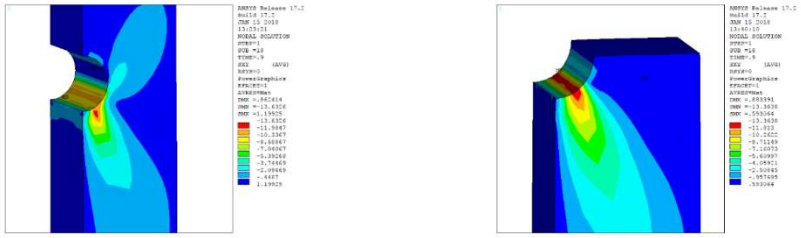

(a) (b)

Figure 3.11: In-plane shear stress pattern for: (a) Full-hole model at 1.1 mm loading (b) Half-hole model at 0.9 mm loading

The FE model for full-hole specimens indicated that maximum shear stress reached 13.6 MPa at 1.1mm displacement (Fig3.11a) which corresponds well with the experimental shear strength of 13.2 MPa at mean 1.2 mm loading (given in Table 3.1). For half-hole specimen, maximum shear stress was predicted to be 13.3 MPa at 0.9mm loading (Fig. 3.11b) compared to experimental value of 13.2 MPa at mean 1.0 mm loading. Both experimental and FE models confirmed that half-hole specimens fail at less displacement than full-hole specimens.

The Tsai-Wu failure criteria was employed to predict insipient failure location based on a combined stress state of shear and tensile stress perpendicular to grain. This criterion is a general quadratic interaction equation in which the failure surface is in the form of a tensor polynomial:

$$F_i\sigma_i + F_{ij}\sigma_i\sigma_j = 1 \quad \text{for } i,j=1,2,\ldots,6 \tag{2.12}$$

F_i : First rank stress tensor

F_{ij}: Fourth rank stress tensor

F parameters are experimentally determined and can be expressed in terms of uniaxial and shear strength except for F_{12} that needs biaxial test to be determined. Hence, when applying Tsai-Wu failure criteria, these F parameters were requested through ANSYS dialogue box:

-Longitudinal and transverse tensile strength (obtained from Table 3.1).

-Longitudinal and transverse compressive strength (obtained from Table 3.1).

-Longitudinal and transverse Shear strength (obtained from Table 3.1).

-Stress coupling coefficient (XY, YZ, XZ): This parameter equals $2F_{ij}$ in ANSYS nomenclature. The value F_{ij} was assumed 0.00012 using glubam off-axis test data (Yang et al.2014).

Figures 3.12 and 3.13 shows how the Tsai-Wu criteria effectively predicts location of insipient failure. In Fig3.12a (after disregarding the value at a singularity due to contact chattering) it is shown that the full-hole model fails at 1.1mm loading and the most probable failure area includes the central lower part up to the lower 1/6th of the hole perimeter. While in the half-hole model (Fig3.13a) the failure location is predicted to be just off-center and at the lower 1/6th of the hole perimeter. Considering these results, the Tsai-Wu criteria appears to be a good measure to predict failure of the LVB dowel joint.

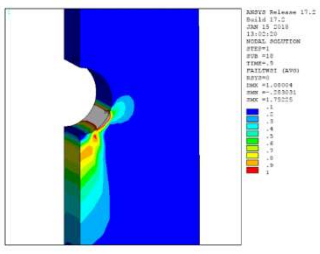

(a)

(b)

Figure 3.12: Full-hole model at 1.1mm loading: (a)Tsai wu failure criteria compared to (b)actual failure pattern

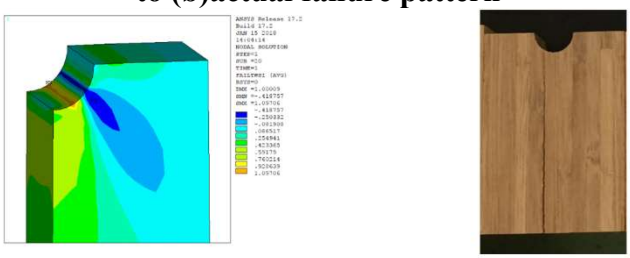

(a) (b)

Figure 3.13: Full-hole model at 1.1mm loading: (a)Tsai wu failure criteria compared to (b)actual failure pattern

3.4.2 Frictional Stresses in the Contact Zone

Sjodin et. al. (2008) showed that for softwood species, roughening the surface area of the dowel increases shear stresses and decreases tensile stresses in the perpendicular to grain direction. And, since tensile stresses perpendicular-to-grain are the dominant factor in defining strength of wood specimens, they suggest that designing dowel joints with rough contact surface ($0.3<\mu<0.5$) improves the load bearing capacity.

Given that in the LVB dowel joint (which is arguably similar to a hard wood species) the determining factor of load bearing capacity is shear stress, the effect of a friction coefficient on shear stress results are of particular interest. Consequently, two FE models of dowel joints were considered here: one with $\mu=0.2$ and the other with $\mu=0.4$.

Both models are the same in terms of material properties and boundary conditions except for the coefficient of friction. Figure 3.14, which represents the contact status in both models, shows that the FE model with $\mu=0.4$ has a larger area in sticking status for the same applied displacement. This leads to less sliding distance in this model according to Figure 3.15. Consequently, the frictional stresses are much higher in $\mu=0.4$ FE model (Fig3.16) which in turn leads to higher shear stresses as shown in Figure 3.18. By increasing the coefficient of friction to 0.4, the maximum shear stress has increased by 4%,

which - compared to results for softwood species (Rodd,1973) - is not significant. However, it confirms that in dowel joints with similar size and material and loading conditions, shear stresses are higher in the dowel with rough contact surfaces. This means that, contrary to wood connections, the smoother contact surface contributes to higher strength of LVB dowel connections. It is noted that this conjecture should be confirmed in a future study by carrying out experiments on rough and smooth surfaces for LVB material.

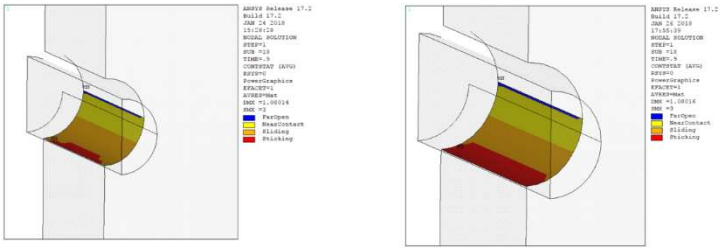

(a) μ=0.2 (b) μ=0.4

Figure 3. 14: Contact status at 1.1 mm displacement for (a) μ=0.2 (b) μ=0.4

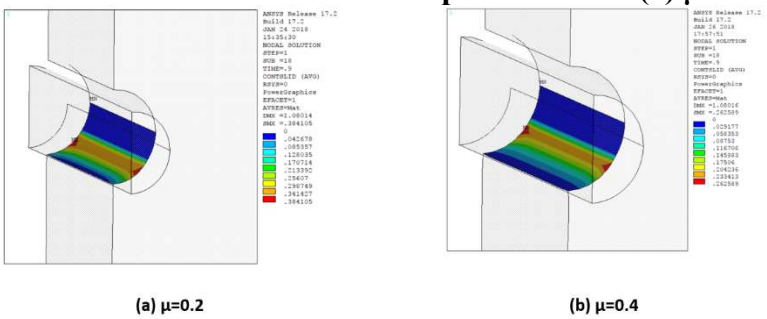

(a) μ=0.2 (b) μ=0.4

Figure 3.15: Contact sliding distance at 1.1 mm displacement for a) μ=0.2 b) μ=0.4

Fig3.17 shows shear stresses in the first sub step of loading in both frictional models. Since the dowel is still in the sticking status for both models, the shear results are equal in the beginning and the maximum shear stress is also closer to the centerline. As the loading increases and the steel dowel begins to slide, the location and the value of maximum shear stresses changes dependent on the coefficient of friction (Fig3.18).

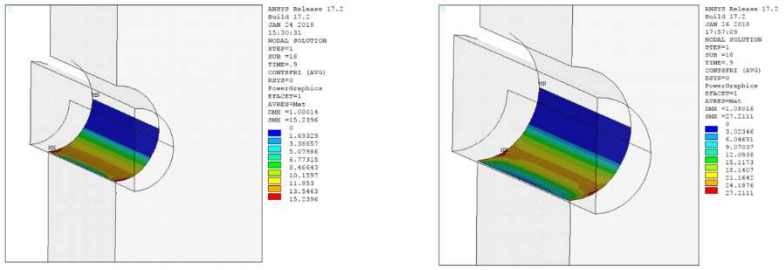

(a) μ=0.2 (b) μ=0.4

Figure 3.16: Contact frictional stresses at 1.1 mm displacement for a) μ=0.2 b) μ=0.4

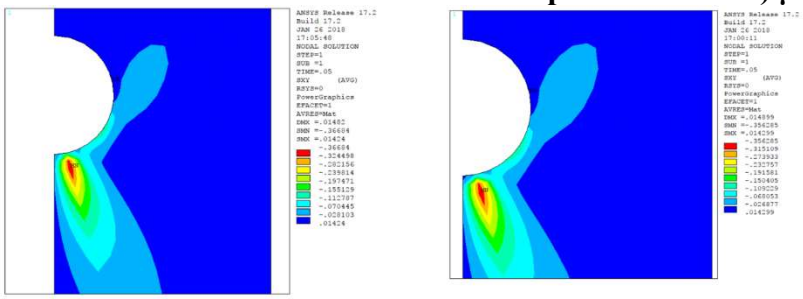

(a) μ=0.2 (b) μ=0.4

Figure 3. 17: Shear stress pattern at 0.1 mm displacement for (a) μ=0.2 (b) μ=0.4

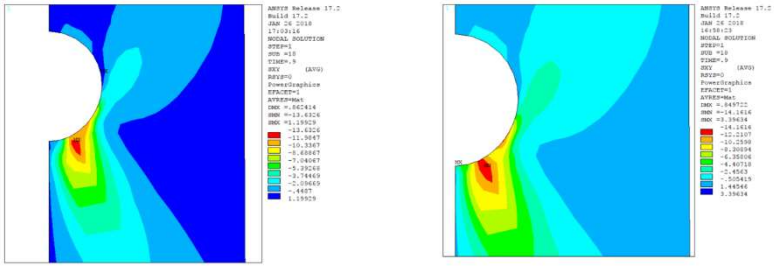

(a) μ=0.2 (b) μ=0.4

Figure 3.18: Shear stress pattern at 1.1 mm displacement for (a) μ=0.2 (b) μ=0.4

In conclusion, both FE and experimental analysis revealed a noticeable difference between the failure behavior of LVB full and half-hole dowel joints: for full-hole specimen a combination of shear stresses (as the main cause of failure) and tensile stresses perpendicular-to-grain (as a secondary cause of failure) is responsible; while for half-hole specimens, shear stresses parallel-to-grain dominate failure.

It was also shown, both numerically and experimentally, that for the same applied displacement, the half-hole specimen fails at slightly less displacement than full-hole

specimens, despite higher load bearing capacity and stiffness. This is because the higher internal shear stresses exceed LVB shear strength sooner than full-hole specimen. This suggests that higher dowel stiffness and load bearing capacity does not lead to stronger joint design for the displacement-based loading.

CHAPTER 4

MODELING LVB DOWEL BEHAVIOR LOADED AT DIFFERENT ANGLES TO GRAIN

4.1 Introduction

Broadly speaking, wood is an orthotropic material and examining embedment strength loaded at different angles to grain is an integral part of studying wood dowels. Though much research has been dedicated to understanding dowel bearing capacity of wood at varying angles to grain, to date, no research has been done on the behavior of LVB dowel connections as such. The focus of this chapter, therefore, is on LVB connections loaded at different angles to the grain to expand the reader's insight towards the application of LVB dowel connection in structural design.

The dowel-bearing behavior is evaluated using experimental data and FE models. Specifically, the critical zone beneath the bolt hole is studied in terms of interactive stresses and then assessed for its applicability with failure criteria known for wood.

4.2 Experimental program

4.2.1Methodology

To evaluate embedment strength, six angles (15°, 30°, 45°, 60°, 75° and 90°) were selected for a dowel diameter of 15.9 mm (5/8 in). This size dowel was chosen because the focus of the study is wood crushing underneath the dowel: smaller diameter dowels tend to result in bending of the steel dowel during the test. As was investigated in the author's previous work (Khoshbakht et al. 2018), the full-hole test set up, described in ASTM

D5764 (2013), *Standard Test Method for Evaluating Dowel-Bearing Strength of Wood and Wood-Based Products,* was chosen as it leads to achieving more realistic results.

4.2.2 Material Preparation

Six samples of laminated bamboo lumber were machined for testing with ten replications for each sample. The material was supplied by Lamboo® Technologies in the form of 2.5-meter lengths of nominal 2x6 in. boards.

The dimensions of specimens were determined using ASTM D5764 to avoid any splitting before completion of the test. The thickness of the boards was roughly 38mm (1.5 in.) and was decreased to 36mm (1.4 in.) with machining tools to both, meet the ASTM restrictions, and to fit properly into the loading apparatus of the MTS machine. First, each board was divided into equal small parts. See Fig 4.1.

The specimens were cut using a miter saw, and wooden jigs were created to provide fast and accurate machining of specimens at different grain angles (Fig4. 2).

A simple vertical mill drill (Fig4.1) was used for drilling holes in the specimens. A steel-cutting 17.5mm (11/16 in.) drill bit was used to drill the dowel hole. Drilling was completed in two steps and with low speed to ensure achieving smooth surface inside the hole. Another jig was built for the vertical drill to fix the specimen correctly, so a consistent location of the hole for all specimens was assured.

Figure4.1: Miter saw, cut LVB Boards and vertical drilling machine

Figure4.2: wooden Jigs for quickly machining uniform specimens

4.2.3 Experimental Testing

A universal MTS 3000 machine was used to test the specimens. Figure 4.3 shows the testing setup and equipment employed. A Linear Variable Differential Transformer (LVDT) was employed to precisely measure strain in the vertical direction on the steel dowel. The dowel connection was centered with the machine crosshead to achieve uniform load distribution on the dowel.

Specimens were tested at 1mm/min, as recommended by ASTM D5764, to allow for completion of the test between 1 and 10 minutes.

The test was stopped when the specimen failed or when the dowel displacement reached 2.5 mm. The load-displacement curves were generated using the data acquisition system of the MTS machine.

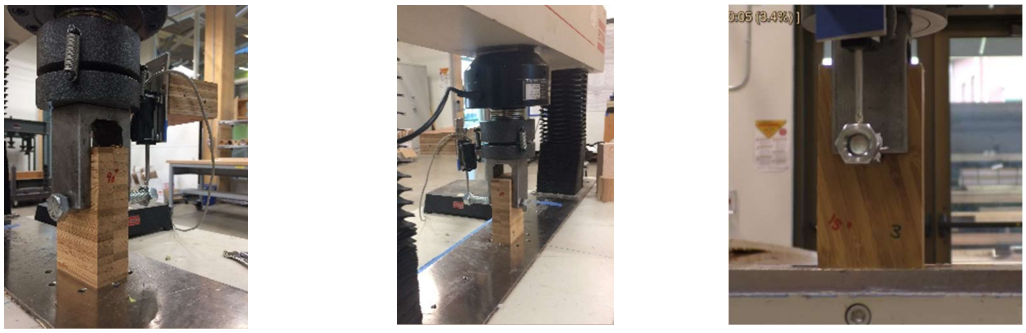

Figure4.3: Test setup according to ASTM D5764

4.2.4 Analysis

Before inspecting LVB dowel load-displacement curves and test data it is helpful to first consider the two concepts of “embedment strength” and “ductility" in wood connections.

4.2.4.1 Embedment strength

Embedment strength of a specimen is defined as the yield load divided by the product of the specimen thickness and the fastener diameter. To find yield load according to ASTM D5764, the linear portion of the load-displacement curve is determined and then it is shifted by 5% of the dowel diameter. Yield load is then attained by intersecting the shifted line and load-displacement curve. If the intersection point passes the peak load, the yield load is assumed to be the peak load.

For LVB specimens, the offset line intersects with the load-slip curve after the peak load. Hence, as we need both peak load and yield load to quantify ductility in the LVB dowel tests, the suggested method in ASTM was deemed to be an improper choice to define yield load.

To find yield load for wood products, several methods exist and are shown in Fig4.4. The details regarding each method are explained in Muñoz & Salenikovich (2008).

Here, we only discuss the method of our choice, which is the method proposed by Yasumura & Kawai (Muñoz & Salenikovich 2008).

Referencing Figure 4. 4e, in the Yasumura & Kawai method, the linear slope of the load-displacement curve is calculated between 10% and 40% of the peak load. Then, a straight line is drawn from 40% of the peak load to 90% of the peak load. Parallel to this line, another line is drawn tangent to the load–displacement curve. If we intersect this tangential line with initial linear slope and project the point of intersection towards the load–displacement curve, we obtain the yield point displacement.

The yield point achieved by this method was then employed to define the ductility of each sample. Embedment strength for loading at each grain angle was also calculated and will be discussed in the last chapter to evaluate application of Hankinson equation for LVB dowel connections.

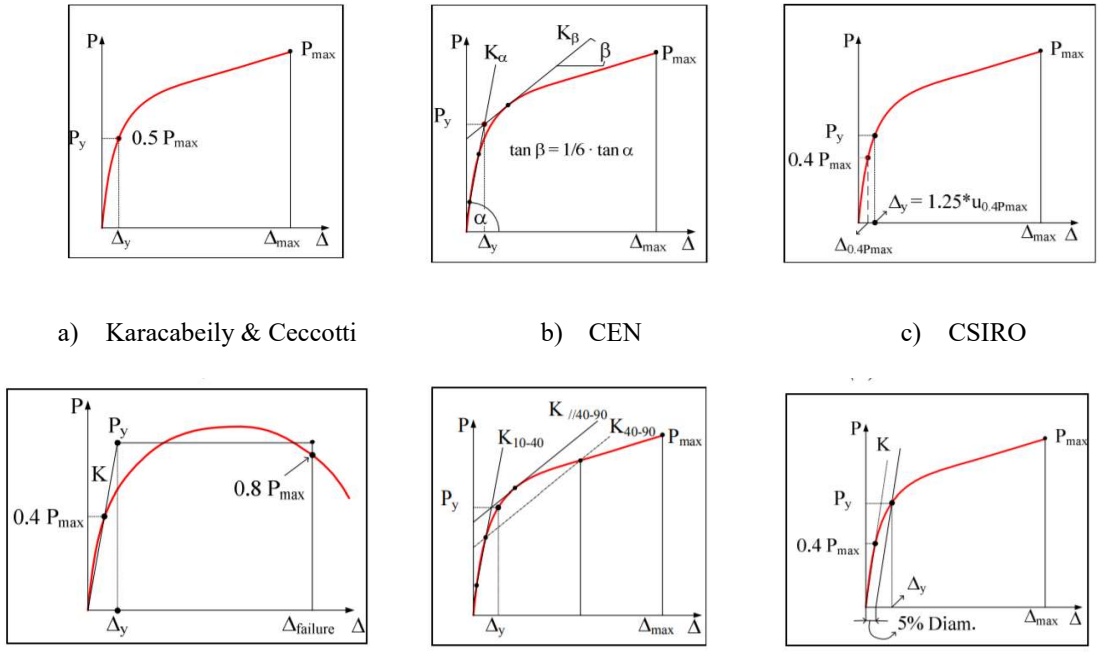

a) Karacabeily & Ceccotti b) CEN c) CSIRO

d) EEEP e) Yasumura & Kawai f) 5% diametet

Figure4.4: Different method to find the yielding point (Muñoz & Salenikovich 2008).

4.2.4.2 Ductility in wood dowel connections

From a practical design standpoint, it is not overly necessary to focus on higher embedment strength in connection design. This is because, no matter how strong a connection is in terms of embedment strength, it doesn't necessarily lead to a safer design because, in some cases, the material might have a brittle failure mechanism. In fact, for connection design purposes, a designer must make sure that the connection contains sufficient ductility. Sufficient ductility in dowel connection design means that: no matter how much the entire system (considering both the steel dowel and the wood together) deforms, the strength should remain approximately the same.

Brühl et al (2011) explains what sufficient ductility is and more importantly, how ductility can be quantified and adopted in structural design. They used Johnson's expression of ductility with the ductility number, D_f, being the ratio of the displacement at failure, u_f and the displacement at the onset of yielding u_y:

$D_f = u_f / u_y$

Hence, $D_f = 1$ corresponds to linear elastic behavior (no ductility)

and $D_f > 1$ to non-linear behavior, with or without hardening.

Fig 4.5 shows the load–slip responses of tested LVB fasteners at different angle to grain. From zero to 45°, the slip curves first show linear elastic behavior followed by plastic deformation and hardening behavior; whereas, from 45° to 90°, the curve initially has nonlinear elastic behavior followed by a hardening branch.

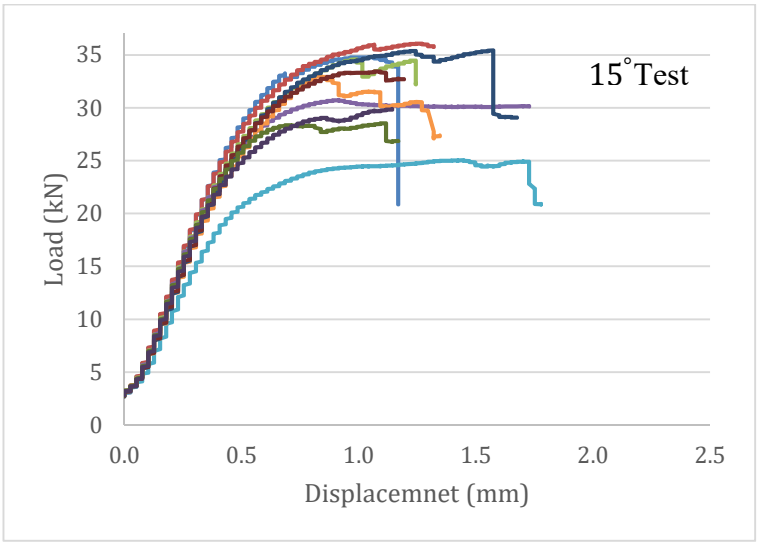

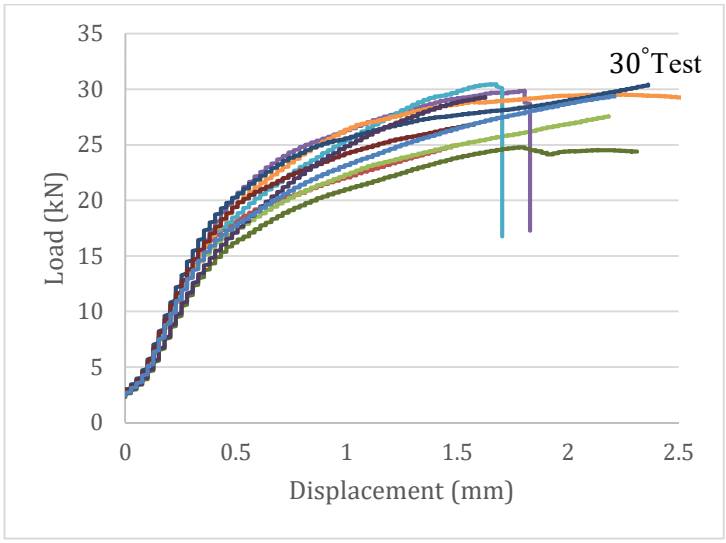

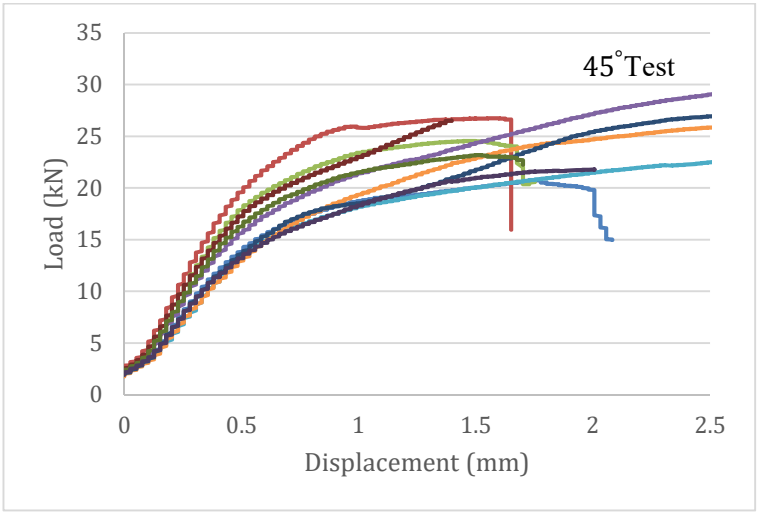

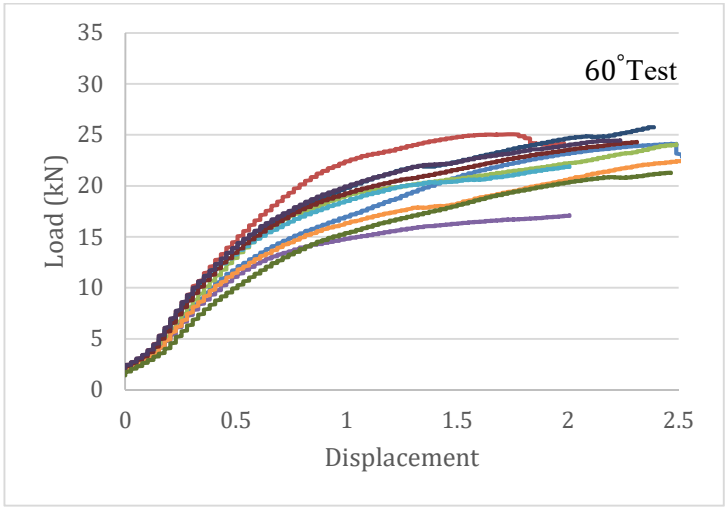

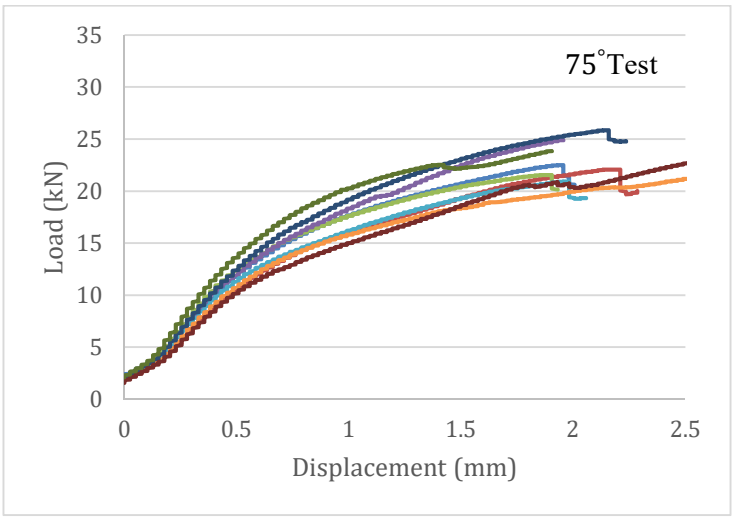

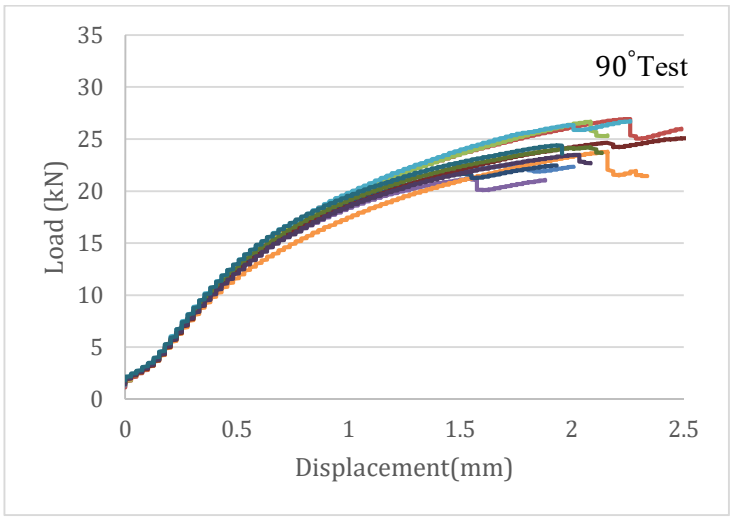

Figure 4. 5: Load-displacement curves for LVB tests at load-to-grain direction

Based on Johnson's definition, all slip curves in Fig4.5 are considered to have ductile behavior since, in each case, $D_f > 1$. However, there exists a more detailed, quantified approach to classify fastener ductility, introduced by Smith et al. (2006).(See Table 4.1). Applying this approach to the test results of the LVB dowel joint produces differing classifications of ductility as shown in Table 4.2.

Table4.1: Classification of fasteners regarding ductility ratio D_i (Smith et al. ,2006)

Classification	Ductility ratio
Brittle	$D_i \leq 2$
Low-ductility	$2 < D_i \leq 4$
Moderate ductility	$4 < D_i \leq 6$
High-ductility	$D_i > 6$

Table4.2: Calculated LVB connection ductility ratio loaded at different angles

	No. of specimens	Calculated D_i		Classification based on Smith et al.
		Lower/upper limits	Mean Value	
0°	10	1.75-4	3	Low ductility / semi-brittle
15°	10	2.1-2.6	2.3	Low ductility / semi-brittle
30°	10	3.8-4	3.9	Low / Moderate ductility
45°(a)	4	3-3.4	3.4	Low ductility
45°(b)	6	4.5-7.6	6.3	High ductility
60°	10	4-4.6	4.3	Moderate ductility
75°	10	3.8-4	3.9	Low / Moderate ductility
90°	10	4.25-5.75	5	Moderate ductility

For each load-to-grain direction, a representative load-displacement curve is given in Fig4.6. Considering together the level of ductility values in Table 4.2 and the graphical information in Fig4.5, it appears that it can generally be said that LVB dowel connections display ductile behavior when loaded at an angle to grain; however, for the lower range of angles, (less than 15degrees) there appears to be less ductility. To say definitively that angles less than a certain threshold are semi-brittle would require more tests on more angles within this lower range.

The ductility within each sample of curves is generally consistent, with the exception of the 45 degree test whereby the curves can be categorized into two groups in terms of ductility according to Table 4.2. Notably, the 45°- b group is defined as “highly ductile” and its behavior is significantly different from all other test groups.

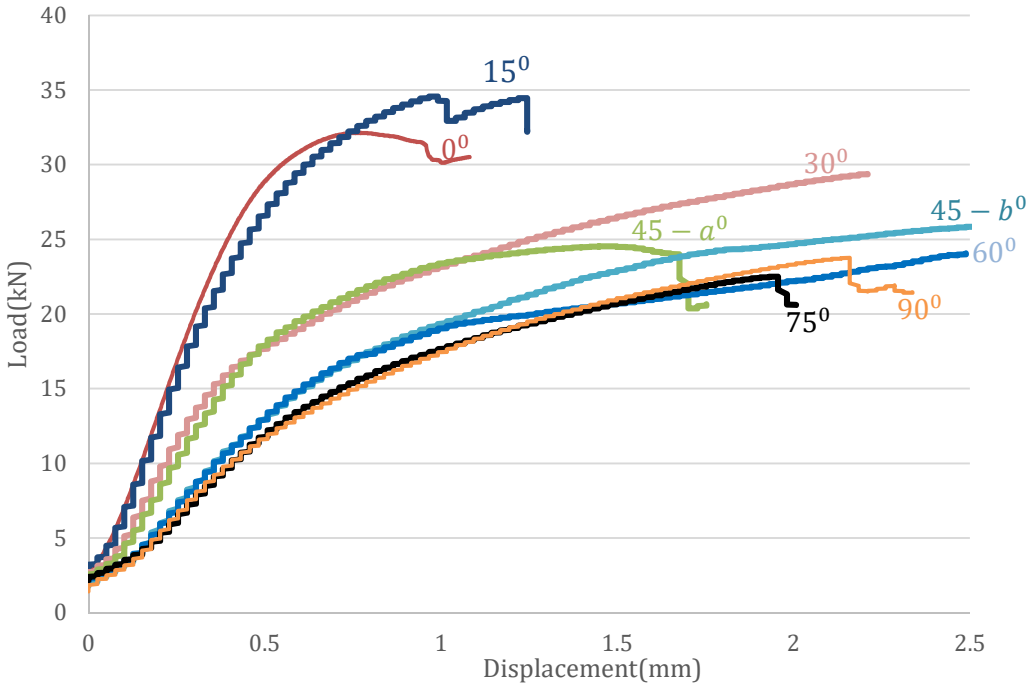

Figure 4.6: Three distinctive load-displacement behaviors: a)0°-30° b)45° c) 60-90°

4.3 Finite Element Model and Analysis

To find a more detailed explanation of failure behavior and understand the fracture behavior of LVB dowel joint under the different loading at angle-to-grain, a non-linear 3D FE model was built for 15°,30°,45°,60°,45° and 90° angles using ANSYS Mechanical APDL17.2.

For the model geometry in the FE models, the dimension of the test specimen following the ASTM D5764 standard was used to match the experimental test results.

Investigating dowel connection strength at different angles-to-grain implies that the dowel loading direction differs from the bamboo grain angle direction. This means that in the computational model, the material axes direction doesn't coincide with the global coordinate system. Hence, in this model, it wasn't possible to take advantage of symmetry so as to model half of the geometry due to asymmetrical loading (Fig4.7). Instead the full geometry was modelled.

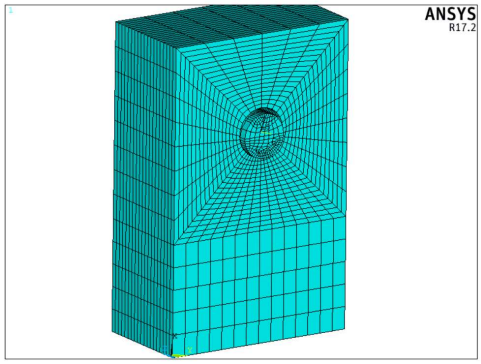

Figure4.7: geometry and meshing of FE models

Furthermore, this model was extended by a) altering the existing contact and frictional applications and settings; b) introducing new contact applications where necessary, and c) applying a new material model to comply with the current test results for the specific angle to grain loading.

The model involved 3-dimensional hexahedra homogenous 20-node elements (SOLID186) for simulating both wood and steel material.

4.3.1 Contact

Contact elements (CONTA174 and TARGE170) were employed for creating flexible surface-to-surface contact for the steel bolt and the LVB hole. Then, an Augmented Lagrange algorithm was used to solve the contact problem by implementing parameter FKN=0.1 which adjusts the contact stiffness in the contact area. The other important contact parameter, contact tolerance (FTOL), was taken to be 0.15 in accordance to descriptions given in our previous work (Khoshbakht et al. 2018). Coefficient of friction between LVB and steel dowel was assumed to be 0.2 according to (Reynolds, Sharma, Harries, & Ramage, 2016).

4.3.2 Boundary Conditions

Displacement-controlled compressive loading was applied to the steel bolt and the specimen model was fixed at the bottom. These models were subjected to the same loading protocol of the experimental test as shown in Fig4.3 allowing the computational model to simulate the connection behavior as accurately as possible.

The bolt hole diameter was modeled to be 1/16th inch larger than the bolt diameter as specified in the National Design Specification for Timber Construction (NDS 2015).

4.3.3 Material Properties

An orthotropic bilinear material model with hardening was assumed for Moso LVB. The constitutive properties were chosen from the LVB material test data (Khoshbakht et al. 2018) for the elastic region. To calculate the required parameters for the plastic region - which is defined by yield stress and tangential modulus - the average slope

and yield load of 10 embedment tests were used for each grain angle and the calculated stress and tangential modulus were incorporated in the FE model (Figure 4.8).

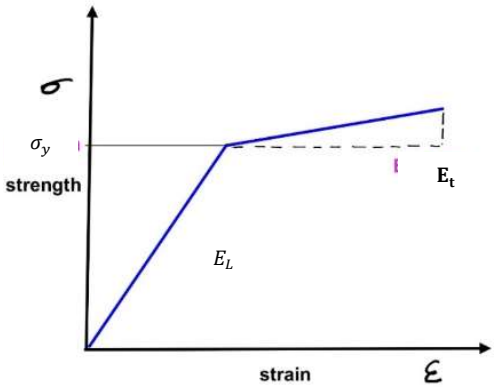

	E_L (MPa)	σ_y (MPa)	E_t (MPa)
15°	2000	49	245
30°	1290	35	177
45°	1026	26.6	111
60°	862	21.5	128
75°	602	36	135
90°	726	23.7	140

Figure4.8: Elastic-plastic material model for 15° , 30°,45°,60°,75° and 90° specimens based on embedment test curves

The Poisson ratio and shear modulus were chosen as 0.25 and 745 MPa respectively. A complete description of how this choice was made has been described in (Khoshbakht et al. 2018). The steel bolt used in the test has a nominal yield strength of 210 GPa and Poisson's ratio of 0.3.

In orthotropic material modeling, care should be taken for choosing the right direction of input material properties. Six FE models were developed and assigned to different grain angles. Six different local coordinate systems were defined to simulate models with loading at different angles to the grain. First, the model geometry was created in the global coordinate system. Then, the strongest direction of LVB material aligned with global X-axis followed by assigning the local coordinate system in a clock-wise direction for 15°,30°,45°,60°,45° and 90° to define the material coordinate system for each FE model (Fig4.9).

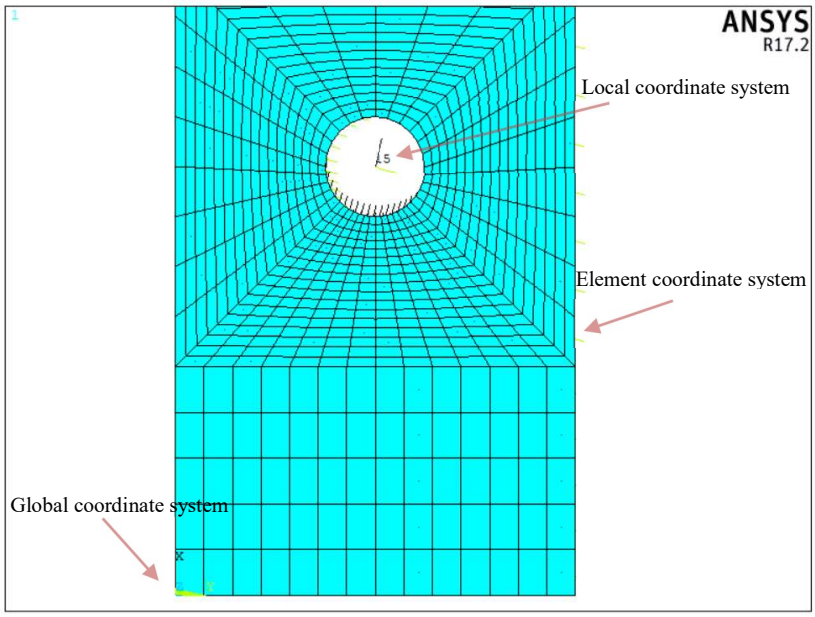

Figure4.9: Global, Local and material coordinate system in ANSYS

4.4 Results and discussion

In this chapter, we discuss the results of the six FE models to see how each model responds to loading, the stress pattern considering σ_y, τ_{xy} , and the Tsai-Wu strength criterion. These numerical results are further compared to experimental results of the respective test specimens.

As a prelude to a detailed analysis for each model, it is helpful to first explain the assumptions of the analyses. For instance, in the LVB dowel bearing test, whenever the material yields, it doesn't necessarily mean that the connection has failed. This is because in some Gauss points, when the stress passes strength, it only creates localized micro-cracks that do not lead to catastrophic failure. This is true mostly for stresses perpendicular to the grain. But, when shear stresses parallel to grain pass shear strength, they usually

create a global splitting failure in the area and largely rule the failure criteria. Shear stresses decrease dramatically in tests (as seen in Fig4.10) as the grain angle increases.

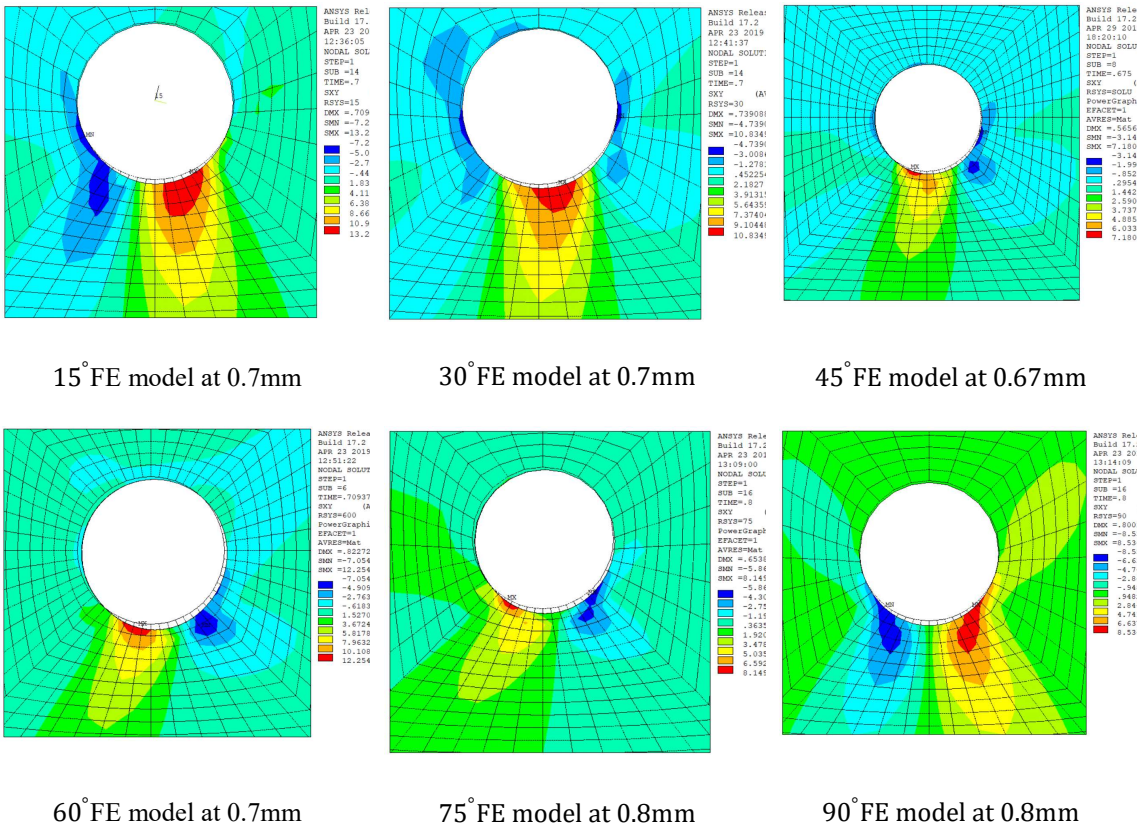

15°FE model at 0.7mm | 30°FE model at 0.7mm | 45°FE model at 0.67mm

60°FE model at 0.7mm | 75°FE model at 0.8mm | 90°FE model at 0.8mm

Figure4.10: shear stress pattern at the time of yielding for each load-to-grain direction: Shear stresses decrease as the grain angle increases

The other phenomenon that was observed in both the experimental specimens and the FE models was the horizontal deviation of dowel displacement (Fig4.11) due to stiffness differences on both sides of the loaded area in tests. As a result, the displacement measured by the MTS machine in the vertical direction does not show the precise displacement of the dowel connection (Fig4.12). Using FE results, the lateral deviation for each angle has been quantified and is shown in Fig 4.12. To quantify this lateral deviation, the displacement of the steel dowel in the horizontal direction was obtained from FE results at the time of 0.5 mm and 1mm loading. Figure 4.12 suggests that the resultant lateral

displacement does not follow a symmetric pattern for angles between 0° and 90°. Also, the initial vertical applied load changes its direction irregularly due to uneven stiffness variation in each direction (Fig4. 13) and contributes to this asymmetric displacement deviation pattern. As seen in Fig4.13, the initial vertical applied load changes its direction towards the side with lower stiffness. The most extreme displacement deviation, shown in Fig4.12, occurs for the 60° grain angle sample in which the error percentile is 16%. Based on the percent error, we decided to neglect the effect of unmeasured lateral movement for predicting the load-displacement curve and embedment strength calculations.

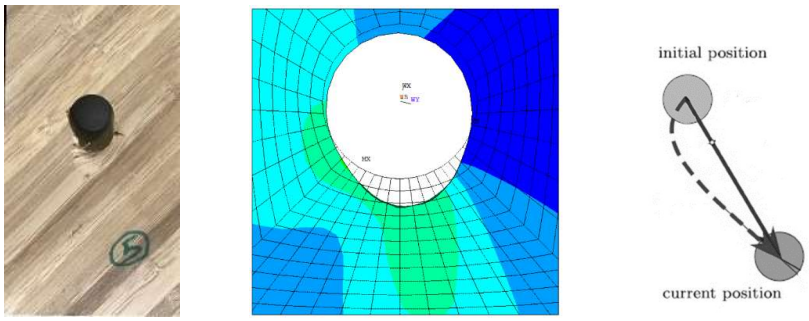

a) b)

Figure4.11: a) LVB Dowel connection loaded at angle to the grain b) The actual displacement of the dowel connection

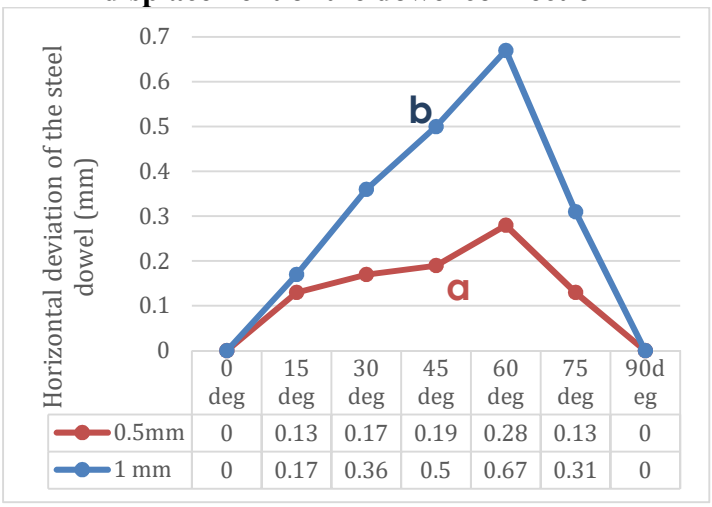

	0 deg	15 deg	30 deg	45 deg	60 deg	75 deg	90deg
0.5mm	0	0.13	0.17	0.19	0.28	0.13	0
1 mm	0	0.17	0.36	0.5	0.67	0.31	0

Figure4.12: Steel dowel lateral deviation in (mm) for each loading-to-grain angle test: a) 0.5 mm loading in vertical direction b) 1mm loading in vertical direction

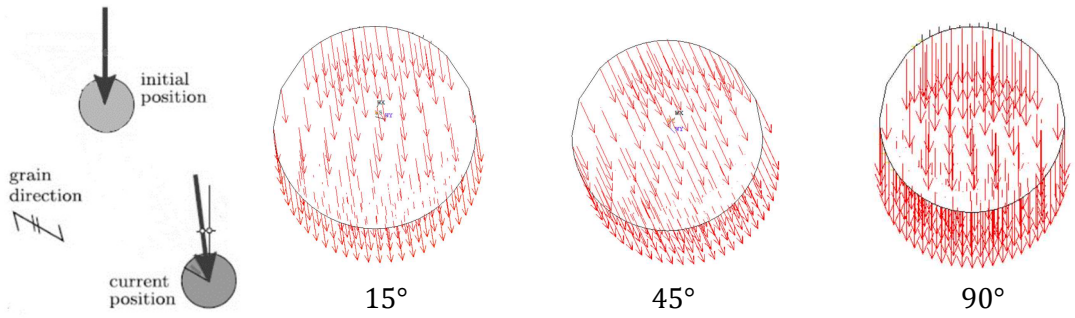

Figure 4.13: a) Change of loading direction as load increases b) Deviation of applied load for 15°,45°,90° grain angle: applied load changes its direction in a different way for different grain angles

4.4.1 Loading at 15° angle to the grain

Fig4.14 shows experiment-related information including load-displacement curves and testing assembly at the time of failure for the 15° grain angle sample. FE results are provided in Fig4.15. Considering the load-displacement curve, the dowel joints yield at 0.7 mm (using the Yasumura & Kawai model for yield point). Correspondingly, considering "0.7mm loading" for the FE results in Fig4.15, the shear stresses parallel to grain almost reach shear strength while, at the same time, the tensile stresses perpendicular to grain exceed the associated strength (5 MPa). In fact, according to FE results (Fig.4.15), tensile stresses create microscopic local cracks in the beginning (at 0.4-0.5mm loading); however, according to the load-displacement curve shown in Fig 4.14, the dowel behavior remains in elastic zone, despite the excessive tensile stresses in the perpendicular-to-grain direction. Hence, for 15° specimens, we can deduce that shear stresses are still dominant and are the primary cause of failure in the dowel joints. Comparing the test specimens under loading

in photographs (Fig4.14a) to the Tsai-Wu criterion (Fig 4.15b), the criterion appears to work well for predicting the failed area underneath the dowel surface at 0.7 mm loading.

a)

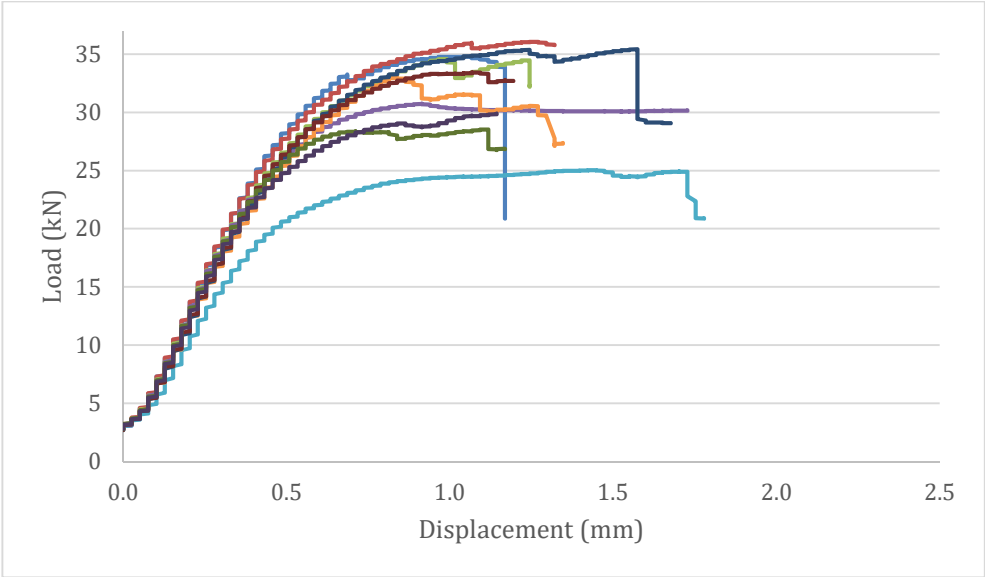

b)

Figure4.14: 15° grain angle: a) testing assembly at the time of failure and b) load-displacement curves

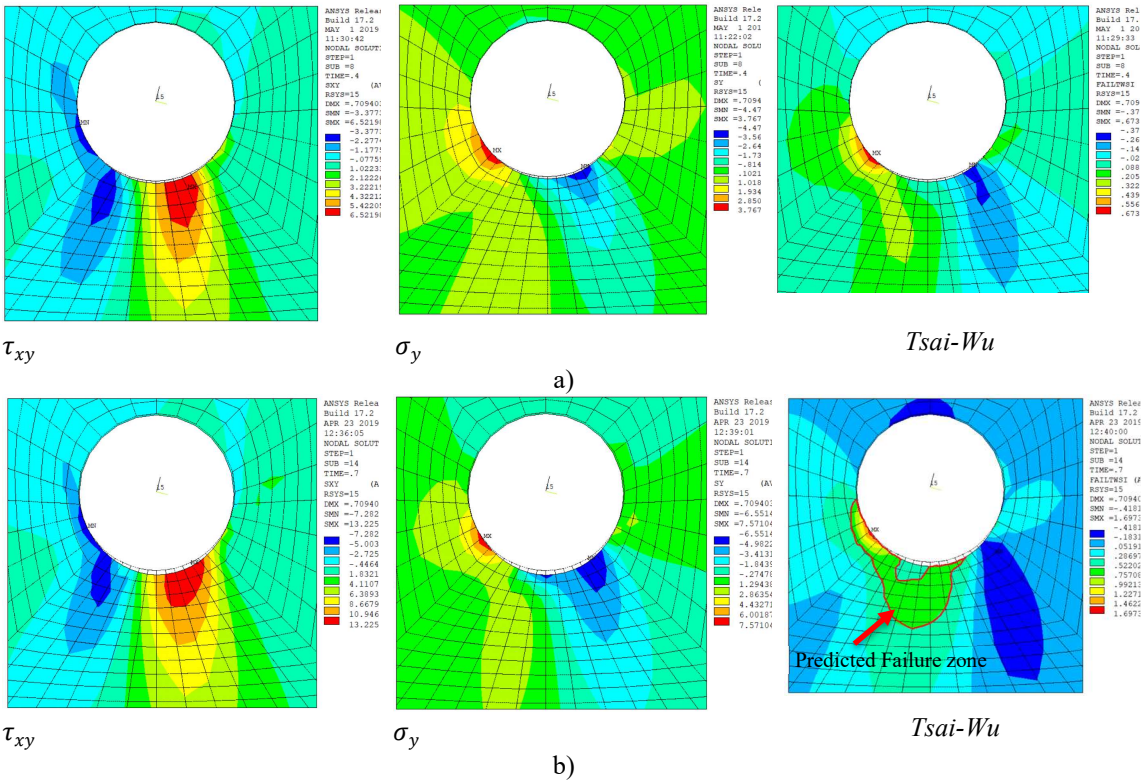

Figure4.15:15° grain angle: FE results a) in elastic zone (at .4mm loading) b) at failure (at .7mm loading)

4.4.2 Loading at 30° angle to the grain

As shown in Fig4.16a, a small crack started to develop around 0.5 mm loading on the lower left side of the hole followed by another small crack on the right side. The LVB consistently displayed ductile behavior, with the exception of specimens 3 and 4 (blue and purple curves in Fig.4.16 b), which failed with a shear split through the specimen.

a)

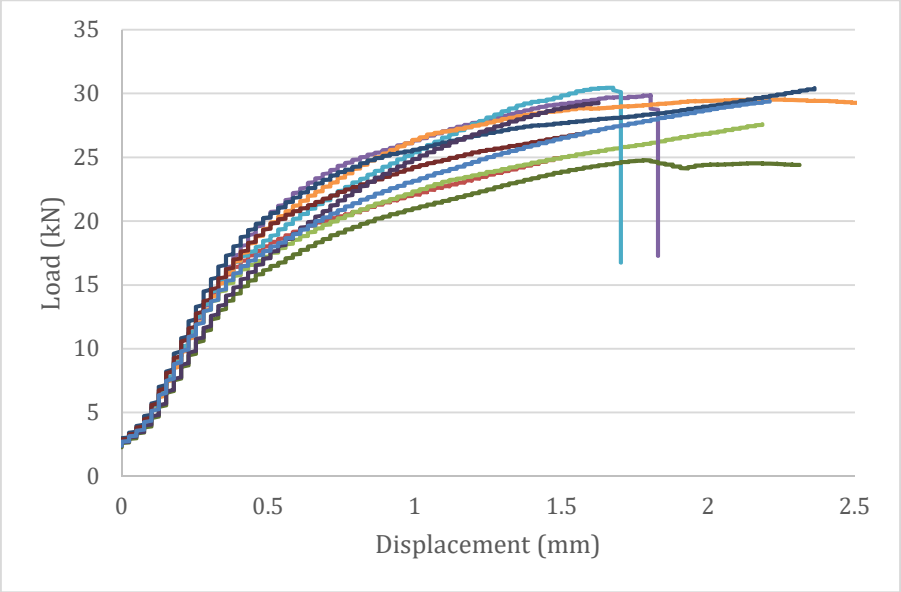

b)

Figure4.16:30° grain angle: a) testing assembly at the time of failure and b) load-displacement curves

The FE results suggest that the LVB material yields at 0.7 mm loading, in which case only tensile stresses exceed strength; whereas, shear stresses do not contribute to failure anymore. However, at 1mm loading, because of high shear stress contribution, (Fig4.17b) a crack can develop leading to brittle behavior, as occurred in specimens 3 and 4..

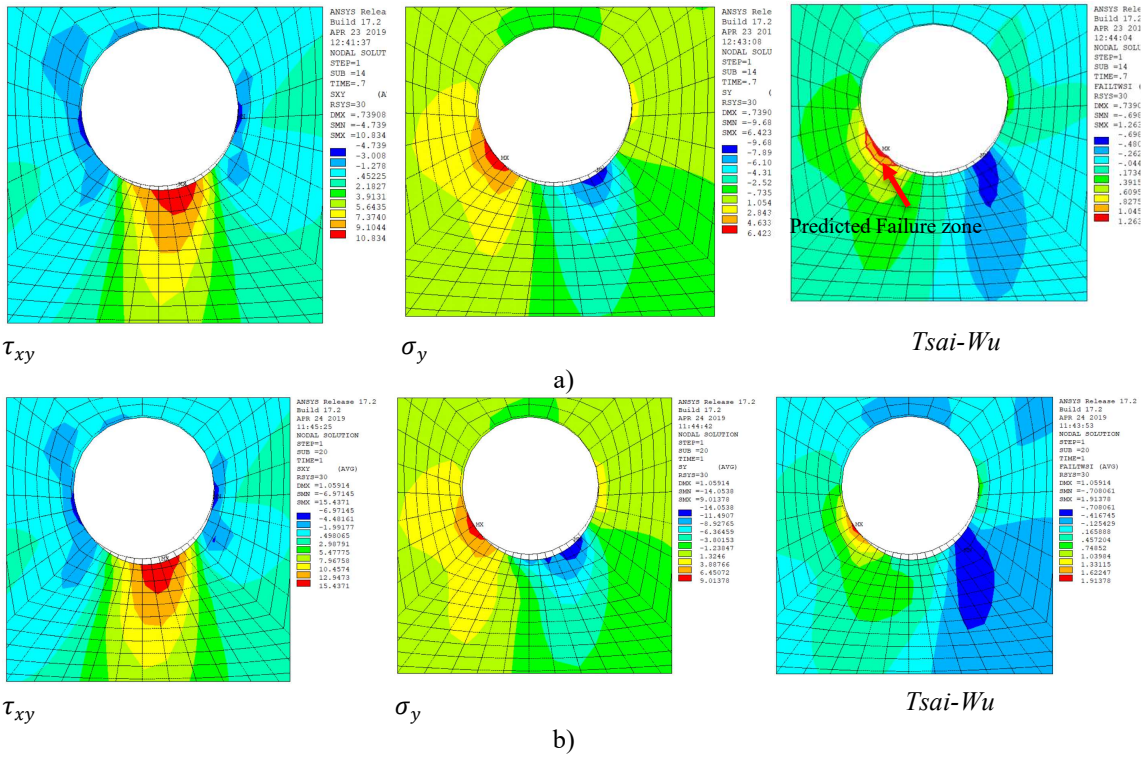

Figure4. 17: 30° grain angle: FE results a) at .7mm loading b) at1mm loading

4.4.3 Loading at 45° angle to the grain

When the connection yields (around 0.7 mm loading), the picture of the specimen under the loading in Fig4.18a shows the appearance of cracks in the lower left side of the connection which is, again, in agreement with the FE model, as seen in Fig4.19.

Fig4.19 shows that these cracks are the result of higher tensile stresses in the lower left corner. Shear stresses are too low at the time of yielding and has minimal contribution to the failure of LVB dowel joint. However, as seen in Fig4. 18b and corroborated by the FE results (Fig4.19b), as the loading increases past 1mm deformation, fracture occurs in the LVB due to high shear stresses parallel to the grain.

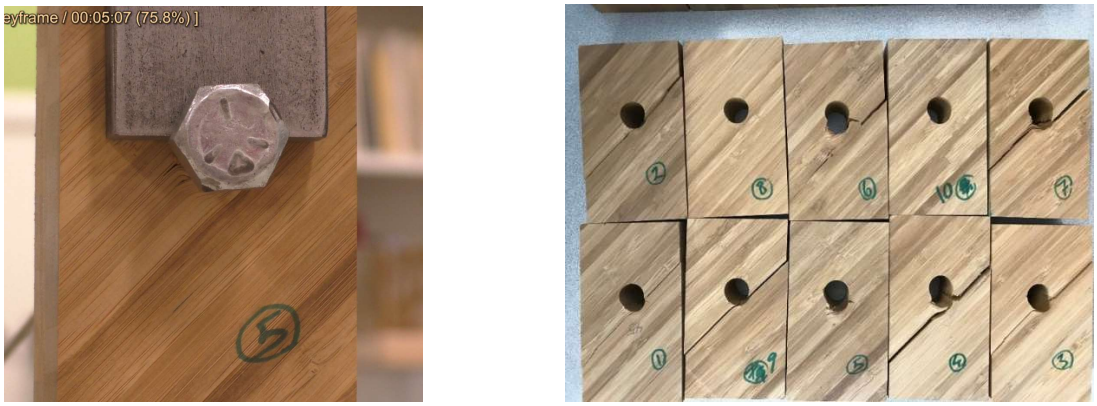

a)

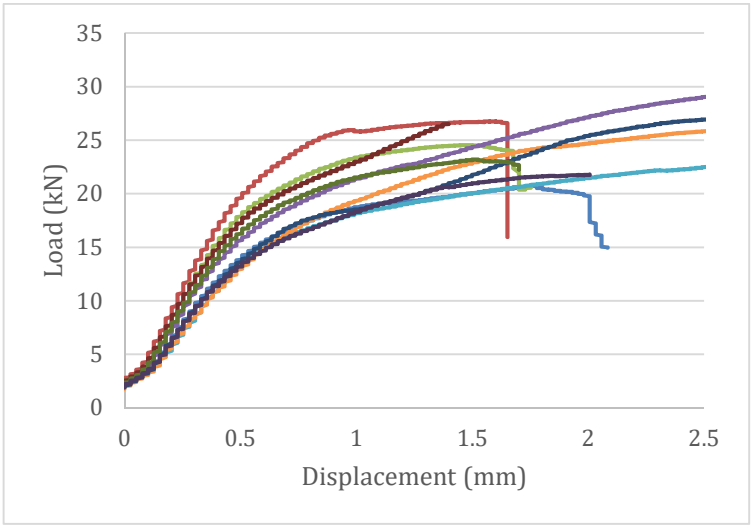

b)

Figure4. 18: a) testing assembly at the time of failure and b) load-displacement curves

4.4.4 Loading at 60°, 75° and 90° angle to the grain

For loading at 60°, 75° and 90° angle to the grain, the dowel connection behavior is almost the same as for the 45 degree (Fig4.20a), with an increasing ductility rate as the loading angle goes up. Also, the yield strength decreases as the grain angle increases.

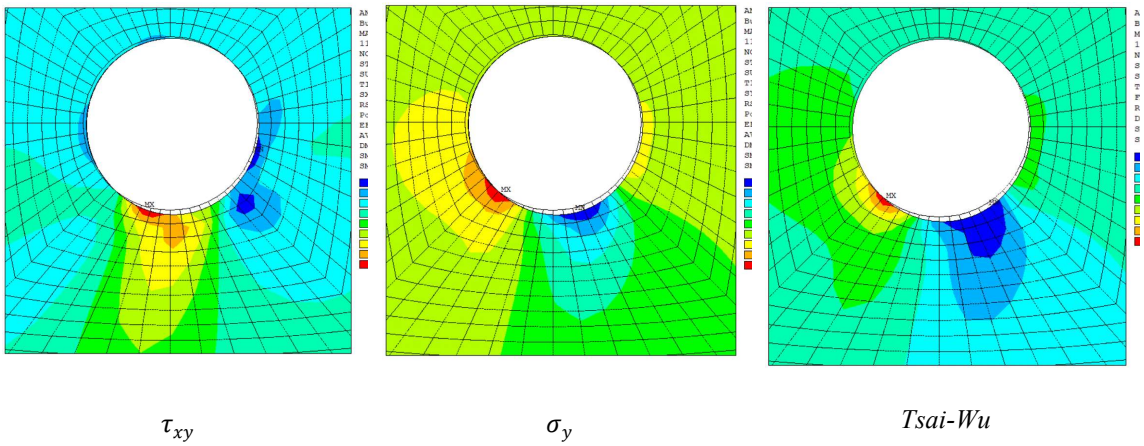

a)

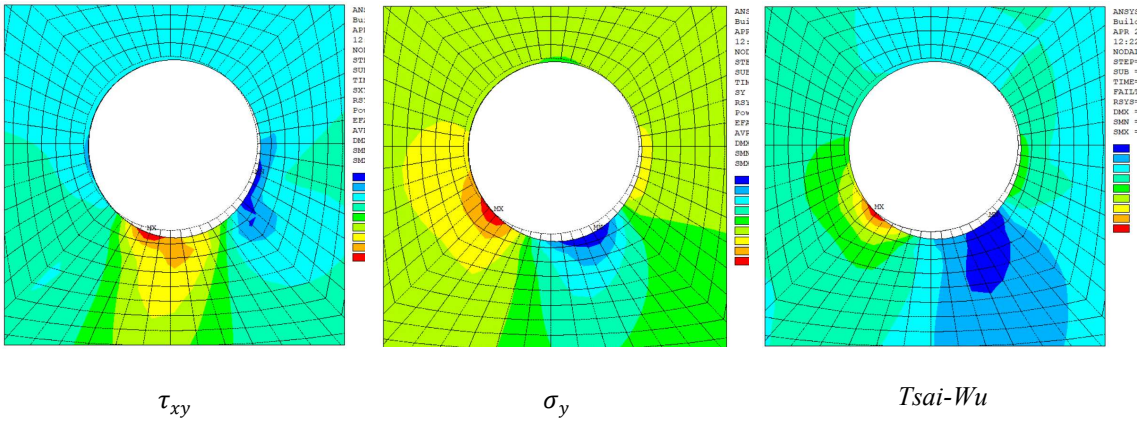

b)

Figure4. 19: 45° grain angle FE results a) at failure (0.67mm loading) b) at1mm loading

Fig4.21 and Fig4.22 show shear stress parallel and tensile stress perpendicular to grain pattern at the yielding onset for each loading-at-angle test set up. Considering data shown in Fig4.20 and Fig4.21 and Fig4.22, the dowel behavior for 60°, 75° and 90° grain angle is to be expected: first, a tiny crack starts in the lower left corner due to tensile stresses perpendicular to the grain and then the material underneath the contact surface densifies toward the direction of lower stiffness in the material. After local densification formation, the cracks in the perpendicular direction begin to propagate until the LVB material fails.

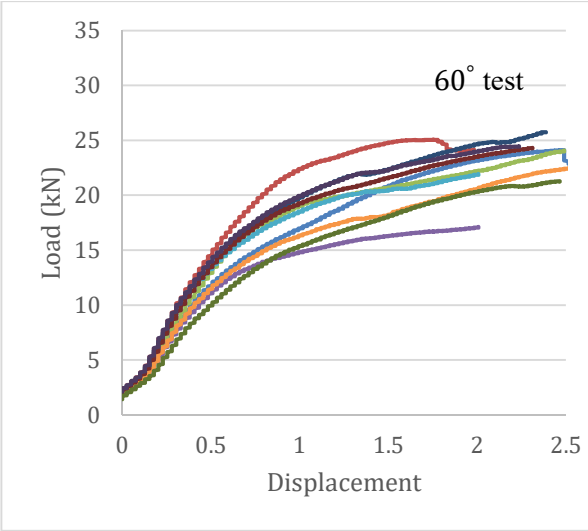

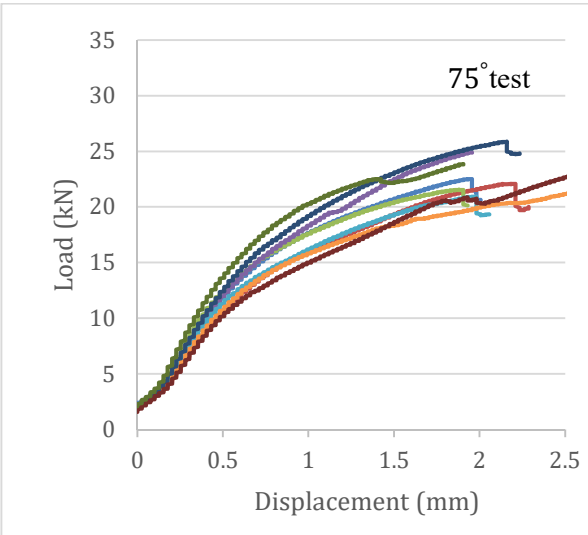

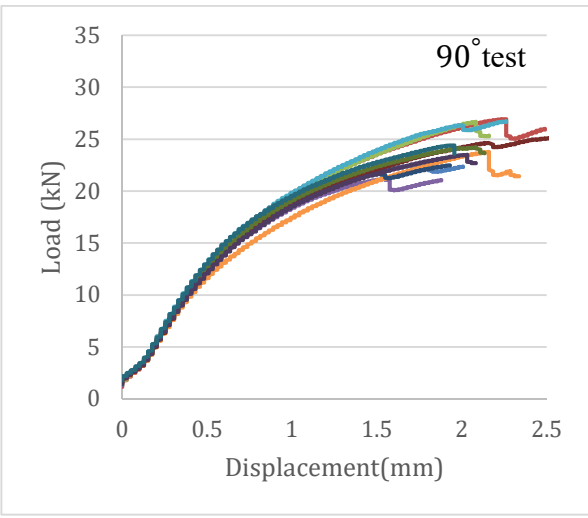

Figure4.20: loading at 60°,75°,90° angle to the grain a) load-displacement curves b) failed specimens

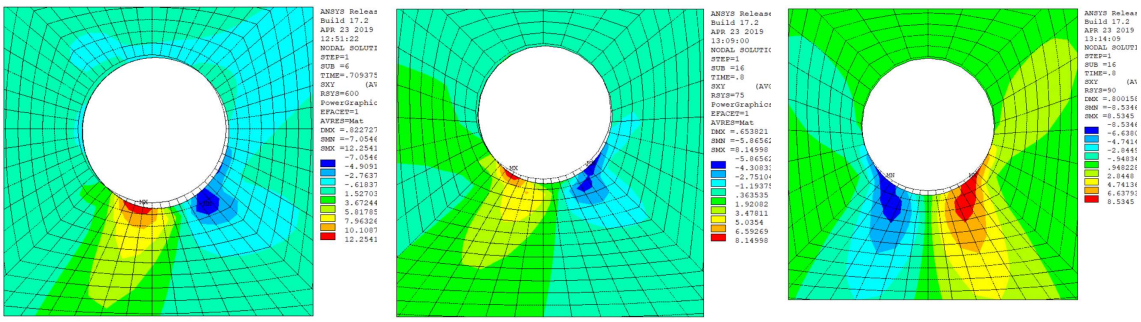

60° FE model at 0.7mm 75° FE model at 0.8mm 90° FE model at 0.8mm

Figure4.21: Shear stress pattern for 60° ,75° and 90° grain angle

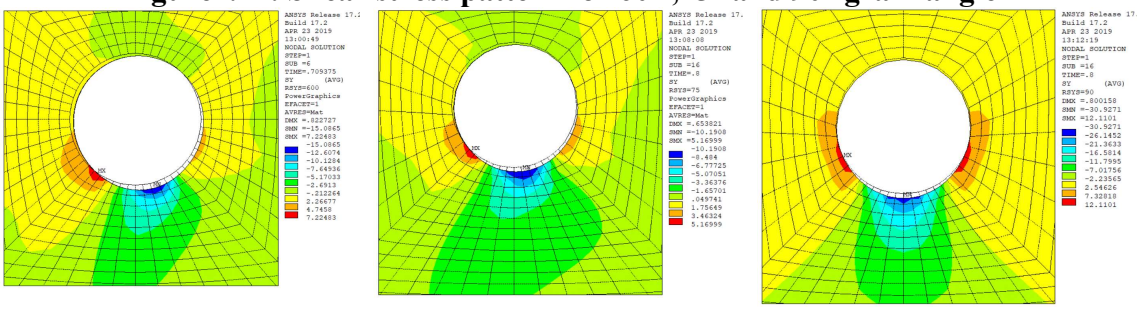

60° FE model at 0.7mm 75° FE model at 0.8mm 90° FE model at 0.8mm

Figure4. 22: Tensile stresses perpendicular to grain for 60°,75° and 90° grain angle

4.5 Evaluation of Hankinson equation for LVB dowel connection

Before proposing a model for predicting LVB dowel connection failure when loaded at an angle to the grain, it is informative to first review both Hankinson and Tsai-Hill criteria as they are the most widely used formula for off-axis loading.

4.5.1 Decision process for chosen failure criteria

4.5.1.1 Hankinson equation

If we consider biaxial stress in an orthotropic material, the simplest way to address the strength interaction criterion is to use a linear form:

$$\frac{\sigma_1}{s_L} + \frac{\sigma_2}{s_T} + \frac{\tau_{12}}{s_{LT}} = 1 \quad (4.1)$$

For off-axis stress state at angle θ, after transformation of stresses (as detailed in Appendix A), we have:

$$\sigma_1\left(\frac{\cos^2\theta}{s_L} + \frac{\sin^2\theta}{s_T} + \frac{\cos\theta\sin\theta}{s_{LT}}\right) = 1 \quad (4.2)$$

Hankinson formula is an empirical formula developed from Equation 1.4 which has excluded the shear term. This was done because with wood products, the interaction equation was found to be insensitive to shear stress.

$$\sigma_1 = s_\theta \rightarrow s_\theta = \frac{s_L s_T}{s_L \sin^2\theta + s_T \cos^2\theta} \quad (4.3)$$

s_θ: $failure\ strength\ at\ angle\ \alpha$ in the loading direction

The Hankinson formula has been widely used (Hankinson, 1921) as a method to predict unidirectional strength at different angles-to-grain loading for wood and wood products.

The most widely used criterion for timber, glulam and LVL products, it was adopted by Eurocode 5 (BSI, 2009) and the NDS for wood construction (NDS,2015).

The Hankinson formula has been generalized as shown in Equation 1.7 in which the term *n* is a constant that is determined from experiments. For the original Hankinson equation, which is based on studies of spruce (Hankinson,1921), *n* equals to 2. It has since been used for many structural wood species. However, for the general formulation, the value *n* can differ based on different strength ratios in orthotropic directions and loading types

(compression and tension) and the range of its variation can be found in the literature (Wood Handbook 2010).

$$s_\theta = \frac{s_L s_T}{s_L \sin^n \theta + s_T \cos^n \theta} \tag{4.4}$$

4.5.1.2 Tsai-Hill Criterion

In general, the general Quadratic failure criterion can be simply written in the form of an ellipsoid:

$$\left(\frac{\sigma_1}{s_L}\right)^2 + \left(\frac{\sigma_2}{s_T}\right)^2 + \left(\frac{\tau_{12}}{s_{LT}}\right)^2 = 1 \tag{4.5}$$

This Quadratic criterion is a modified version of Von Mises (Maximum distortional energy) criterion in which the effect of material anisotropy is considered (Gibson,1994). For a 2D planar surface, the Quadratic criterion has been generalized and extended in the form of the Tsai- Hill criterion:

$$\frac{{\sigma_1}^2}{{s_L}^2} - \frac{\sigma_1 \sigma_2}{{s_L}^2} + \frac{{\sigma_2}^2}{{s_T}^2} + \frac{{\tau_{12}}^2}{{s_{LT}}^2} = 1 \tag{4.6}$$

Again for off-axis stress state at angle θ, after transformation of stresses (as detailed in Appendix B) we have:

$$\frac{(\sigma_x (\cos\theta)^2)^2}{{S_L}^2} - \frac{(\sigma_x \sin\theta \cos\theta)^2}{{S_L}^2} + \frac{(\sigma_x (\sin\theta)^2)^2}{{S_T}^2} + \frac{(\sigma_x \cos\theta \sin\theta)^2}{{S_{LT}}^2} = 1$$

$$\sigma_x = \left[\frac{(\cos\theta)^4}{{S_L}^2} - \left(\frac{1}{{S_L}^2} - \frac{1}{{S_{LT}}^2}\right)(\sin\theta)^2(\cos\theta)^2 + \frac{(\sin\theta)^4}{{S_T}^2}\right]^{-1/2} \tag{4.7}$$

4.5.1.3 Tsai-Hill vs. Hankinson Criterion

In summary, the following two equations were employed to evaluate the angle to grain test results:

Hankinson (uniaxial test):

$$\sigma_X\left(\frac{\cos^2\theta}{s_L}+\frac{\sin^2\theta}{s_T}\right)=1 \tag{4.8}$$

Tsai-Hill (uniaxial test):

$$\sigma_x{}^2\left[\frac{(\cos\theta)^4}{S_L{}^2}-\left(\frac{1}{S_L{}^2}-\frac{1}{S_{LT}{}^2}\right)(\sin\theta)^2(\cos\theta)^2+\frac{(\sin\theta)^4}{S_T{}^2}=1\right. \tag{4.9}$$

It is important to note that:

- Neither of these two criteria can account for differences between tensile and compressive strengths.
- There is no coupling term between normal stresses to account for interaction between terms in either criteria.

As a way to visualize and contrast some of these equations, Fig4.23 depicts tensile strength vs. angle to grain for different thicknesses of OSB panels (Aicher and Klöck 2001). It can be seen that the quadratic interaction criterion results are closer to experimental data (being a more flexible criterion) while the linear criterion is too conservative but consistently so for every angle.

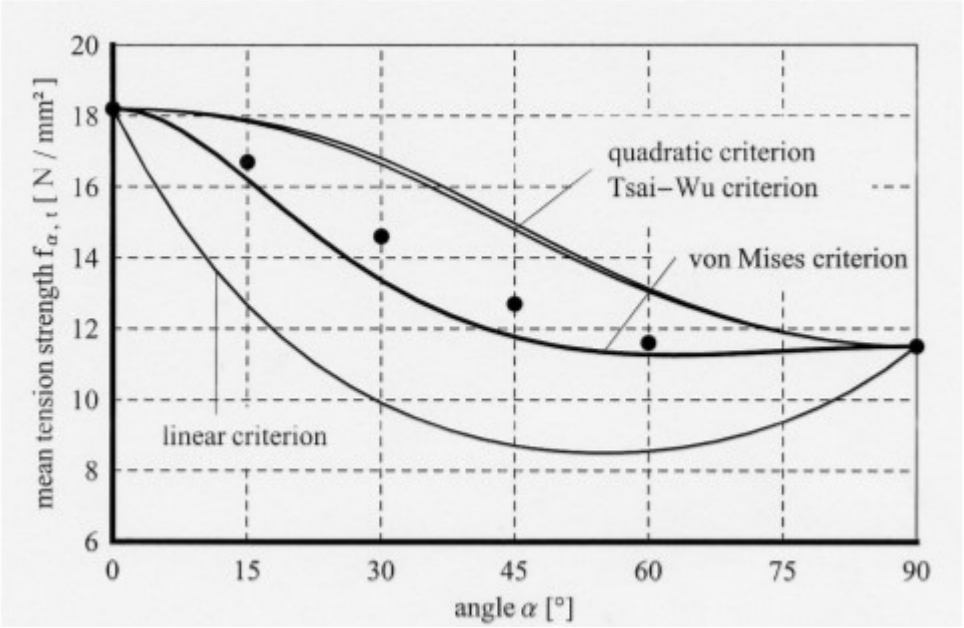

Figure4.23: off-axis tension strength of OSB panels for different strength criteria (Aicher,S. Klöck,W. , 2001)

Since the intent of this work is to devise a formula that can be safely used by engineers and designers, a linear interaction criterion was deemed the most practical; hence, the Hankinson formula for LVB dowel strength evaluation was chosen moving forward.

4.5.2 LVB dowel experimental data analysis

Using the test data from a total of 70 specimens, as described in section 4.2, statistics were generated for various parameters. The range of embedment strengths and the average for each angle were plotted against grain angle (Fig4.24).

Fig4.24 shows the strength of LVB dowel connections at different load-to-grain directions of 0°, 15° ,30°,45°, 60°, 75° and 90° angle. For each load-to-grain direction, 10 specimens were tested in accordance with the ASTM D5764 method. This was followed

by ANOVA analyses to statistically test for differences between the samples' means (Appendix C).

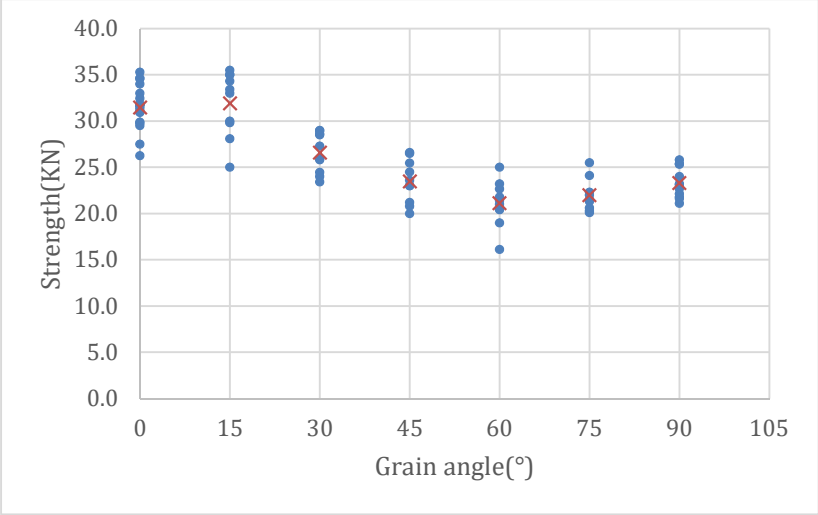

Figure4.24: LVB dowel connection strength at different load-to-grain directions based on ASTM D5764

To find the best theory that explains the LVB behavior at different load-to-grain directions, the experimental mean values (shown in Fig4.25) were compared to results of Hankinson and Tsai-Hill criterion for the off-axis test (Fig4.26)using LVB material properties attained through LVB dowel tests.

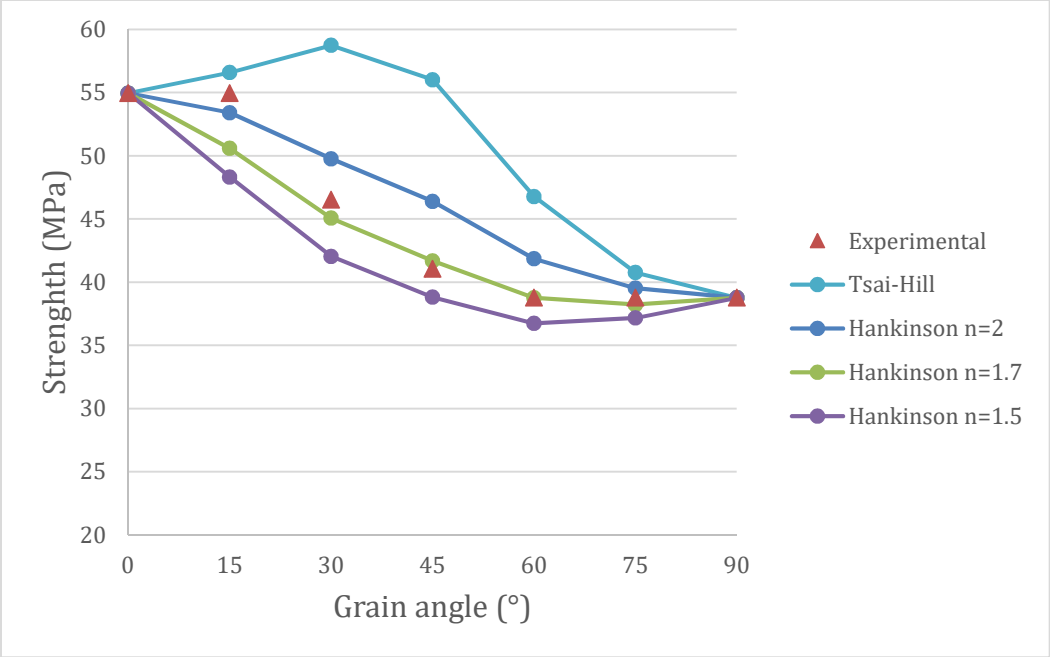

Figure4.25: Comparison of LVB dowel strength test results with most relevant failure theories applied to LVB material

As shown in Fig4.25, the Tsai-Hill failure criterion overestimates the strength of LVB loaded at different load-to-grain directions. The original Hankinson equation (n=2) does the same except the strength is particularly lower than experimental data for 15°angle. The Hankinson equation with n=1.7 curve is the closest curve to experimental data. Nonetheless, to be on the safe side the best choice for prediction of LVB dowel joints would be Hankinson equation with n=1.5.

By choosing n=1.5 the strength at 15° will be underestimated by 12 % which is acceptable since using the adjusted formula with n=1.5 leads us to the safer design of LVB dowel connection towards the end. However, it is statistically hard to claim that the taken sample size is a true representative for the entire LVB product population and more samples are needed from different batches to draw robust conclusion. Also, different dowel diameters are needed to be tested to achieve revised Hankinson formula for LVB dowel connection.

CHAPTER 5

CONCLUSION AND RECOMMENDATIONS

5.1 Introduction

The intention of this dissertation was to study the failure behavior of LVB dowel connections, which will contribute to safer design and implementation of LVB bolted connections and the development of a standard test method for LVB dowel connections. To achieve this goal, we followed these steps:

First, a series of experimental tests were conducted to measure tension, compression, and shear properties of LVB which were further used as input into the finite element material model.

Second, a preliminary study on LVB dowel connection was done using a 2D elastic, plane strain finite element model developed for a 15.9mm (5/8th inch) diameter bolt with a bolt hole size of 17.5mm (11/16th inch) following a full-hole specimen protocol per ASTM D5764. Full-hole tests were conducted in accordance with ASTM D5764 and the finite element model was calibrated to match experimental results. Verified FE model was then used to inspect stress distributions at various levels of displacement in the critical zone under the bolt. The model included contact elements assuming a rigid-target contact problem between the bolt and the LVB leading to new information about frictional effects.

Third, the ASTM D5764 standard for testing dowel connections provides a procedure for measuring dowel-bearing strength of wood and wood-based products. Two test methods offered by ASTM5764 standard: full-hole and half hole specimen. A quantitative comparison between these two test methods offered by ASTM5764 standard for wood-

based products was carried out to see if the same condition holds for LVB dowel connections. Then the most appropriate test was chosen to be the basis for modeling FE representations and fabricating LVB test specimens. For the purpose of this study, 3D bilinear finite element models for half-hole and full-hole specimens were incorporated in accordance with ASTM D5764 when loaded in compression parallel-to-grain followed by experimental investigation of two ASTMD5764 methods.

The effect of friction on the contact surface of our 3D FE model was also studied to see if it complies with what has been advised in the literature.

Finally, the bearing strength of any wood dowel connection is influenced by the angle of the load to grain direction and laminated veneer bamboo (LVB) is not an exception. In the final chapter, the dowel bearing strength of LVB has been characterized by loading test specimens at different angles to the grain. Then a 3-dimensional FE model was developed for each load-to-grain direction. The failure behavior of LVB material in each setting was explained using stress patterns and Tsai-Wu failure criterion around the bolt hole. Using LVB embedment strength data attained from the tests, the Hankinson formula and Tsai-Hill criteria were evaluated to see if they can be used as an engineering tool to estimate LVB embedment strength at any loading-at-angle to the grain and finally a revised Hankinson equation was proposed for further engineering applications.

5.2 General conclusions

For the purpose of investigating the embedment response of LVB when loaded by a steel dowel in compression parallel-to-grain,a Finite element model was built to simulate this test, was calibrated to match experimental results, and was then used to inspect stress

distributions at various levels of displacement in the critical zone under the bolt. The model was novel in that it included contact elements assuming a rigid-target contact problem between the bolt and the LVB leading to new information about frictional effects.

The key findings of this study were as follows:

- In calibrating the Finite Element model, it was found necessary to define a functional local modulus of elasticity (E_L) to be used in place of bulk modulus (E_B), the two values differing by a factor of about 10.2 (1,140MPa vs 11,600MPa). This calibration approach is consistent with that conducted in a previous study on Guadua Bamboo by Ramirez et al. (Ramirez, Correal, Yamin, Atoche, & Piscal, 2012).

- The FE model predicted that the LVB dowel joint begins to fail at approximately 0.95 mm of applied displacement, matching experimental results within reasonable limits of statistical variability.

- Both the experimental and FEM results indicate that in-plane shear stress was the primary cause of LVB failure through concurring measures of both failure load and location. Failure typically occurred off hole center, at 1/6th of the hole perimeter left or right of center, which according to the FEM is in the high shear stress zone where tension perpendicular-to-grain stresses were moderate. The model further elucidates that with each load increment, the location of maximum shear stress moves further outward from the hole center and further underneath the contact surface.

- Tension perpendicular-to-grain stresses were shown to be a secondary contributing factor to failure. Maximum tensile stress occurred 7.4mm beneath the

hole, at the center of the contact region with an increasingly heightened distribution as applied displacement increased.

- The FE model showed high sensitivity to frictional forces indicating that they play an important role in how the model predicts the location of maximum shear stresses. It is suggested that future studies delve further into this area of how coefficient of friction between the steel bolt and LVB material influence LVB failure.

After a preliminary study of LVB dowel joints, ASTM full and half-hole methods were evaluated using LVB material properties. After performing a mixed mode analysis of internal stresses and investigating the LVB fracture behavior in experiments, both FE and experimental analysis revealed a noticeable difference between the failure behavior of LVB full and half-hole dowel joints: for full-hole specimen a combination of shear stresses (as the main cause of failure) and tensile stresses perpendicular-to-grain (as a secondary cause of failure) is responsible; while for half-hole specimens, shear stresses parallel-to-grain dominate failure.

It was also shown, both numerically and experimentally, that for the same applied displacement, the half-hole specimen fails at slightly less displacement than full-hole specimens, despite higher load bearing capacity and stiffness. This is because for half-hole specimen, the high internal shear stresses exceed shear strength sooner than it occurs for the full-hole specimen. This suggests that higher dowel stiffness and load bearing capacity does not lead to a stronger joint design for the displacement-based loading.

The dowel bearing strength of LVB at different angles to grain was also studied both numerically and experimentally and results are as follows:

- In some cases when stress passed strength in FE model, only local cracks appeared on the real specimen. In other word the specimen didn't fail at that point and as the loading increased, the dowel failed in different locations which was predicted by Tsai-Wu criterion in FE model. Eventually, the FE models' prediction of displacement at failure was confirmed through comparison with experimental results.
- Results from finite element models revealed that 15° grain angle behaves almost like parallel grain angle in which shear stresses parallel to the grain were the main cause of failure (khoshbakht et al. 2018) while for 30°,45°,60°,75° and 90°grain angle the connection failed due to high tensile stresses perpendicular to the grain.
- Also based on experimental data the connection ductility in each grain angle test setting was studied. Semi-brittle behavior was noticed for 0°,15° grain angle and for 30°,45°,60°,75° and 90°ductile behavior was observed.
- In conclusion, LVB dowel connection behavior could be considered ductile rather than brittle which makes it a good choice for connection design application especially when loaded at an angle to the grain direction.

Finally, using LVB embedment strength data attained from the tests, the Hankinson formula was evaluated and revised to fit LVB experimental data. It was found that using n=1.5 in the general formulation, leaves Hankinson equation a decent tool for designing LVB dowel connection loaded at any angle to the grain. However, it is important to remember that we used the method described in ASTM D5764 to achieve yielding point and consequently embedment stress as the original Hankinson equation follows the same method.

5.3 Recommendations

In view of all mentioned above, the authors recommend that only the full-hole specimen test procedure be used to evaluate LVB dowel joint behavior as it more closely represents real-life connections conditions.

In this dissertation, a 15.9mm (5/8th inch) diameter bolt with a bolt hole size of 17.5mm (11/16th inch) was used to represent the mode I failure in the dowel connection since our focus was on the wood failure underneath the dowel. The same approach might be applied for different diameters to achieve a better understanding of the LVB connections and finding a cohesive interrelation among the strengths when the connection is loaded at different angles to the grain. The effect of width-to-diameter ratio for LVB dowel connection was not investigated in this study and might be considered as the future study to expand existing knowledge of LVB connection characteristics.

It has been advised in the literature to incorporate the frictional property of the dowel in the standard dowel test methods. Contrary to the findings for typical wood connections, as was mentioned in the third chapter since the failure mechanism of LVB dowel joint is different from timber and shear stresses are determinant factor for the strength calculations, further experimental program is suggested to see the importance of surface smoothness in LVB and other engineered wood materials with similar orthotropic properties.

APPENDICES

APPENDIX A

FINDING OFF-AXIS STRESS STATE FOR LINEAR STRENGTH INTERACTION DRITERION

For calculating Hankinson formula, one can start from linear form of strength interaction criterion. This is a linear strength interaction criterion form for biaxial test:

$$\frac{\sigma_1}{s_L}+\frac{\sigma_2}{s_T}+\frac{\tau_{12}}{s_{LT}}=1 \qquad (1)$$

For off-axis stress state at angle θ, after transformation of stresses equation (2) is resulted from equation (1).

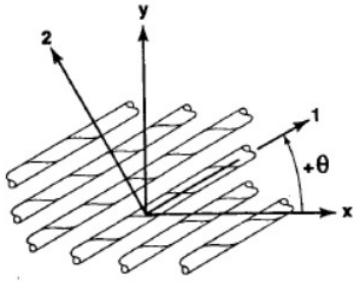

$$\begin{Bmatrix}\sigma_1\\ \sigma_1\\ \tau_{12}\end{Bmatrix}=[T]\begin{Bmatrix}\sigma_x\\ \sigma_y\\ \tau_{xy}\end{Bmatrix},\ [T]=\begin{bmatrix} c^2 & s^2 & 2cs\\ s^2 & c^2 & -2cs\\ -cs & cs & c^2-s^2\end{bmatrix}$$

Where c=cos θ and S =sin θ

For off-Axis test:

$$\frac{(\sigma_x\,(\cos\theta)^2)^2}{{S_L}^2}-\frac{(\sigma_x\sin\theta\cos\theta)^2}{{S_L}^2}+\frac{(\sigma_x(\sin\theta)^2)^2}{{S_T}^2}+\frac{(\sigma_x\ \cos\theta\ \sin\theta)^2}{{S_{LT}}^2}=1$$

$$\frac{\sigma_1}{s_L}+\frac{\sigma_2}{s_T}+\frac{\tau_{12}}{s_{LT}}=1$$

And

$$\begin{cases}\sigma_1=\sigma_x\,(\cos\theta)^2+\ \sigma_y(\sin\theta)^2+2\tau_{xy}\cos\theta\sin\theta\\ \sigma_2=\sigma_x\,(\sin\theta)^2+\ \sigma_y(\cos\theta)^2-2\tau_{xy}\cos\theta\sin\theta\\ \tau_{12}\ =-\cos\theta\sin\theta\ \ \sigma_x+\sigma_y\cos\theta\sin\theta+\tau_{xy}((\cos\theta)^2-(\sin\theta)^2)\end{cases}\xrightarrow{\sigma_y=0\ and\ \tau_{xy}=0}$$

$$\sigma_X\left(\frac{\cos^2\theta}{s_L}+\frac{\sin^2\theta}{s_T}+\frac{\cos\theta\sin\theta}{s_{LT}}\right)=1 \qquad (2)$$

$\sigma_X = uniaxial\ stress$

APPENDIX B

FINDING OFF-AXIS STRESS STATE AT ANGLE θ FOR QUADRATIC FAILURE CRITERION

For 2D planar surface, the Quadratic criteria has been generalized and extended in form of Tsai- Hill criterion:

$$\frac{{\sigma_1}^2}{{S_L}^2} - \frac{\sigma_1\sigma_2}{{S_L}^2} + \frac{{\sigma_2}^2}{{S_T}^2} + \frac{{\tau_{12}}^2}{{S_{LT}}^2} = 1 \qquad (5)$$

To find off-axis stress state at angle θ, stresses will be transformed :

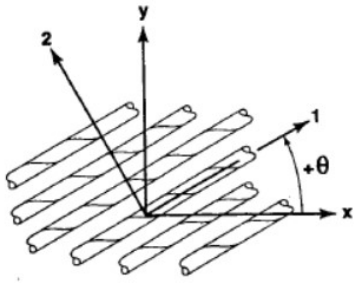

$$\begin{Bmatrix}\sigma_1\\ \sigma_1\\ \tau_{12}\end{Bmatrix} = [T]\begin{Bmatrix}\sigma_x\\ \sigma_y\\ \tau_{xy}\end{Bmatrix}, \quad [T] = \begin{bmatrix} c^2 & s^2 & 2cs \\ s^2 & c^2 & -2cs \\ -cs & cs & c^2 - s^2 \end{bmatrix}$$

Where c=cos θ and S =sin θ

Considering condition below for off-axis test:

$$\begin{cases} \sigma_1 = \sigma_x(\cos\theta)^2 + \sigma_y(\sin\theta)^2 + 2\tau_{xy}\cos\theta\sin\theta \\ \sigma_2 = \sigma_x(\sin\theta)^2 + \sigma_y(\cos\theta)^2 - 2\tau_{xy}\cos\theta\sin\theta \\ \tau_{12} = -\cos\theta\sin\theta\ \sigma_x + \sigma_y\cos\theta\sin\theta + \tau_{xy}((\cos\theta)^2 - (\sin\theta)^2) \end{cases} \xrightarrow{\sigma_y=0\ and\ \tau_{xy}=0}$$

And $\frac{{\sigma_1}^2}{{S_L}^2} - \frac{\sigma_1\sigma_2}{{S_L}^2} + \frac{{\sigma_2}^2}{{S_T}^2} + \frac{{\tau_{12}}^2}{{S_{LT}}^2} = 1$,

then we will have:

$$\frac{(\sigma_x\,(\cos\theta)^2)^2}{{S_L}^2}-\frac{(\sigma_x\sin\theta\cos\theta)^2}{{S_L}^2}+\frac{(\sigma_x(\sin\theta)^2)^2}{{S_T}^2}+\frac{(\sigma_x\ \cos\theta\ \sin\theta)^2}{{S_{LT}}^2}=1$$

$${\sigma_x}^2[\frac{(\cos\theta)^4}{{S_L}^2}-(\frac{1}{{S_L}^2}-\frac{1}{{S_{LT}}^2})(\sin\theta)^2(\cos\theta)^2+\frac{(\sin\theta)^4}{{S_T}^2}=1$$

$$\sigma_x=[\frac{(\cos\theta)^4}{{S_L}^2}-(\frac{1}{{S_L}^2}-\frac{1}{{S_{LT}}^2})(\sin\theta)^2(\cos\theta)^2+\frac{(\sin\theta)^4}{{S_T}^2}]^{-1/2}$$

APPENDIX C

ANOVA ANALYSIS OF TEST SAMPLES (MICROSOFT EXCEL 2016)

ANOVA analysis between 0°and 15°group:

Anova: Single Factor

SUMMARY

Groups	*Count*	*Sum*	*Average*	*Variance*
Angle 0	10	309100	30910	2465444.444
Angle 15	10	319100	31910	12385444.44

ANOVA

Source of Variation	*SS*	*df*	*MS*	*F*	*P-value*	*F crit*
Between Groups	5000000	1	5000000	0.673360368	0.422617174	4.413873419
Within Groups	133658000	18	7425444.444			
Total	138658000	19				

There were no statistically significant differences between 0°and 15°group means as determined by one-way ANOVA.

ANOVA analysis between 15°and 30°group:

Anova: Single Factor

SUMMARY

Groups	*Count*	*Sum*	*Average*	*Variance*
Angle 15	10	319100	31910	12385444.44
Angle 30	10	265950	26595	4674138.889

ANOVA

Source of Variation	*SS*	*df*	*MS*	*F*	*P-value*	*F crit*
Between Groups	141246125	1	141246125	16.55915297	0.000719759	4.413873419
Within Groups	153536250	18	8529791.667			
Total	294782375	19				

There were significant differences between 15°and 30°group means as determined by one-way ANOVA.

ANOVA analysis between 30°and 45°group

Anova: Single Factor

SUMMARY

Groups	*Count*	*Sum*	*Average*	*Variance*
Angle 30	10	265950	26595	4674138.889
Angle 45	10	234645	23464.5	5413380.278

ANOVA

Source of Variation	*SS*	*df*	*MS*	*F*	*P-value*	*F crit*
Between Groups	49000151.25	1	49000151.25	9.715005333	0.005955085	4.413873419
Within Groups	90787672.5	18	5043759.583			
Total	139787823.8	19				

There were significant differences between 15°and 30°group means as determined by one-way ANOVA.

ANOVA analysis between 45°and 60°group:

Anova: Single Factor						
SUMMARY						
Groups	*Count*	*Sum*	*Average*	*Variance*		
Angle 45	10	234645	23464.5	5413380.278		
Angle 60	10	211070	21107	5881601.111		
ANOVA						
Source of Variation	*SS*	*df*	*MS*	*F*	*P-value*	*F crit*
Between Groups	27789031.25	1	27789031.25	4.920597971	0.039638914	4.413873419
Within Groups	101654832.5	18	5647490.694			
Total	129443863.8	19				

There were significant differences between 45°and 60°group means as determined by one-way ANOVA.

ANOVA analysis between 60°and 75°group:

Anova: Single Factor						
SUMMARY						
Groups	*Count*	*Sum*	*Average*	*Variance*		
Angle 60	10	211070	21107	5881601.111		
Angle 75	10	219700	21970	2882333.333		
ANOVA						
Source of Variation	*SS*	*df*	*MS*	*F*	*P-value*	*F crit*
Between Groups	3723845	1	3723845	0.84981124	0.368797439	4.413873419
Within Groups	78875410	18	4381967.222			
Total	82599255	19				

There were no statistically significant differences between 60°and 75°group means as determined by one-way ANOVA.

ANOVA analysis between 75°and 90°group:

Anova: Single Factor						
SUMMARY						
Groups	*Count*	*Sum*	*Average*	*Variance*		
Angle 75	10	219700	21970	2882333.333		
Angle90	10	232950	23295	2983583.333		
ANOVA						
Source of Variation	*SS*	*df*	*MS*	*F*	*P-value*	*F crit*
Between Groups	8778125	1	8778125	2.992925232	0.100738005	4.413873419
Within Groups	52793250	18	2932958.333			
Total	61571375	19				

There were no statistically significant differences between 75°and 90°group means as determined by one-way ANOVA.

BIBLIOGRAPHY

ADINA. (2012). ADINA Theory and Modeling Guide. <http://www.adina.com/adinadownloads/docs/tmg-a_89.pdf.>. (Dec. 8, 2016).

ADINA. (2014). ADINA Primer. < http://www.adina.com/adinadownloads/docs/primer_89.pdf>. (Dec. 8, 2016).

Aicher, S. Klöck,W. .2001."Linear Versus Quadratic Failure Criteria for In plane Loaded Wood Based Panels" Otto-Graf-Journal Vol. 12, 2001.

Askarinejad, S., Kotowski, P., Shalchy, F., & Rahbar, N. (2015). Effects of humidity on shear behavior of bamboo. Theor. Appl. Mech. Lett., 5(6), 236-243. doi:10.1016/j.taml.2015.11.007

ASTM D143. (1994). Standard Methods of Testing Small Clear Specimens of Timber. ASTM. Philadelphia, PA.

ASTM D2915. (1999). Standard Practice for Evaluating Allowable Properties for Grades of Structural Lumber. ASTM. Philadelphia, PA.

ASTM3500D. (2009). Standard Test Methods for Structural Panels in Tension. ASTM. Philadelphia, PA.

ASTMD2016. (1991). Standard Test Methods for Moisture Content of Wood. ASTM. Philadelphia, PA.

ASTM D5764-97. (2013). Standard Test Method for Evaluating Dowel-Bearing Strength of Wood and Wood-Based Products. ASTM. Philadelphia, PA.

ASTM D5456-17e1. (2017). Standard specification for evaluation of structural composite lumber products, ASTM International, West Conshohocken, PA, www.astm.org DOI: 10.1520/D5456-17E01.

Awaludin, A., Smittakorn, W., Hirai, T., & Hayashikawa, T. (2007). Bearing properties of Shorea obtusa beneath a laterally loaded bolt. Journal of wood science, 53(3), 204-210.

AWC (American Wood Council). (2015). NDS, national design specification for wood construction (2012 ed.). AWS, Leesburg, VA.

Bathe, K. (1996). Finite Element Procedures. New Jersey, NJ: Prentice Hall.

Branco, J., Cruz, J., & Piazza, M. (2009). Experimental analysis of laterally loaded nailed timber-to-concrete connections. Constr. Build. Mater., 23(1), 400-410.

BS EN 1995-1-1:2004+A2:2014 Eurocode5.Design of timber structures. General. Common rules and rules for buildings, BSI.

BSI. (2009). Timber structures. Test methods. Determination of embedding strength and foundation values for dowel type fasteners. Brussels.

Brühl, F., Kuhlmann, U., & Jorissen, A. (2011). Consideration of plasticity within the design of timber structures due to connection ductility. Engineering Structures,33(11), 3007-3017. doi:10.1016/j. engstruct.2011.08.013

Clouston, P., Lam, F., & Barrett, J. (1998). Interaction Term of Tsai-Wu Theory for Laminated Veneer. Journal of Materials in Civil Engineering, 10(2), 112-116.

Diesen, K., & Clouston, P. (2014). Building with Bamboo: A Review of Culm Connection Technology. Journal of Green Building, 8(4), 83-93.

Dixon, P., & Gibson, L. (2014). The Structure and Mechanics of Moso Bamboo Material. Journal of the Royal Society Interface, 11(99), 22-23. doi:http://dx.doi.org/10.1098/rsif.2014.0321

EN 383 (2007): Determination of embedding strength and foundation values for dowel type fasteners, Timber structures, Test methods, CEN (European Committee for Standardization), Brussels, Belgium.

European Committee for Standardization., & British Standards Institution. (1994). Eurocode 5: Design of timber structure. Brussels: BSI.

Franke, S. and Magniere, N. (2014).” Discussion of testing and evaluation methods for the embedment behaviour of connections”, INTER: Proceedings of Meeting 47, INTER/47-15-6, Bath, United Kingdom.

Flinn, A. 2013.Honors Thesis: “Evaluating Dowel-Bearing Strength for Laminated Bamboo Lumber (LBL) in Structural Applications” Department of Civil and Environmental Engineering University of Massachusetts, Amherst.

Forest Products Laboratory, Wood Handbook (2010) “ Wood as an Engineering Material, General Technical Report “, Department of Agriculture, Forest Service, Forest Products Laboratory, Madison, USA.

Frastia, L. (2007). Numerical solution of elastic bodies in contact by FEM utilizing equilibrium displacement fields. Comput. Mech., 41, 159-174.

Hankinson, R.L. (1921).” Investigation of crushing strength of spruce at varying angles of grain,” Air Service Information circular, Washington, DC, 3(259),130.

Hong, J.P., Barrett, J.D. & Lam, F (2011). Three-dimensional finite element analysis of the Japanese traditional post-and-beam connection. Journal of Wood Science. 57:119–125. DOI 10.1007/s10086-010-1151-0.

Johansen, K. W. (1949). Theory of timber connections. International Association for Bridge and Structural Engineering, 9, 249-262.

Jones, R. (1999). Mechanics of Composite Materials. Taylor & Francis Inc. Levittown, PA.

Jorissen, A. (1998) Double shear timber connections with dowel type fasteners. Ph.D. thesis. Technical University of Delft, Delft, The Netherlands (ISBN 90-407-1783-4).

Jorissen, A. (1999). Double shear timber connections with dowel type fasteners. Heron, Vol. 44(3). ISSN 0046-7316.

Kharouf, N., McClure, G., & Smith, I. (2003). Elasto-plastic modeling of wood bolted connections. Comput. Struct., 81,747-754.

Khoshbakht, N., Clouston, P.L., Arwade, S.R., and Schreyer, A.C.(2018)" Computational Modeling of Laminated Veneer Bamboo Dowel Connections" J. Mater. Civ. Eng.,30(2): 04017285, pages 1-11 , ISSN (print): 0899-1561 | ISSN (online): 1943-5533 .

Khoshbakht, N., P. Clouston, P., Arwade, S., and Schreyer, A. (2019) "Evaluation of ASTM D5764 Dowel Connection Tests for Laminated Veneer Bamboo (LVB)." Journal of Testing and Evaluation ,Vol.47(4): 2717–2736.. https://doi.org/10.1520/JTE20180385.

Kim, N.-H. (2015). Introduction to nonlinear finite element analysis. Springer. New York.

Lee, A., Bai, X., & Peralta, P. (1994). Selected physical and mechanical properties of giant timber bamboo grown in South-Carolina. Forest Products Journal, 44(9), 40-46. http://search.proquest.com/docview/214634490?accountid=14572

Lekhnit͡skiĭ, S. G. (1968). Anisotropic plates. New York: Gordon and Breach.

Mahdavi, M., Clouston, P. L., & Arwade, S. R. (2011). Development of Laminated Bamboo Lumber: Review of Processing, Performance, and Economical Considerations. ASCE, J. Mater. Civ. Eng., 23(7), 1036-1042.

Muñoz, W., & Salenikovich, A.J. (2008). Determination of Yield point and Ductility of Timber Assemblies: in search for harmonized approach.

Oudjene, M., & Khelifa, M. (2009). Elasto-plastic constitutive law for wood behavior under compressive loading. Constr. Build. Mater.,23(11),3359-3366. doi: 10.1016/j.conbuildmat.2009.06.034

Patton-Mallory, M., Cramer, S. M., Smith, F. W., & Pelican, P. J. (1997). Nonlinear material models for analysis of bolted wood connections. J. Struct. Eng., 123(8), 1063-1070.

Patton-Mallory, M., Cramer, S. M., Smith, F. W., & Pelican, P. J. (1997). Nonlinear material models for analysis of bolted wood connections. Journal of Structural Engineering, 123(8), 1063-1070.

Patton-Mallory, M., Pelicane, J. P., & Smith, F. W. (1998). Experimental Analysis of Blted Joints in Wood. Jornal of Testing and Evaluation, 26(1), 45-52.

Patton-Mallory, M., Pelicane, J. P., & Smith, F. W. (1998). Qualitative Assessment of Failure in Bolted Connections: Tsai-Wu Criterion. Jornal of Testing and Evaluation, 26(1), 489-497.

R.Z. Yang, Y. X. (2014). Failure analysis of typical glubam with bidirectional fibers by off-axis. Construction and Building Materials, 85, 9-15.

Ramirez, F., Correal, J., Yamin, L., Atoche, J., & Piscal, C. (2012). Dowel-Bearing Strength Behavior of Glued Laminated Guadua Bamboo. J. Mater. Civ. Eng., 24(11), 1378-1387.

Reynolds, T., Sharma, B., Harries, K., & Ramage, M. (2016). Dowelled structural connections in laminated bamboo and timber. Composites Part B. doi: 10.1016/j.compositesb.2015.11.045

Rodd P.D. (1973) The analysis of timber joints made with circular dowel connectors. PhD thesis, University of Sussex, England.

Santos, C. L., de Jesus, A., Morais, J., & Lousada, J. (2010). A Comparison Between the EN 383 and ASTM D5764 Test Methods for Dowel-Bearing Strength Assessment of Wood: Experimental and Numerical Investigations. Strain. 46(2), 159-174 DOI: 10.1111/j.1475-1305.2008.00570. x.

Schoenmakers, J., & Jorissen, A. (2011). Failure mechanisms of dowel-type fastener connections perpendicular to grain. Engineering Structures,33(11), 3054-3063. doi:10.1016/ j.engstruct.2011.05.018

Sjodin,J., Serrano,E.,Enquist,B. (2008).“An experimental and numerical study of the effect of friction in single dowel joints” Holz Roh Werkst (2008) 66: 363–372. https://doi.org/10.1007/s00107-008-0267-z.

Smith, I., A. Asiz, M. Snow, and Y.H. Chui. 2006. Possible Canadian/ISO approach to deriving design values from test data. International Council for Research and Innovation in Building and Construction.Working Commission W18–Timber Structures. 39th meeting, August 2006, Florence, Italy.

Soltis, L. A. (1991). European Yield Model for Wood Conncetions. 9th structures congress proceedings (pp. 60-63). Indianapolis, IN. NewYork: American Society of Civil Engineers. Stelmokas, J., Zink, A., Loferski, J., & Dolan, J. (1997). Image correlation Analysis of Multiple-bolt wood. Wood and Fiber Science, 29(3), 210-227. doi:10.1520/JTE11362J

Takeuchi, C. P., Estrada, M., & Linero, D. L. (2015). The Elastic Modulus and Poisson's Ratio of Laminated Bamboo Guadua angustifolia. Key Engineering Materials, 668, 126-133.

Tsai, S. W., & Wu, E. M. (1971). A General Theory of Strength for Anisotropic Materials. Journal of Composite Materials, 5(1), 58-80. doi:10.1177/002199837100500106

Van der Put, T. A. (2008). Derivation of the bearing strength perpendicular to the grain. Holz als Roh- und Werkstoff , 409-417.

United States Department of Agriculture, Forest Service, Forest Products Laboratory, 2010. "Mechanical Properties of Wood," in Wood Handbook: Wood as Engineering Material (Madison, WI: United States Department of Agriculture), 5.

Wiggers, P. (2006). Computational contact mechanics. New York, NY: Springer.

Yang, R. Z., Lam, F., & Xiao, Y. (2014). Failure analysis of typical glubam with bidirectional fibers by off-axis. Constr. Build. Mater., 85, 9-15.

Yu, Y., Tian, G., Wang, H., Fei, B., & Wang, G. (2011). Mechanical characterization of single bamboo fibers with nanoindentation and microtensile technique. Holzforschung, 65(1). doi:10.1515/hf.2011.009